The synthesis of novel semicarbazide compounds and investigation of their chemical and biological behaviour have gained more importance in recent decades for biological, medicinal, and agricultural reason. This work is mainly focused to the detailed structural behaviour of the molecule analysis by FT-IR, FT-Raman, UV-Vis and NMR spectra of semicarbazide molecules were recorded and subjected to the new trends of theoretical methods have proved to be very efficient and cost effective tool for structural elucidation of bioactive molecules. This work has been determined the vibrational frequencies and various properties of certain prominent particles using the Gaussian program, which is developed for performing DFT estimations.

**Dr. M. Raja** works at Dept. of Physics, Govt. Thirumagal Mills College, Gudiyattam, Vellore.

**Mrs. E. Dhanalakshmi** works at Dept. of Physics, Vels Institute of Science, Technology & Advanced Studies.

**Dr. D. Vijayalakshmi** is Assistant Professor at Dept. of Physics, Vels Institute of Science, Technology & Advanced Studies.

9 786207 488421

Spectroscopic and Theoretical Study



M. Raja, E. Dhanalakshmi, D. Vijayalakshmi

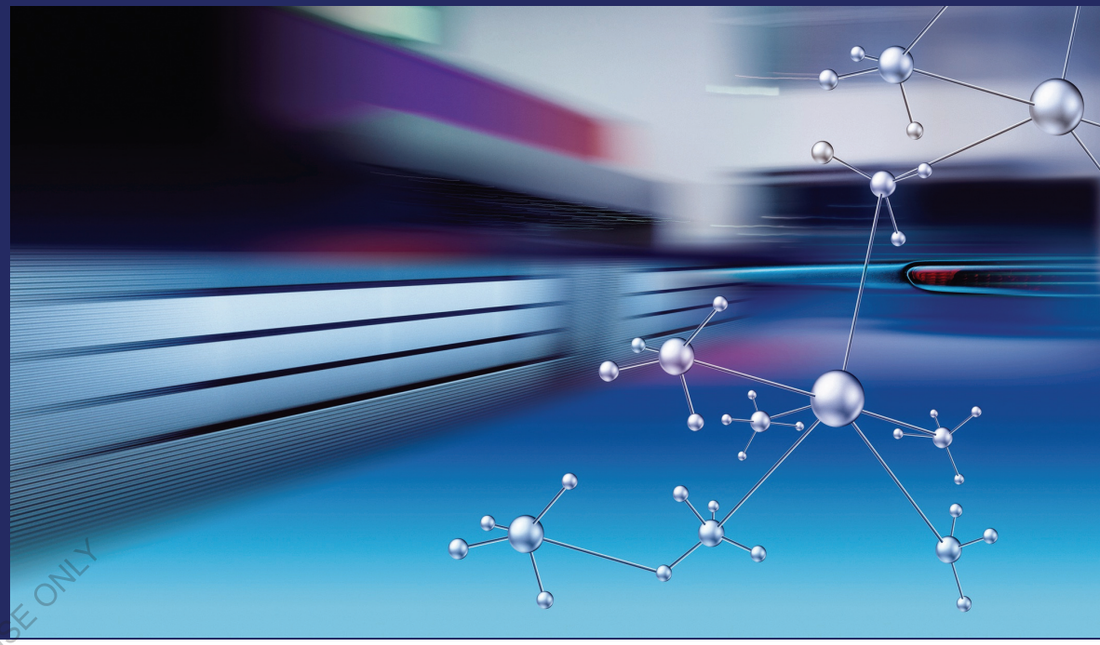

M. Raja
E. Dhanalakshmi
D. Vijayalakshmi

# Spectroscopic and Quantum Calculations on Semicarbazide Derivatives

## Post-Graduate and Research Based

LAP LAMBERT Academic Publishing

**M. Raja**
**E. Dhanalakshmi**
**D. Vijayalakshmi**

# Spectroscopic and Quantum Calculations on Semicarbazide Derivatives

M. Raja
E. Dhanalakshmi
D. Vijayalakshmi

# Spectroscopic and Quantum Calculations on Semicarbazide Derivatives

**Post-Graduate and Research Based**



LAP LAMBERT Academic Publishing

**Imprint**
Any brand names and product names mentioned in this book are subject to trademark, brand or patent protection and are trademarks or registered trademarks of their respective holders. The use of brand names, product names, common names, trade names, product descriptions etc. even without a particular marking in this work is in no way to be construed to mean that such names may be regarded as unrestricted in respect of trademark and brand protection legislation and could thus be used by anyone.

Cover image: www.ingimage.com

Publisher:
LAP LAMBERT Academic Publishing
is a trademark of
Dodo Books Indian Ocean Ltd. and OmniScriptum S.R.L publishing group

120 High Road, East Finchley, London, N2 9ED, United Kingdom
Str. Armeneasca 28/1, office 1, Chisinau MD-2012, Republic of Moldova, Europe
Printed at: see last page
**ISBN: 978-620-7-48842-1**

## CONTENTS

# CHAPTER – I

## Spectroscopic Techniques and Quantum Chemical Calculation on Semicarbazide Derivatives

### 1.1. Introduction

Spectroscopy is the interaction of electromagnetic radiation with matter. Absorption spectroscopy is most widespread and energy quanta from electromagnetic radiation are absorbed by the sample illuminated by the radiation. Depending upon the wavelength (frequency) of the electromagnetic radiation, transitions between different kinds of energy states are induced in the molecules of the sample. Spectroscopy consists in the recording of absorption changes as the frequency of the radiation is varied over a given range. A plot of absorption of energy versus frequency known as the spectrum usually shows a number of absorption bands whose characteristic position, intensity, width and shape yield important information. Spectroscopy is one of the important experimental techniques for determining the electronic structure of atoms and molecules [1, 2]. It is mainly useful for determining structure and dynamics of biological molecules. Time-resolved spectroscopy enables visualization and tracking of fundamental events such as molecular reaction mechanisms or protein folding. Advanced systems utilizing high-power pulse lasers enable the study of dynamics of fast processes occurring in the region of picoseconds. Spectroscopy has found its way from academic laboratories into practical applications across a range of diverse fields including biomedical, pharmaceutical, agricultural, forensic and much more. Most commonly used characterization techniques are Fourier Transform Infrared (FT-IR), Fourier Transform Raman (FT-Raman), Ultraviolet-Visible (UV-Vis) and Nuclear magnetic resonance (NMR) spectroscopy. They require very small

quantities and can be used in the examination of samples in all phases of matter [3-10]. While FT-IR spectroscopy measures decrease in intensity of incident light due to excitation of vibrational energy levels in a molecule, FT-Raman spectroscopy measures light elastically scattered from a sample with a frequency different from that of incident light.

Frontiers of spectroscopy are very wide, as technique is applicable to solids, crystals, powder, liquids, solutions, melt, gases, films and absorbed species. It's important application are Molecular structural determinations, calculation of intra-molecular & inter-molecular forces, computation of the degree of association in condensed phases, elucidation of molecular symmetries, identification and characterization of new molecules, deducing thermo dynamical properties of molecular systems, etc [11]. NMR is the technique used for determining the structure of organic molecules and biomolecules in solution. Covalent structure, stereochemistry, and conformation are available techniques that measure direct distances and bond dihedral angles. Specific NMR signals can be identified and assigned to each hydrogen and carbon in the molecule.



This introductory chapter is deals with the instrumentation technique of infrared, Raman, UV-Visible (UV-Vis) and Nuclear Magnetic Resonance spectroscopy (NMR). Important facts relevant to the carried out research work, mainly theoretical background, instrumentation and sample handling. Different quantum computational methods, Vibrational energy distribution analysis and Importance of semicarbazide derivative materials are explained briefly.

## 1.2. Instrumentation techniues

### 1.2.1. Infrared Spectroscopy

Infrared spectroscopy is one of the most powerful analytical techniques, which offers the possibility of molecular confirmation. The most advantage of infrared spectroscopy over the other usual methods of structural analysis is that it provides useful information about the structure of the molecules quickly without tiresome evaluation methods. The infrared region of the electromagnetic spectrum lies between the red end of the visible spectrum and the beginning of the microwave region. Conventional infrared spectroscopy is concerned with mid infrared range extending from approximately 4000-400 $cm^{-1}$. Each functional group absorbs characteristic frequencies of infrared radiation uniquely and hence the infrared spectrum is a finger print of the chemical groups [12-15]. An infrared spectrum originated from molecular vibrations causes a change in the dipole moment of the molecule. Such a spectrum, therefore, reflects the structure of the molecule, especially the masses of the constituent atoms and the intermolecular forces acting between them, as well as the intermolecular forces operating in crystalline state.



With most forms of spectroscopy the spectrum is a plot of the absorbance of the sample against wavelength but in infrared the transmittance is plotted against wavenumber. An infrared spectrum has characteristically four main features namely (i) the number of bands present (ii) the wavenumber position (iii) shape of the bands and (iv) the intensities of the bands. The infrared region of the spectrum encompasses radiation with wave numbers ranging from about 12,800 to10 $cm^{-1}$ or wavelengths from 0.78 to 1000 μm. From instrumentation and application point of view, the infrared region has been subdivided into near IR region

(overtone region), mid IR region (vibration rotation region) and far IR region (rotation region). When a molecule absorbs infrared radiation the usual vibrational transitions is from ground state to the first excited state, producing bands of fundamental frequencies. In addition to this other transition can also occur, although not common, giving rise to weaker bands than the fundamentals and are called as overtones. If two fundamental vibrations are simultaneously excited, then these are called combination bands. The actual position of a band in infrared spectrum depends on the force constant that binds the atoms. The various bands can be interpreted according to the characteristic functional groups present in the compound [16].

### 1.2.2. Fourier Transform Infra-red (FT-IR)

Fourier transform spectroscopy simultaneously exposes a sample to the entire range of IR frequencies. Frequencies not absorbed by the sample constitute the "sample beam", which reaches the detector at 100% transmittance. As this takes place, another beam of IR radiation reaches the detector. This "reference beam" has not passed through the sample. The sample beam and the reference beam are allowed to interfere with each other as they reach the detector and the resulting data is used to construct an interferogram. This interferogram is converted to a normal spectrum by performing a Fourier transformation. Once data has been collected by the spectrometer, it is sent to the computer as an interferogram. The computer determines the frequency and intensity of each component wave of the interferogram, by performing a Fourier transform of the data. These frequencies and intensities make up the peaks of an IR spectrum.

### *1.2.2.1. Michelson interferometer*

Interferometer is an important part of FT-IR spectrometer. It consists of two perpendicular mirrors as shown in Fig.1.1. One of them is a stationary mirror while the other one is a movable mirror that can be displaced perpendicularly towards the fixed mirror at a constant velocity. Between the two mirrors, there is a beam splitter placed at 45° from the identical position of the movable mirror. When a parallel beam of radiation from the source is passed on to the mirrors through the beam splitter, the beam splitter divides the beam and transmits half of the incoming radiation to the fixed mirror and the other half to the movable mirror.

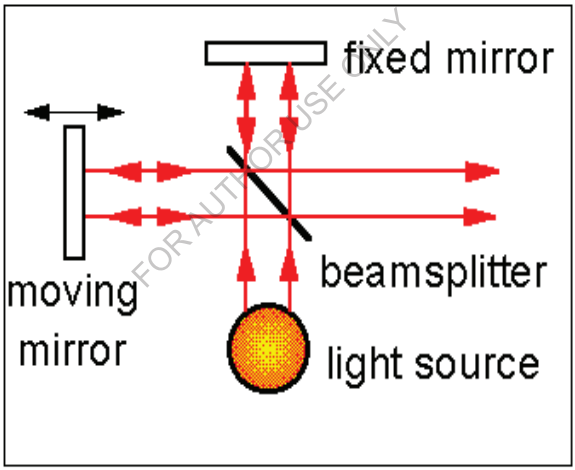



**Fig. 1.1. Michelson interferometer**

### *1.2.2.2. FT-IR Instrumentation*

The IFS 66v/S is a flexible vacuum FT-IR spectrometer whose spectral range may be expanded from far-IR to the near UV. The working and schematic diagram of FT-IR spectrometer has been given below in Fig. 1.2. The FT-IR spectra of the sample were recorded in the wavelength

region of 4000–400 $cm^{-1}$. This spectrometer consists of an Interferometer between source (Globar) and sample compartment. The working of Interferometer has been explained above. The sample compartment is located between the interferometer and the detector. The radiation from the interferometer incident on the sample, then it goes to the detector. The compound in the present work is solid. So, the KBR pellet method was used for recording spectrum. The sample was then pelletized with KBr and the signals were recorded.

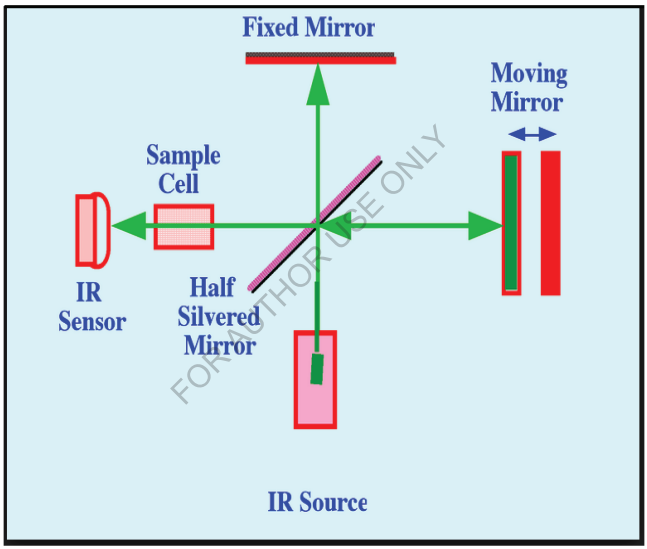


**Fig.1.2. Simplified diagram of Fourier transform infrared spectrometer**

### *1.2.2.3. Sample handling techniques*

Sample handling is considered as an important technique in infrared spectroscopy. There are various methods of sample preparation to enable almost any type of sample to be examined. Some significant problems arise when trying to construct sample containers for vibrational

spectrometry, because every material has some vibrational absorption. The material of choice for IR spectroscopy is a solid potassium bromide plate. Such plates are used in a number of ways. Polyethylene pellets are used for recording the far IR spectra.

***a. Solids***

Solids are sampled in a wide variety of ways. If the sample is soluble, it may be dissolved and handled as for a liquid. Solid samples for which no solvent is suitable can be prepared for analysis by incorporating them into a pressed pellet of alkali halide, usually potassium bromide. Sample is mixed with a weighed amount of powdered potassium bromide and the mixture is admitted to a pressure of several tones in a dye, to produce a highly transparent plate or disc which can be inserted into the spectrophotometer. The use of KBr eliminated the problems of additional bands due to mulling agent. KBr does not absorb infrared light in the region 2.5 – 15 μm and a complete spectrum of the sample is obtained. Solid samples have also been examined in the form of a thin layer deposited by sublimation or solvent evaporation on the surface of a salt plate. Another method, called mulling has also been developed, in which the powdered sample is mixed to form a paste with little heavy paraffin oil. The mull is sandwiched between salt plates for measurement. Mulls are formed by grinding 2 to 5 mg of finely powdered sample in the presence of one or two drops of heavy hydrocarbon oil called Nujol [17-22].



***b. Liquids***

In most instances the spectra of liquids are measured in either a demountable type cell or in fixed thickness or sealed cells. The spectra of pure samples can be measured as very thin films squeezed between two alkali halide windows of a demountable cell. This technique can produce a

film of thickness 0.01 mm or less. This method is most useful for qualitative work only because the sample thickness cannot be controlled. Liquid cells consist of two alkali halide windows usually NaCl or KBr, separated by a spacer of suitable thickness made of Teflon or lead which limits the volume of the cell [17-22].

***c. Gases***

Absorption spectra of gases can be measured in a wide variety of gas cells ranging from a few centimeters to several meters that can be directly placed in the path of the infrared beam. The end walls of the cell are usually made of sodium chloride which is transparent to infrared. The low frequency vibrational changes in the gaseous phase often split the high frequency vibrational bands [23].



***d. Solvents***

Solvents of good infrared transparency over a convenient frequency range are available and the spectra of the sample dissolved in carbon tetrachloride and carbon disulphide provide the complete range. Chloroform is considered to be an important solvent and is frequently used because it shows absorptions though it is less symmetric molecule than carbon tetrachloride and carbon disulphide.

***1.2.2.4. Advantages of Fourier Transform Infrared Technique***

The main advantages of FT spectroscopy are the greater ease and speed of measurement. The entire spectrum can be recorded within few seconds using sophisticated computers. Recent developments in FT Infrared spectrometers have thus led to higher resolution, total wavelength coverage, higher accuracy in frequency and intensity measurements. It can also be used in the characterization of all kinds of samples. In FT method,

all the source energy passes through the instrument and the resolving power is constant over the entire spectrum. The signal to noise ratio is also improved [24]. The smoothening of peaks and the vertical and horizontal expansion of selective region is also possible.

### 1.2.3. Theory of Raman Effect

Raman spectroscopy is an optical analysis technique based on an effect discovered by Chandrasekhara Venkata Raman. Raman was a self-made scientist who was known for his outrageous ideas, simple experimental design and in-depth observations. An interest in optical phenomena led him to demonstrate in 1921 that the scattering of light is responsible for the colour of the ocean rather than sky reflection or absorption as previously thought [25]. Then in 1928 he discovered the inelastic scattering of light, or Raman Effect, which won him the Nobel Prize two years later [26]. These experiments used a narrow band photographic filter to produce a monochromatic light source from sunlight, a "crossed" filter to block scattered light and the human eye as a detector. Raman and his co-worker Krishnan found that when a benzene sample was irradiated by this intense monochromatic light source, light of a different frequency passed through the "crossed" filter. Since these early days of crude instrumentation, Raman spectroscopy has gradually developed to become a well-established scientific tool. The effect was subject to intensive research in the first decade after its discovery. However, during the Second World War it became overshadowed by the infrared spectroscopy, a technique that was enhanced by the development of sensitive detectors and advances in electronics. The popularity of Raman spectroscopy was not restored until the invention of the laser in the early 1960s and has grown steadily since. In recent years, instrumentation has

progressed with the availability of durable and affordable lasers and increasing accessibility of high-powered computer technology. Nowadays Raman spectroscopy is widely used to analyze materials well beyond the capabilities of other methods, with the ability to obtain a detailed account of the physical and chemical makeup of a material at the molecular level. The fundamental process of the Raman Effect is the transfer of energy between light and matter.

Raman spectroscopy employs this effect by measuring the scattering of light from molecules in different vibrational states of a material and the consequent energy exchange between the incoming light and the molecules [27]. When a beam of monochromatic electromagnetic radiation impinges on a material, it can be either scattered or absorbed (Fig. 1.3.).



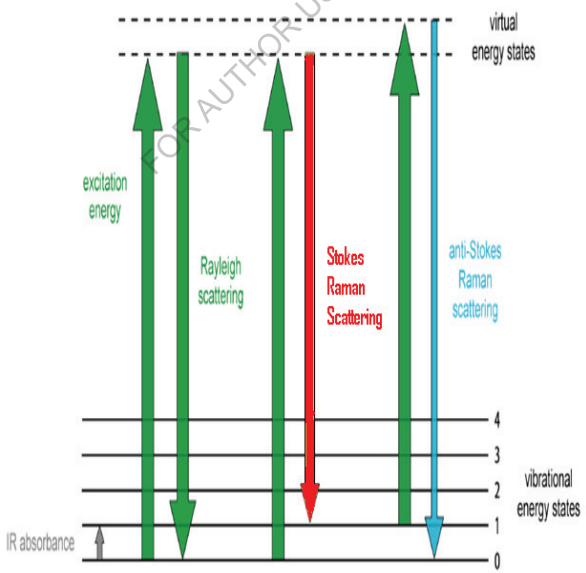


**Fig. 1.3. Energy Level Diagram**

If light is scattered from an atom or molecule within the material, most photons are elastically scattered. This is known as Rayleigh scattering, in which the scattered photons have the same energy E as the incident photons given by

$$E = h\nu_0 \qquad (1.1)$$

where h is Plank's constant and $\nu_0$ is the frequency of the incident light. However, a small fraction of scattered light (approximately 1 in every billion photons) undergoes what is known as inelastic or Raman scattering. In this case light is scattered from molecules with frequencies of oscillation that vary from the frequency of the incident photons. It is this difference in frequency, or energy between the incoming and outgoing light that is the measurable quantity used as the basis of Raman spectroscopy.



***1.2.3.1. Stokes and Anti-stokes Raman Scattering***

The Raman Effect comprises of two distinct types of scattering, known as Stokes and anti-Stokes scattering (Fig.1.3). The most likely to occur is Stokes scattering, in which the incident light interacts with a molecule that absorbs energy from it. This molecule is excited from its ground state to the "virtual state" and then relaxes back down to finish in a vibrational excited state. In this case photons are scattered that are lower in energy and frequency than the incoming photons and therefore longer in wavelength. Anti-Stokes scattering is the less probable and weaker effect, which occurs when light interacts with a molecule that is already in a vibrational excited state. After being excited up to the "virtual state" this molecule falls down to the ground state, causing the incident photons to gain energy and scatter at a higher frequency and shorter wavelength.

A classical treatment of Raman scattering demonstrates the occurrence of these two effects mathematically [28]. The electric field strength E of the incoming electromagnetic radiation is given by

$$E=E_0 \cos(2\pi\upsilon_0 t) \quad (1.2)$$

where t is time, $E_0$ is the vibrational amplitude of the electric field and $\nu_0$ is the frequency of the radiation. When this light interacts with a molecule, it induces an electric dipole moment

$$P= \alpha E = \alpha E_0 \cos(2\pi\upsilon_0 t) \quad (1.3)$$

where α is known as polarisability. Molecular polarisability can be interpreted as the deformability of the electron cloud by the external electric field. In general, α is a tensor that depends on E. However, for simplicity the tensor properties of polarisability are neglected here. The above oscillatory dipole moment allows scattering to occur, as the molecule moves to an excited state. The charge distribution in the material is then vibrating with a frequency ν and nuclear displacement



$$q=q_0 \cos(2\pi\upsilon t) \quad (1.4)$$

where $q_0$ is the vibrational amplitude. These oscillations may induce a change in the polarizability of the molecule. When $q$ is small, polarisability varies linearly with displacement and can be approximated by a Taylor series expansion of $\alpha$ resulting in

$$\alpha = \alpha_0 + \left[\frac{\partial\alpha}{\partial q}\right]_0 q_0 + \ldots\ldots \quad (1.5)$$

where $\alpha_0$ is the polarisability at equilibrium and produces elastic scattering, whilst $(\partial\alpha/\partial q)_0$ is the rate of change of $\alpha$ with respect to $q$ at this point and is the origin of inelastic scattering. Combining the previous three equations, making substitutions and simplifying gives

$$P = \alpha E_0 \cos(2\pi \upsilon_o t) + \frac{1}{2}\left[\frac{\partial \alpha}{\partial q}\right]_0 q_0 E_0[\cos\{2\pi(\upsilon_0 - \upsilon)t\} + \cos\{2\pi(\upsilon_0 + \upsilon)t\}] \quad (1.6)$$

The result is an expression consisting of two terms. The first term represents the outgoing light that remains unchanged from when it enters the material, possessing the frequency of the incident light $\nu_0$. This is Rayleigh scattering. The second term represents the inelastically scattered light and contains two frequency shifts ($\nu_0 - \nu$) and ($\nu_0 + \nu$) arising from Stokes and anti-Stokes Raman scattering respectively.

The key to using Raman scattering to investigate the physiochemical makeup of a material is the change in photon energy between the incident and scattered light, measured as the shifts in frequency derived previously. As shown in Fig. 1.4, light exits a material at a number of different energies that are shifted from the original energy of the incoming photons *E*. In this case the more probable Stokes scattering is demonstrated, in which there is a loss in energy and therefore a decrease in frequency. These different energy changes, $\Delta E_1$ etc, correspond to light scattering from molecules being excited to a number of distinct vibrational energy levels. The frequency shifts corresponding to these different molecular vibrational modes, $(\nu_0 - \nu_1)$ etc, are displayed as a spectrum of peaks. The position and intensity of each peak relates to a specific type of molecular vibration such as the stretching, bending, torsion or deformation of a bond, combining to form a spectrum that represents the chemical fingerprint of a material.

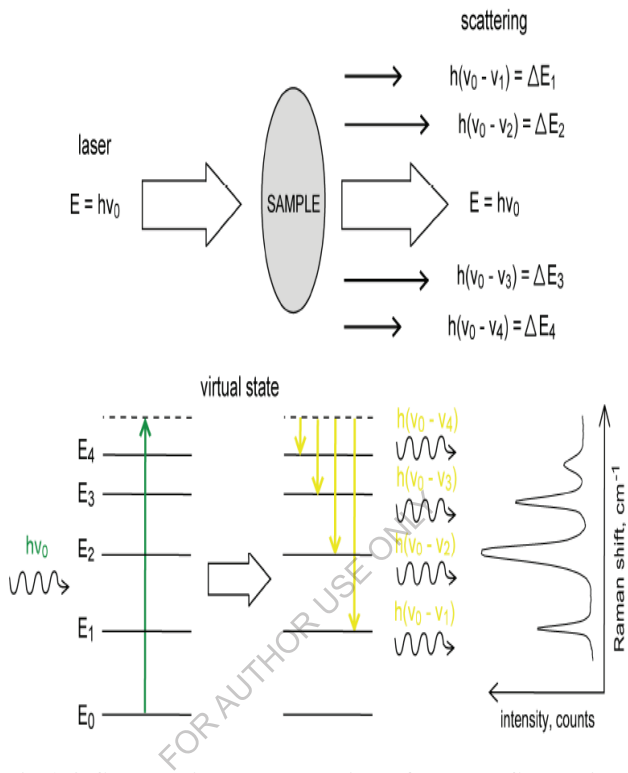




**Fig.1.4. Schematic representation of Raman Scattering**

The Stokes and anti-Stokes Raman bands are much weaker than the Rayleigh line and occur symmetrically on either side of it, corresponding to the same amount of energy lost and gained respectively by the incident photons. The Boltzmann distribution indicates that within a system at thermal equilibrium, the lower energy state is more populated than the higher energy state. For a material, this translates to a larger number of molecules in lower energy states than in higher energy states. Therefore in a Raman spectrum the bands relating to Stokes scattering are more intense than those corresponding to anti-Stokes scattering. These peaks have a

magnitude of light intensity, or counts, and are usually displayed as a Raman shift ν . This parameter is common to vibrational spectroscopy. It is essentially wavenumber with units of $cm^{-1}$ and is related to wavelength λ and frequency ν via

$$\tilde{\nu} = \frac{\upsilon}{C} = \frac{1}{\lambda} \qquad (1.7)$$

where c is the speed of light. In Raman spectroscopy, the unit of wavenumber is used simply for convenience. If wavelength or frequency were used, the position of peaks in a spectrum would be determined by the wavelength of the excitation light that they originated from. Instead spectra are displayed in Raman shifts from the Rayleigh peak, which is always set to 0 $cm^{-1}$. This means that the positions of peaks for a particular material are independent of the excitation wavelength.



Experimentally, a Raman shift can be determined from

$$\tilde{\boldsymbol{\nu}}\ (cm^{-1}) = 10^7[(1/\lambda_0)-(1/\lambda_R)] \qquad (1.8)$$

where $\lambda_0$ and $\lambda_R$ are the laser wavelength and Raman scattering wavelength respectively, both in nanometers.

### *1.2.3.2. FT-Raman measurements*

FT-Raman spectra of the samples were recorded using the Bruker RFS 100/S spectrophotometer that uses 1064 nm laser excitation and provides a $4cm^{-1}$ resolution (Fig.1.5). The solid sample was taken in sample holder and was subjected to laser irradiation. The orientation of the sample holder was adjusted to obtain maximum amplitude.

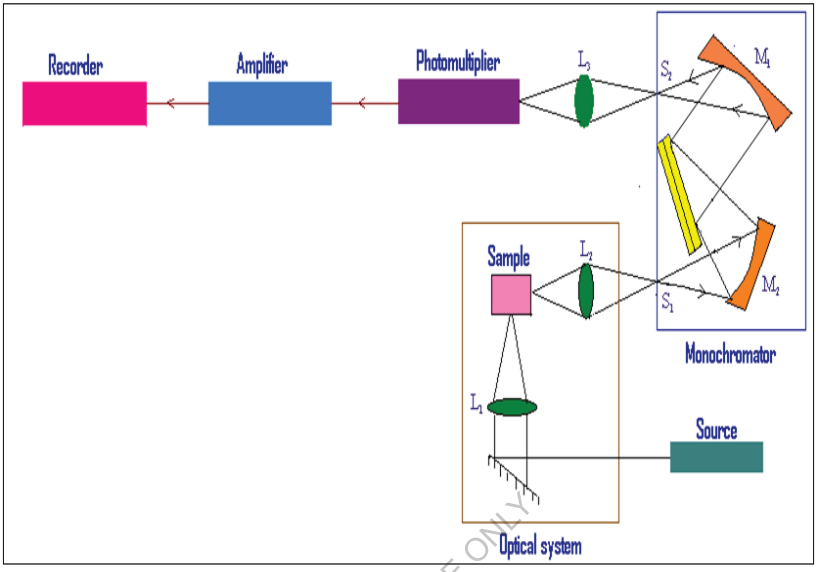


**Fig. 1.5. Simplified diagram of FT- Raman Spectrometer**



### *1.2.3.3. Excitation laser*

The FT-Raman spectrometers currently available use Nd: YAG lasers operating at nm. The laser output is filtered by nm band pass filter to remove spontaneous emission, and then directed to the sample. Some spectrometers have a provision for 180° geometry or 90°. Since an interferometer has a large aperture than the slit of the dispersive/CCD system, it is not always necessary to focus the laser on to a small spot. For this reason, the beam steering mirror (or prism M3) is placed to the right of the collection lens. An optical focusing lens, that may be easily removed and placed in the laser beam path, is used. An unfocused or weakly focused laser is advantageous in FT-Raman because it lowers the power density at the sample and relaxes the tolerance on alignment of laser, collection optics and sample.

### *1.2.3.4. Collection optics*

The collected light can be coupled directly with parallel path of the interferometer, but it usually passes through an aperture. This aperture called jacquinot stop and it permits control of the degree of collimation in the interferometer and excludes severely of axis light.

### *1.2.3.5. Interferometers*

Interferometers were developed for FT-IR and adapted for FT-Raman with minimal change. The FT-Raman accessory consists of a laser, sample chamber, filter and detector that are added to a stand-alone FT-IR spectrometer. The schematic representation of Interferometers is shown in Fig.1.1.



### *1.2.3.6. Laser Rejection Filters*

The laser rejection filter serves the essential function of reducing the strong elastically scattered laser relative to the weak Raman scattering. The noise in FT-Raman spectrum is proportional to the square root of the average intensity of light across entire spectrum. The laser rejection filters are variations of the holographic notch filters, which enhance the possibility of observing low frequency shifts of the order 85$cm^{-1}$.

### *1.2.3.7. Detectors*

Currently available detectors for the 1100 to 1700nm wavelength range appropriate to FT-Raman are low band gap semiconductors, particularly germanium (Ge) and indium gallium arsenide (InGaAs). The parameters used to specify the efficiency and performance of the detector is the dark signal and quantum efficiency. These parameters critically affect the detector performance.

### *1.2.3.8. Sample handling techniques*

Sample handling techniques for Raman spectroscopic measurements is simpler than for infrared spectroscopy because glass can be used for windows, lenses and other optical components instead of the more fragile and atmospherically less stable crystalline halides. In addition, the laser source is easily focused on slit. Consequently very small samples can be investigated. In fact, a common sample holder for non-absorbing liquid sample is an glass melting-point capillary.

#### *a. Liquid Samples*

The spectrum of a liquid can be recorded as neat or in solution. Ordinarily about 0.3 ml of a liquid may be required. The sample could be taken in glass or silica containers or capillaries. The spectra can be measured directly from the reaction vessel. Water is a good solvent for recording the Raman spectra. Water absorbs strongly in the infrared but it is a poor Raman scattered. Raman spectroscopy is thus a valuable tool for studying water soluble biological materials.



#### *b. Solid samples*

The Raman spectra of solids as polycrystalline material or as a single crystal can be recorded. No medium such as null, KBr or solvent is needed. A few milligrams of the solid samples are required. Solid can be packed into capillary tubes as a powder. The crystal can be mounted in a goniometer on a glass or silica fiber. The spectra can be measured for different orientation of the crystal. For single crystals, the Raman spectrum varies depending on the direction of the crystal axis, when polarized light is used as incident radiation. Raman spectra of adsorbed species can be recorded at different temperatures and pressures.

*c. Gas samples*

The Raman spectra of gases are generally weaker than those of liquids or solids and hence may require cells of larger path length. The gas may be filled in a glass or silica tube of 1 to 2 cm diameter. If the resolving power of the instrument is good and if the molecule has sufficiently low moment of inertia, the rotational fine structure may be observed on either side of the Rayleigh line. Generally a broadband contour may be observed. The main advantage of Raman spectroscopy is that it may be used for a wide variety of sizes and forms of the sample. Samples in gas, liquid and solid states can be examined easily.

***1.2.3.9. Advantages and disadvantages***

Raman spectroscopy has long been used in many areas of physics, chemistry and materials science [29]. However, more recent applications of the technique have been in biological and medical research, both in vitro and in vivo [30, 31]. Raman spectroscopy offers many benefits to work in these fields:



(1) It is non-invasive, requiring no labeling or other preparation of the sample;

(2) As long as suitable laser wavelengths, powers and exposure times are used, it does not cause significant damage to biological cells and tissue;

(3) It can be used under a wide range of conditions such as varying temperature or pressure;

(4) Typical "background" species such as carbon dioxide and water do not significantly interfere with spectra, as they have weak Raman scattering;

(5) It allows the investigation of samples in physiological conditions, therefore lengthening the time period for measurements and making it possible to experiment in real-time.

For any application, the lack of sample preparation needed prior to analysis with Raman spectroscopy is one of the greatest advantages of the technique. This allows it to be a very rapid analytical technique, leading to high quality data in very short periods of time. Furthermore, Raman scattering originates from the surface of a sample (typically no deeper than several hundred microns), so there is no concern with sample thickness, size or shape.

Raman spectroscopy can be used for a variety of purposes. The technique is often used as a qualitative or identification tool, as it provides exceptional chemical specificity. A Raman spectrum contains a wealth of analytical information and no two molecules will give the same one. Raman spectroscopy also has a greater sensitivity to chemical functional groups not seen strongly by other similar methods. The selection rules governing the technique require a change in the polarisability of a molecule in order to be Raman-active, a condition that is unique to Raman spectroscopy. In addition, the intensity of scattered light is related to the amount of material present, allowing Raman spectroscopy to be used in quantitative applications.



As with any scientific technique, Raman spectroscopy also has its limitations. The most significant disadvantage of Raman spectroscopy is the interference it suffers from fluorescence. This phenomenon originates from different mechanisms to Raman scattering; however, they can occur together. Fluorescence is broad and more intense than Raman scattering,

often overwhelming it. There are ways to avoid such interferences, as discussed in the following chapter, but the potential for fluorescence must always be considered during applications of Raman spectroscopy. Other disadvantages of Raman spectroscopy include equipment cost and the sensitivity of the technique. The Raman Effect is very weak, therefore efficient collection and detection of scattering requires sensitive and highly optimized instrumentation.

### 1.2.4. Ultraviolet-Visible spectroscopy

#### *1.2.4.1. Basic principles*

Ultraviolet (UV) and visible radiation comprise only a small part of the electromagnetic spectrum, which includes such other forms of radiation as radio, infrared (IR), cosmic and X rays. The energy associated with electromagnetic radiation is defined by the following equation:



$$E=h\upsilon \qquad (1.9)$$

where E is energy (in joules), h is Planck's constant ($6.62 \times 10^{-34}$ Js), and n is frequency (in seconds). Electromagnetic radiation can be considered a combination of alternating electric and magnetic fields that travel through space with a wave motion. Because radiation acts as a wave, it can be classified in terms of either wavelength or frequency, which is related by the following equation:

$$\upsilon=c/\lambda \qquad (1.10)$$

where υ is frequency (in seconds), c is the speed of light ($3 \times 10^{8}$ $ms^{-1}$), and l is wavelength (in meters). In UV-visible spectroscopy, wavelength usually is expressed in nanometers (1 nm = $10^{-9}$ m). It follows from the above equations that radiation with shorter wavelength has higher energy. In UV-visible spectroscopy, the low-wavelength UV light has the highest

energy. In some cases, this energy is sufficient to cause unwanted photochemical reactions when measuring sample spectra.

### *1.2.4.2. Origin of UV-Visible spectra*

When radiation interacts with matter, a number of processes can occur, including reflection, scattering, absorbance, fluorescence/phosphorescence (absorption and reemission) and photochemical reaction (absorbance and bond breaking). In general, when measuring UV-visible spectra, we want only absorbance to occur.

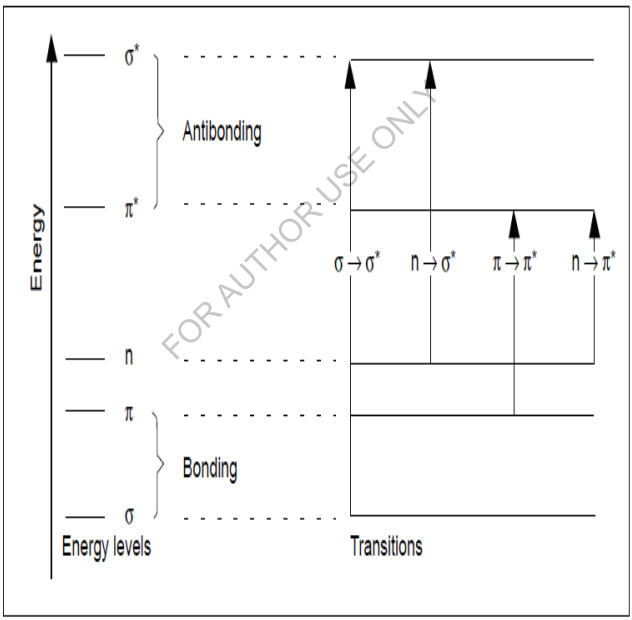



**Fig.1.6. Electron transitions in ultraviolet/visible spectroscopy**

Because light is a form of energy, absorption of light by matter causes the energy content of the molecules (or atoms) to increase. The total

potential energy of a molecule generally is represented as the sum of its electronic, vibrational and rotational energies:

$$E_{total} = E_{electronic} + E_{vibrational} + E_{rotational} \quad (1.11)$$

The amount of energy a molecule possesses in each form is not a continuum but a series of discrete levels or states. The differences in energy among the different states are in the order:

$$E_{electronic} > E_{vibrational} > E_{rotational}$$

In some molecules and atoms, photons of UV and visible light have enough energy to cause transitions between the different electronic energy levels. The wavelength of light absorbed is that having the energy required to move an electron from a lower energy level to a higher energy level.



### *1.2.4.3. Origin of the absorptions*

Valence electrons can generally be found in one of three types of electron orbital:

1. Single or σ bonding orbitals
2. Double or triple bonds (π bonding orbitals) and
3. Non-bonding orbitals (lone pair electrons)

Sigma bonding orbitals tend to be lower in energy than π bonding orbitals, which in turn are lower in energy than non-bonding orbitals. When electromagnetic radiation of the correct frequency is absorbed, a transition occurs from one of these orbitals to an empty orbital, usually an antibonding orbital, σ* or π*. The exact energy difference between the orbitals depends on the atoms present and the nature of the bonding system. Most of the transitions from bonding orbitals are of too high a frequency (too short a wavelength) to measure easily, so most of the

absorptions observed involve only $\pi \rightarrow \pi^*$, $n \rightarrow \sigma^*$ and $n \rightarrow \pi^*$ transitions (Fig.1.6).

### *1.2.4.4. Absorption laws*

Beer's law tells us that absorption is proportional to the number of absorbing molecules -ie. to the concentration of absorbing molecules (this is only true for dilute solutions) - and Lambert's law tells us that the fraction of radiation absorbed is independent of the intensity of the radiation. Combining these two laws, we can derive the Beer-Lambert Law:

$$\log_{10} (I_0/I) = \varepsilon lc \qquad (1.12)$$

Where $I_0$ = the intensity of the radiation

I = the intensity of the transmitted radiation

ε = a constant for each absorbing material, known as the molar absorption coefficient

l = the path length of the absorbing solution in cm

c = the concentration of the absorbing species in mol $dm^{-3}$.



The value of $\log_{10} (I_0/I)$ is known as the absorbance of the solution and can be read directly from the spectrum as 'absorbance units'. The wavelength at which maximum absorption occurs is represented by $\lambda_{max}$. The values of both ε and $\lambda_{max}$ are strongly influenced by the nature of the solvent, and for organic compounds, by the degree of substitution and conjugation.

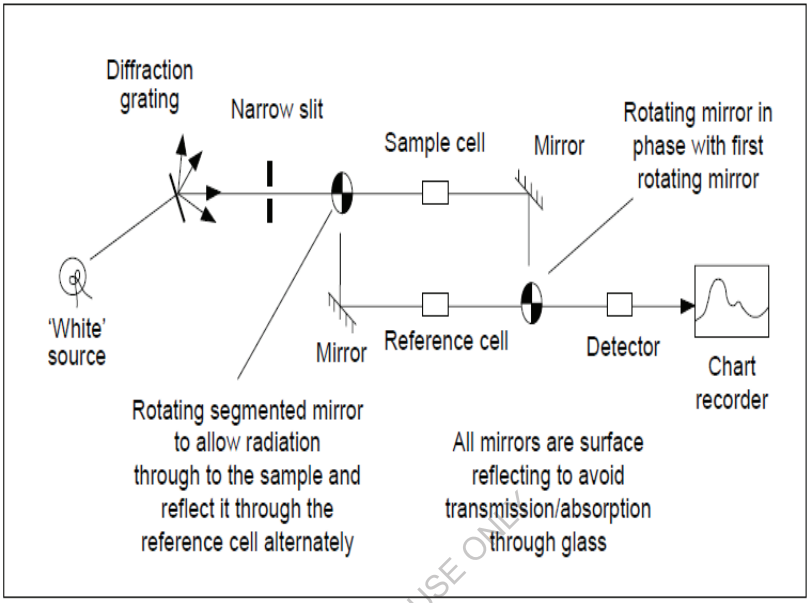


**Fig.1.7. Simplified diagram of UV-visible Spectrometer**



### *1.2.4.5. Instrumentation*

Because only small number of absorbing molecules is required, it is convenient to have the sample in solution. In conventional spectrometers electromagnetic radiation is passed through the sample which is held in a small square-section cell (usually 1cm wide internally). Radiation across the whole of the ultraviolet/visible range is scanned over a period of approximately 30 s, and radiation of the same frequency and intensity is simultaneously passed through a reference cell containing only the solvent. Photocells then detect the radiation transmitted and the spectrometer records the absorption by comparing the difference between the intensity of the radiation passing through the sample and the reference cells (Fig.1.7.). In the latest spectrometers radiation across the whole range is monitored simultaneously.

A hydrogen or deuterium discharge lamp covers the ultraviolet range, and a tungsten filament (usually a tungsten/halogen lamp) covers the visible range. The radiation is separated according to its frequency /wavelength by a diffraction grating followed by a narrow slit. The slit ensures that the radiation is of a very narrow waveband – i.e. it is monochromatic.

The cells in the spectrometer must be made of pure silica for ultraviolet spectra because soda glass absorbs below 365 nm, and pyrex glass below 320 nm. Detection of the radiation passing through the sample or reference cell can be achieved by either a photomultiplier or a photodiode, which converts photons of radiation into tiny electrical currents; or a semiconducting cell (that emits electrons when radiation is incident on it) followed by an electron multiplier similar to those used in mass spectrometers. The spectrum is produced by comparing the currents generated by the sample and the reference beams. Modern instruments are self-calibrating, though the accuracy of the calibration can be checked if necessary. Wavelength checks are made by passing the sample beam through glass samples (containing holmium oxide) that have precise absorption peaks, and the absorption is calibrated by passing the sample beam through either a series of filters, each with a specific and known absorption, or a series of standard solutions.



### *1.2.4.6.* Applications

UV-VIS spectroscopy is routinely used for quantitative determination of analyses solutions in transition metal ions and highly conjugated organic compounds.

Solutions of transition metal ions can be coloured (i.e., absorb visible light) because d electrons within metal atoms can be excited from one electronic state to another.

- While charge transfer complexes also give rise to colors, colors are often too intense to be used for quantitative measurement.
- Absorbance of a solution is directly proportional to concentration of absorbing species in solution and path length. Thus, for a fixed path length, UV/VIS spectroscopy can be used to determine concentration of absorber in a solution.

### 1.2.5 Nuclear Magnetic Resonance (NMR)

Phenomenon of NMR deals with transitions between energy levels that arise because of different orientations of nuclei moment of nuclei placed in a magnetic field. These transitions are studied by means of a resonance method which is called NMR [32]. It is a powerful analytical technique used to characterize organic molecules by identifying carbon-hydrogen frameworks within molecules. Two common types of NMR spectroscopy are used to characterize organic structure: $^{1}H$ NMR is used to determine the type and number of H atoms in a molecule; $^{13}C$ NMR is used to determine the type of carbon atoms in molecule. Source of energy in NMR is radio waves which have long wavelengths and thus low energy and frequency. When low-energy radio waves interact with a molecule, they can change nuclear spins of some elements, including $^{1}H$ and $^{13}C$.



#### *1.2.5.1 Basic principles of NMR Spectroscopy*

Atoms consist of electrons and a nucleus and the most important property of a nucleus for NMR spectroscopy is its spin. In its most simple form, spins can be described as an electric charge rotating around its own

axis. This rotation generates a small magnetic moment which interacts with an external applied magnetic field. Interaction of a single isolated nuclear spin I, with a magnetic moment $\overline{\mu} = \gamma . I . \hbar$, and a static field along z-direction, $\overline{B_0}\, r$ , is called Zeeman interaction. Hamiltonian describing this interaction is:

(1.13)

Most nuclei which are studied in liquid state NMR spectroscopy ($^{1}$H, $^{13}$C, $^{15}$N, $^{19}$F and $^{31}$P) have a spin quantum number 1 of 1/2. This means that for spin-1/2 nuclei two spin energy levels exist, i.e. +1/2 and -1/2 which are commonly denoted as α and $\beta$ respectively.

Energy difference between both states is called Zeeman splitting and equals:

(1.14)

as schematically represented in Fig. 1.8. Observed frequency is called Larmor frequency.



Every nucleus is surrounded by a cloud of electrons in constant motion. Under the influence of the magnetic field these electrons are caused to circulate in such a manner as to oppose the field. This has the effect of partially shielding the nucleus from feeling the full value of the external field. Thus either the frequency or the field will have to be changed slightly to bring the shielded nucleus into resonance. It is generally accomplished by an adjustment of the magnetic field through an auxiliary winding carrying varying direct current which sweeps the field over a narrow span. The value of the shift depends on the chemical environment of the proton. Because this is the source of variations in shielding by electrons, it is called the chemical shift [33].

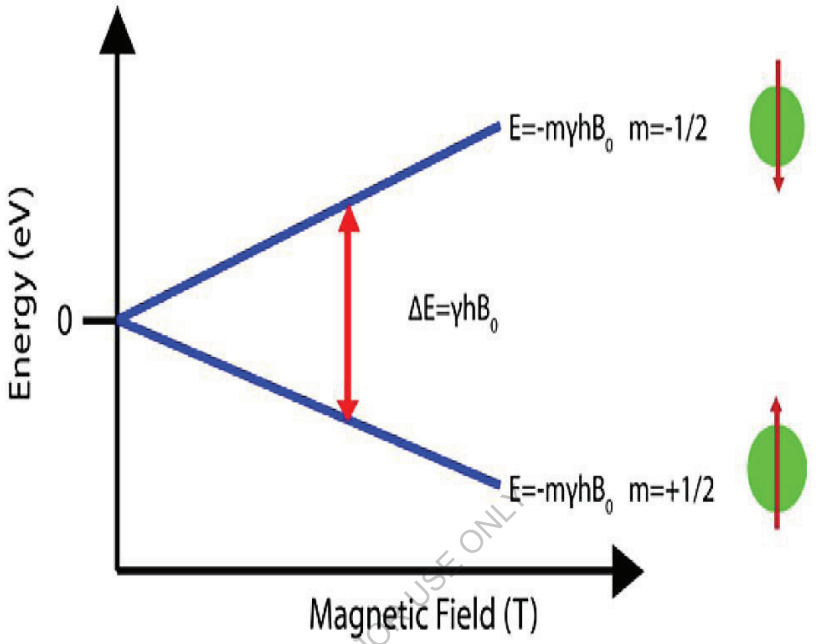




**Fig. 1.8. Splitting of degenerate nuclear energy levels under an applied magnetic field**

***1.2.5.2 Instrumentation***

Basis of NMR experiment is to induce a transition between two consecutive energy levels that result when a nucleus is placed in a magnetic field.

Two types of NMR spectrometers are commonly used. They are:

(a) Continuous wave (CW) NMR spectrometer

(b) Fourier Transform (FT) NMR spectrometer

### *1.2.5.3 Fourier Transform (FT) NMR Spectrometer*

In order to carry out a normal continuous wave NMR experiment, strength of magnetic field or frequency of applied radiation must be varied. In order to acquire signals with low intensity, it is necessary to run experiment repeatedly in order to average noise associated with measurement.

Fourier transform operation converts a signal from time domain to frequency domain. It can essentially separate out a complex wave into many constituent waves of a fixed frequency. Instead of individually scanning frequency domain, sample can be excited by a single pulse or multiple pulses of strong radio-waves and free induction decay (FID) picked up on a receiver. By Fourier transforming FID, a multi-frequency based NMR spectrum is observed. This can be completed in a few seconds or less, making it far less time consuming to perform than multiple scans needed for continuous wave method.



## 1.3. Antimicrobial Studies

Microbes are microscopic life forms, usually too small to be seen by the naked eye. Although many microbes are single-celled, there are also numerous multi-cellular organisms. Microorganisms are very diverse and include bacteria, fungi and algae. Microorganisms live in all parts on the earth where there is liquid water, including hot springs, on the ocean floor, high in the atmosphere and deep inside rocks within the Earth's crust. Certain microbes have adapted to withstand unusual environmental conditions, including extreme pressure, temperature, acidity and radiation. These microscopic organisms are found in plants and animals as well as in the human body. An antimicrobial is a substance that kills or inhibits the growth of microorganisms such as bacteria, fungi and orprotozoans.

Antimicrobial drugs either kill microbes (microbiocidal) or prevent the growth of microbes (microbiostatic).

### 1.3.1 Antibacterial Activity Study

Antibiotics are generally used to treat bacterial infections. The toxicity to humans and other animals from antibiotics is generally considered to be low. However, prolonged use of certain antibiotics can decrease the number of gut flora, which can have a negative impact on health. Some recommend that, during or after prolonged antibiotic use, one should consume probiotics and eat reasonably to replace destroyed gut flora.

### 1.3.2 Antifungal Activity Study

Fungi are multi-celled organisms with structures analogous but not identical to plants. They can be found in air, in soil, on plants and in water. Thousands, possibly millions, of different types of fungi exist on Earth. The common types are mushrooms, yeast, mold and mildew. Some live in the human body, usually causing illness. Fungal diseases are called mycoses which can affect human skin, nails, body hair and internal organs such as lungs and body systems such as the nervous system. Aspergillus fumigatus, for instance, can cause aspergillosis, a fungal infection in the respiratory system.



Antifungals work by exploiting differences between mammalian and fungal cells to kill off the fungal organism without dangerous effects on the host. Unlike bacteria, both fungi and humans are eukaryotes. Thus, fungal and human cells are similar at the molecular level, making it more difficult to find a target for an antifungal drug to attack that does not also exist in the infected organism. An antifungal drug is medication used to

treat fungal infections such as athlete‟s foot, ring worm, candidiasis, serious systemic infections such as cryptococcal meningitis and others.

## 1.4. Quantum Chemical Calculations

### 1.4.1. Computational Chemistry

The term theoretical chemistry may be defined as the mathematical description of chemistry. The term computational chemistry is generally used when a mathematical method is sufficiently well developed that it can be automated for implementation on a computer. Computational chemistry is the branch of theoretical chemistry whose major goals are to create efficient computer programs that calculate the properties of molecules (such as total energy, dipole moment, vibrational frequencies) and to apply these programs to concrete chemical objects. In theoretical chemistry, chemists and physicists together develop algorithms and computer programs to allow precise predictions of atomic and molecular properties and reaction paths for chemical reactions. Computational chemists in contrast mostly "simply" use existing computer programs and methodologies and apply these to specific chemical questions. Computational chemistry may be defined as the application of mathematical and theoretical principles to the solution of chemical problems. Molecular modeling, a subset of computational chemistry, concentrates on predicting the behavior of individual molecules within a chemical system. The most accurate molecular model use ab initio or 'first principles' electronic structure methods, based upon the principles of quantum mechanics, and are generally very computer-intensive. However, due to advances in computer storage capacity and processor performance, molecular modeling has been a rapidly evolving and expanding field, to

the point that it is now possible to solve relevant problems in an acceptable amount of time.

The types of predictions possible for molecules and reactions include [34]:

- Heats of formation
- Bond and reaction energies
- Molecular energies and structures (thermo chemical stability)
- Energies and structures of transition states (activation energies)
- Reaction pathways, kinetics and mechanisms
- Charge distribution in molecules (reactive sites)
- Substituent effects
- Electron affinities and ionisation potentials
- Vibrational frequencies (IR and Raman spectra)
- Electronic transitions (UV/Visible spectra)
- Magnetic shielding effects (NMR spectra)



This work presents a review of computational chemistry techniques, focusing on electronic structure methods. Electronic structure methods, particularly DFT calculations, are capable of consistent predictions with high accuracy over a wide range of systems – a critical prerequisite for the successful modeling of Synthetic organic materials.

The programs used in computational chemistry are based on many different quantum-chemical methods that solve the molecular Schrodinger equation. The ultimate goal of most quantum chemical approaches is the "approximate" solution of the Schrodinger equation. Several methods have been developed and implemented in computational programs to solve the Schrodinger equation. The methods that do not include empirical or semi-

empirical parameters in their equations are called ab initio methods. The most popular classes of ab initio methods are:

Hartree-Fock, Moller-Plesset perturbation theory, configuration interaction, coupled cluster, reduced density matrices and density functional theory. Each class contains several methods that use different variants of the corresponding class, typically geared either to calculating a specific molecular property, or, to application to a special set of molecules. The abundance of these approaches shows that there is no single method suitable for all purposes. Computational chemistry can be used to carry out the following:

Molecular energy and structures

- Energies and structure of transition states
- Molecular orbital
- IR and Raman spectra
- NMR properties
- Performing geometry optimizations. Geometry optimization depends primarily on the gradient of the energy (the first derivative of the energy with respect to atomic positions).
- Computing the vibrational frequencies of a molecule resulting from inter atomic motion within the molecule. Frequencies depend on second derivative of the energy with respect to atomic structure. Frequency calculations are not possible or practical for all computational chemistry methods.



### 1.4.2. Computational chemistry methods

All molecular modeling techniques can be classified under three general catagories: ab initio electronic structure calculations, semi-

empirical methods and molecular mechanics. Ab initio or 'first principles' electronic structure methods are based upon quantum mechanics and therefore provide the most accurate and consistent predictions for quantum chemical systems. However ab inito methods are extremely computer intensive. Semi-empirical methods are also founded upon quantum mechanics, but speed computation by replacing some explicit calculations with approximations based upon experimental data. Molecular mechanics techniques are purely empirical methods based on the principles of classical physics and as such are computationally fast. Molecular mechanics methods completely neglect explicit treatment of electronic structure, and are therefore severely limited in scope.



### *1.4.2.1. Ab initio methods*

Ab initio quantum chemistry methods are computational chemistry methods based on quantum chemistry [35]. The term ab initio was first used in quantum chemistry by Robert Parr and coworkers, including David Craig in a semiempirical study on the excited states of benzene [36].

Of the three, ab initio molecular orbital methods are the most accurate and consistent because they provide the best mathematical approximation to the actual system. The term ab initio implies that the computations are based solely on the laws of quantum mechanics, the masses and charges of electrons and atomic nuclei, and the values of fundamental physical constants, such as the speed of light (c=2.998 x 108 m/s) or Planck's constant (h= 6.626 x $10^{-34}$ Js), and contain no approximations. Molecular orbital methods solve Schrodinger's equation for the chemical system using a basis set of functions that satisfy a series of rigorous mathematical approximations. Molecular properties can be assessed from a user specified input (single point energy calculation or

SPE), or the molecule can be allowed to relax to a minimum energy configuration (geometry optimization).

Ab initio molecular orbital computations can provide accurate quantitative predictions of chemical properties for a wide range of molecular systems. However, they place a considerable demand on computer resources. The choice of theoretical method and basis set determine the duration of the calculation; thus, a sophisticated method and a large basis set will provide more accurate results, but will also require more computer resources.

***1.4.2.2. Semi-empirical methods***

Semi-empirical methods increase the speed of computation by using approximations of ab initio techniques (e.g., by limiting choices of molecular orbitals or considering only valence electrons) which have been fitted to experimental data (for instance, structures and formation energies of organic molecules). Until recently, the size of many energetic molecules placed them beyond the scope of ab initio calculations, so preliminary theoretical studies were performed using semi-empirical techniques. However, semi-empirical methods have been calibrated to typical organic or biological systems and tend to be inaccurate for problems involving hydrogen-bonding, chemical transitions or nitrated compounds [37, 38].



Several semi-empirical methods are available and appear in commercially available computational chemistry software packages such as HyperChem and Chem3D. Some of the more common semi-empirical methods can be grouped according to their treatment of electron-electron interactions

### *1.4.2.3. Molecular mechanics*

Molecular mechanics (MM) is often the only feasible means with which to model very large and non-symmetric chemical systems such as proteins or polymers. Molecular mechanics is a purely empirical method that neglects explicit treatment of electrons, relying instead upon the laws of classical physics to predict the chemical properties of molecules. As a result, MM calculations cannot deal with problems such as bond breaking or formation, where electronic or quantum effects dominate. Furthermore, MM models are wholly system-dependent; MM energy predictions tend to be meaningless as absolute quantities, and are generally useful only for comparative studies. Despite these shortcomings, MM bridges the gap between quantum and continuum mechanics, and has been used quite extensively to study 'mesoscopic' effects in energetic materials. Applications include modelling reaction and dissociation on classical potential energy surfaces, studies of equilibrium crystal properties (e.g., density, packing, specific heats) , dynamic investigations of shock interactions with crystals and defects and simulating detonation in molecular crystals.



The basic assumptions of typical molecular mechanics methods are listed below.

- Each atom (i.e., electrons and nucleus) is represented as one particle with a characteristic mass.
- A chemical bond is represented as a 'spring,' with a characteristic force constant determined by the potential energy of interaction between the two participating atoms. Potential energy functions can describe in*tra*molecular bond stretching, bending and torsion, or intermolecular phenomena such as electrostatic interactions or van der Waals forces.

- The potential energy functions rely on empirically derived parameters obtained from experiments or from other calculations.

Current molecular mechanics models are characterised by the set of potential energy functions used to describe the chemical forces. These force fields depend upon:

- Atomic displacements (i.e., bond lengths)
- Atom types, that is, the characteristics of an element within a specific chemical context (e.g., a carbonyl carbon versus a methyl carbon) and
- One or more parameter sets relating atom types and bond characteristics to empirical data.

### 1.4.3. Ab initio molecular orbital theory

#### *1.4.3.1. The physico-chemical model*



The basis of electronic structure methods is the assumption that all chemistry can be described in terms of the interactions between electronic charges within molecules. Hence, chemical bonds can be loosely defined as a redistribution of electronic charge that stabilises the molecule with respect to a collection of its (isolated) constituent atoms.

Relative stabilities are expressed in terms of the total energy of the system, which defined by a differential equation,

$$\hat{H} = \hat{T} + \hat{V} \qquad (1.15)$$

where $\hat{H}$ is the Hamiltonian operator representing the sum of kinetic $\hat{T}$ and potential $\hat{V}$ energies.

In quantum mechanical systems, the kinetic energy of a particle is

$$\hat{\mathrm{T}} = -\frac{\hbar^2}{2\mathrm{m}} + \nabla^2 \qquad (1.16)$$

where m is the mass of the particle, $\hbar$ is Planck's constant ($\hbar$ = 1.055x10$^{-34}$ J.s) and

$$\nabla^2 = \frac{\partial^2}{\partial x^2} + \frac{\partial^2}{\partial y^2} + \frac{\partial^2}{\partial z^2} \qquad (1.17)$$

For electrostatic systems, the potential energy is generally expressed in terms of pairwise interactions between charged particles.

$$\hat{\mathrm{V}} = \frac{\mathrm{q_1 q_2}}{4\pi\mathcal{E}_0} \frac{1}{|\mathrm{r_2 - r_1}|'} \qquad (1.17)$$

where $\mathcal{E}_0$ is the permittivity of free space ($\mathcal{E}_0$ = 8.854x10$^{-12}$ C$^2$/N-m$^2$), and $|\mathrm{r_2 - r_1}|'$ is the distance between charges $\mathrm{q_1}$ and $\mathrm{q_2}$.



### *1.4.3.2. The molecular Hamiltonian*

Under the basic assumption of electronic structure methods, a molecule is a collection of charged quantum particles. The molecular Hamiltonian has the form of **Eq. 1.15**, however the kinetic energy is now a summation over all the particles in the molecule

$$\hat{\mathrm{V}} = \frac{-\hbar^2}{2\mathrm{m}} \sum_{\mathrm{i}} \frac{1}{\mathrm{m_i}} \left( \frac{\partial^2}{\partial x_{\mathrm{i}}^2} + \frac{\partial^2}{\partial y_{\mathrm{i}}^2} + \frac{\partial^2}{\partial z_{\mathrm{i}}^2} \right) \qquad (1.19)$$

and the potential energy is the Coulomb interaction between each pair of charged particles (electron-nucleus attraction, nucleus-nucleus repulsion and electron-electron repulsion):

$$\hat{\mathrm{V}} = \frac{1}{4\pi\mathcal{E}_0} \sum_{\mathrm{i}} \sum_{\mathrm{j}} < j \frac{\mathrm{q_i q_j}}{|\mathrm{r_k - r_j}|'} \qquad (1.20)$$

For electrons, q=-e (e=1.602x10$^{-19}$C), and for nuclei of atomic number Z, q=+Ze

### *1.4.3.3. Hartree-Fock theory*

#### *1.4.3.3.1. The Schrodinger equation*

The quantum mechanical description of chemical bonds is given by a space- and time- dependent probability distribution: the molecular wavefunction. The molecular wavefunction is defined by the Schrödinger equation

$$\hat{\mathrm{H}}_{mol}\psi_{mol}(t) = i\hbar \frac{\partial\psi_{mol}(t)}{\partial t} \tag{1.21}$$

If the potential energy operator is time-independent, then the solution obtained by separation of variables, leads to the molecular wavefunction

$$\psi_{\mathrm{mol}}(\mathrm{t}) = \psi_{\mathrm{mol}} \mathrm{e}^{-\mathrm{iE_{mol}t}/\hbar} \tag{1.22}$$

Where $\psi_{\mathrm{mol}}$ satisfies the time-independent Schrödinger equation

$$\hat{\mathrm{H}}_{mol}\psi_{mol} = \mathrm{E}_{mol}\psi'_{mol}{}' \tag{1.23}$$

and $E_{mol}$ is the total energy of the molecule. Solutions of the time-independent Schrodinger equation represent various stationary states of the molecule (corresponding to stable or meta-stable electronic configurations). The set of wavefunctions $\psi$ which satisfy **Eq.1.23** are its eigen functions and the energies of the molecule, $E_{mol}$ in each stationary state are its eigen values. The stationary state with the lowest energy is called the 'ground state'.

#### *1.4.3.3.2. Antisymmetry and electron spin*

Standard electronic structure methods assume that the molecular wavefunction describing several electrons can be written as a product of

single-electron wavefunctions called 'orbitals', that is, for a molecule containing n electrons,

$$\psi_{mol}(1,2,...n) = \psi(1)\psi(2)...\psi(n) \quad (1.24)$$

Electrons possess an intrinsic angular momentum or 'spin' with a value of ±½. A half integer spin quantum number implies that electrons are antisymmetric with respect to exchange –in other words, a wavefunction describing a pair of electrons i and j must change sign when the electrons are interchanged:

$$\psi(i,j) = -\psi(j,i) \quad (1.25)$$

The simplest antisymmetric combination of molecular orbitals(MOs) is a matrix determinant. A HF wavefunction is constructed by assigning electrons to molecular orbitals $\phi(r)$ in pairs of opposite spin and then forming a determinant using two spin functions α and β, where

$\alpha(\uparrow) = 1$ $\quad \alpha(\downarrow) = 0$

$\beta(\uparrow) = 0$ $\quad \beta(\uparrow) = 1$



For two electrons i and j the total wavefunction takes the form:

$$\Psi(i,j) = \phi(r)\begin{vmatrix}\alpha(i) & \beta(i)\\ \alpha(j) & \beta(j)\end{vmatrix} \quad (1.26)$$

with a determinant

$$\Psi(i,j) = \frac{\phi(r)}{\sqrt{2}}[\alpha(i)\beta(j) - \beta(i)\alpha(j)] \quad (1.27)$$

which satisfies the antisymmetrisation condition of Eq.1.22. For a molecule containing n electrons, the wavefunction is referred to as a 'Slater determinant' and takes the form:

$$(1)\alpha(1)\ \phi_1(1)\beta(1)\ \phi_2(1)\alpha(1)\ \phi_2(1)\beta(1) \qquad {}^{n}/_{2}(1)\alpha(1) \quad {}^{n}/_{2}(1)\beta(1)$$

$$\frac{}{\sqrt{n}}\lfloor\phi\ (n)\alpha(n)\ \phi_1(n)\beta(n)\ \phi_2(n)\alpha(n)\ \phi_2(n)\beta(n) \qquad {}^{n}/_{2}(n)\alpha(n) \quad {}^{n}/_{2}(n)\beta(n)\rfloor$$

(1 28)

***1.4.3.3.3. Ab inito essentials***

For systems of more than two interacting particles, the Schrodinger equation cannot be solved exactly. Therefore, all ab initio calculations for many body systems (e.g. molecules) involve some level of approximation and indeed, some level of empirical parameterization. Nevertheless, ab inito methods for molecular calculations must satisfy a set of stringent criteria:

1. Solutions must be well defined and specified by both the structure and the electronic states of the molecule.
2. The Potential energy of the molecule must vary smoothly and continuously with respect to displacements of the atomic nuclei.
3. The model must contain no bias (e.g., assuming a chemical bond exists between two atoms).
4. The model must be 'size consistent' – that is, solutions and their associated errors must scale in proportion to the size of the molecule.
5. The model must be 'variational' – that is, approximate solutions must provide an upper bound to the true energy of the system. Consequently, the approximate solution having the lowest energy represents the closest fit to the true wavefunction, within the constraints of the method.

*1.4.3.3.4. Born-Oppenheimer approximation*

Electrons in molecules are much lighter than nuclei, and therefore generally have much higher velocities. Hence, under most circumstances, once can assume that electrons respond instantaneously to nuclear displacements. In practice, this means that the molecular Hamiltonian can be written assuming the nuclear positions are fixed (i.e., neglecting nuclear kinetic energy terms):

$$\hat{H} \quad \hat{T} \quad -- \Sigma \quad -- \Sigma_j \Sigma \quad \frac{}{|r \quad j|} \quad (1.29)$$

Most ab initio calculations solve only the electronic part of the molecular wavefunction, and therefore cannot account for systems where the electronic states are strongly coupled to nuclear vibrations.



*1.4.3.3.5. Single particle approximation*

Standard electronic structure methods approximate the total wavefunction of a many electron system as the product of single electron wavefunctions. This is the essence of Hartree Fock theory, which describes each electron in a molecule as moving in the average electric field generated by the other electrons and nuclei. As a single particle theory, HF theory systematically overestimates molecular energies because it neglects the correlated motion of electrons resulting from Coulomb interactions.

*1.4.3.3.6. Linear combination of atomic orbitals (LCAO)*

Although there is no exact analytical solution to the time-independent molecular Schrodinger equation for systems containing more than one electron, approximate solutions can be obtained using standard numerical techniques. The approach of all ab initio techniques is to build

the total wavefunction from a 'basis' set of mathematical functions capable of reproducing critical properties of the system. An individual molecular orbital may then be expressed as

$$\text{(r)} \quad \sum \quad \text{(r)} \qquad (1.30)$$

Where $\chi_\mu(\mathrm{r})$ are the basis functions and the coefficients $\mathrm{C}_{\mu\mathrm{i}}$ are adjustable parameters. For a molecular wavefunction, the electronic orbitals of the constituent atoms form a natural set of basis functions. These atomic orbitals can in turn be represented by different types of mathematical functions. A highly accurate set of atomic orbitals (Slater type orbitals or STO) are based on hydrogenic wavefunctions having the form

$$(\mathrm{r}) \sim \mathrm{Ce}^{-\alpha \mathrm{r}} \qquad (1.31)$$

Exponential functions are not well suited to numerical manipulation, so most electronic structure calculations approximate STOs with a linear combination of Gaussian-type functions

$$(r) \sim \quad \sum \qquad (1.32)$$

Where $d_{\mu v}$ and $\alpha_v$ are adjustable parameters. Gaussian-type functions provide reasonable approximations of STOs, except at very small or very large electron-nucleus separations.Linear combinations of 'primitive' gaussian functions are referred to as 'contracted' Gaussians. Gaussian software offer a choice of basis sets containing contracted guassians optimized to reproduce the chemistry of a large range of molecular systems.

### 1.4.4. Density functional theory

A technique that has gained considerable ground in recent years to become one of the most widely used techniques for the calculation of molecular structure is density functional theory (DFT). Its advantage include less demanding computational effort, less computer time and better agreement with the experimental values than is obtained from Hartree-Fock procedures. The central focus of DFT is the electron density ρ, rather than the wavefunction ψ. The 'functional' part of the name comes from the fact that the energy of the molecule is a function of the electron density, written E[ρ], and the electron density is itself a function of position, ρ(r), and in mathematics a function of a function is called as functional.

#### *1.4.4.1. The Kohn-Sham approach*

Density functional theory [39-41] is based on the Hohenberg-Kohn theorem [42], which states that the total energy of a system in its ground state is a functional of that system's electronic density, ρ(r), and that any density, ρ'(r), other than the true density will necessarily lead to a higher energy. Therefore, the Hohenberg-Kohn theorem introduces an alternative approach to perform exact, variational, abinitio electronic structure calculations. In conventional ab initio methodology, Schrodinger's equation Eψ=Hψ must be solved. Meanwhile, DFT requires only that we minimize the energy functional, E[ρ(r)]. The conceptual simplification thus offered cannot be overstated. Unfortunately, the exact nature of the energy functional is not known and the total energy of a system cannot be simply output when a trial density, ρ'(r), is given as input. Therfore, we must turn to approximate DFT methods, and though we will not have a wavefunction, we will have to make use of one –electron Kohn-Sham

molecular orbitals, which rather closely resemble molecular orbitals from the well known Hartree-Fock (HF) method.

Early applications of DFT tended to be within the physic community, concentrating on systems where the HF approximation is a particularly poor starting point [43]. Therefore, the vast majority of the applications were on metallic systems, because a single determinantal approach is notoriously bad in such cases. Since DFT works with the density, and not the wavefunction, systems that would require a great number of electronic configurations to be well described by conventional ab initio approaches are in principle neither harder nor more expensive, for DFT than the systems that are well described by a single configuration. Correlation effects, absent within the HF approximation, are also built into the approximate energy functional used in modern DFT applications. Therefore, DFT methods are in principle able to treat the entire periodic table with unvarying ease and accuracy



Though the Hohenberg-Kohn Theorem clearly established that one could, in principle, work directly with the density in ab inito calculations, it was the subsequent work of Kohn and Sham (KS) that offered a practical approach to perform DFT calculations. In the KS approach, the unknown Hohenberg-Kohn energy functional, $E[\rho(r)]$, is partitioned in the following manner [43]

$$E[\rho(r)] = U[\rho(r)]+T[\rho(r)]+E_{XC}[\rho(r)] \quad (1.33)$$

In this partitioning scheme, $U[\rho(r)]$ is simply the classical electrostatic energy, the sum of the electron-nucleus attractions and the electron-electron repulsions.

$$U[\rho(r)] = \left(\sum_A \int \frac{-Z_A \rho(r)}{|r-R_A|}\, dr\right) + \frac{1}{2} \iint \frac{\rho(r)\rho(r')}{|r-r'|} dr dr' \qquad (1.34)$$

The next term, T[ρ(r)], is defined as the kinetic energy of a system of non interacting electrons with the same density ρ(r), as that of the real system of interacting electrons being studied. This may seem to introduce a severe error. However, this is not the case, because the final term $E_{XC}$ [ρ(r)] is made to contain, in addition to the exchange and correlation (XC) contributions to the energy, the difference between T [ρ(r)] and the true electronic kinetic energy of the system.

Following KS, ρ(r) of an N-electron system (with $N_\alpha$ spin up electrons and $N_\beta$ spin down electrons) is expressed as the sum of the square moduli of single occupied, orthonormal KohnSham molecular orbitals[44].

$$\rho(r) = \rho^\alpha(r) + \rho^\beta(r) = \sum_i^{N^\alpha} |\psi_i^\alpha(r)^2| + \sum_i^{N^\beta} \left|\psi_i^\beta(r)^2\right| \qquad (1.35)$$



Having done this, T[ρ(r)] can now be defined as

$$T[\rho(r)] = \sum_{\sigma=\alpha\beta} \sum_i^{N^\sigma} \int \psi_i^\alpha(r) \frac{-\nabla^2}{2} \psi_i^\sigma(r) dr \qquad (1.36)$$

One should note that T[ρ(r)] is not a true density functional, because the KS orbitals are required. Alternate forms of T[ρ(r)] that depend only on the electronic density and do not require KS orbitals have been proposed [45]. However, they are too imprecise to be of any practical use in chemistry.

Finally, recalling the fact that the energy functional is minimized by the true ground state density ρ(r), the energy functional E[ρ(r) must be stationary with respect to any arbitrary variation in either of the spin densities [43] ie.,

$$\frac{[\rho(r)]}{\alpha(r)} \qquad \frac{[\rho(r)]}{\beta(r)} \tag{1.37}$$

This condition yields the one – electron KS equations

$$\left\{ -\sum \frac{}{|r \quad A|} \int \frac{\rho(r)}{|r \quad r'|} \qquad \frac{[\rho(r)]}{\sigma(r)} \right\} \quad (r) \qquad (r) \tag{1.38}$$

$$\sigma = \beta\alpha \tag{1.39}$$

Thus, a scheme for performing practical DFT calculation emerges. With an initial guess at the total spin densities, $\rho^{\sigma}(r)$ and $\rho^{\beta}(r)$, the KS equations are constructed and solved, and the resulting set of KS-orbitals, $\psi_i^{\sigma}(r)$ are then used to generate new guesses at $\rho^{\sigma}(r)$ and $\rho^{\beta}(r)$. This procedure is repeated until self-consistency is achieved, that is, the same densities and KS orbitals are generated.

In this preceding discussion, we avoided to deal with the precise nature of the XC energy functional $E_{XC}$ [ρ(r)] and the XC potentials, which are the functional derivatives of $E_{XC}$ [ρ(r)] with respect to $\rho^{\sigma}(r)$ and $\rho^{\beta}(r)$;

$$\frac{[\rho(r)]}{\sigma(r)} \tag{1.40}$$

$$\frac{[\rho(r)]}{\beta(r)} \tag{1.41}$$

If the true XC energy functional, $E_{XC}$ [ρ(r)], were known, this scheme would yield the true ground state density and in turn, exact values for all ground state properties. Unfortunately, the precise nature of $E_{XC}$ [ρ(r) is not known, and at the first glance, it may seem that we are no further along to performing practical DFT calculations then when we had only the Hohenberg-Kohn theorem and an unknown total energy functional

$E_{XC}$ [ρ(r) can, perhaps surprisingly to some yield fairly accurate results. The KS approach is therefore of great practical importance and has become the cornerstone of all modern DFT applications.

### 1.4.5. Basis set

A basis set is a mathematical description of the orbital within a system (which in turn combines to approximate the total electronic wave function) used to perform the theoretical calculations. The molecular orbitals which arise in the slater determinant are usually expanded in the form of linear combination of a finite set of one-electron functions known as basis functions. Larger the basis sets, more accurately approximate the orbital by imposing fewer restrictions on the locations of the electrons in space. In the true quantum mechanical picture, electron has finite probability of existing anywhere in space



Standard basis sets for electronic structure calculations use linear combinations of Gaussian functions to form the orbital. Gaussian offers a wide range of pre-defined basis sets, which may be classified by the number of basis functions that they contain. Basis sets assign a group of basis functions to each atom within a molecule to approximate its orbital. These basis functions themselves are composed of a linear combination of Gaussian functions referred as "contracted functions" and the component Gaussian functions are referred as primitives. A basis function consisting of a single Gaussian function is termed as uncontracted function.

#### *1.4.5.1. Minimal basis sets*

The most common minimal basis set is STO-nG, where n is an integer. This n value represents the number of Gaussian primitive functions comprising a single basis function. In these basis sets, the same number of

Gaussian primitives comprises core and valence orbitals. Minimal basis sets typically give rough results that are insufficient for research-quality publication, but are much cheaper than their larger counterparts. Commonly used minimal basis sets of this type are:

- STO-3G
- STO-4G
- STO-6G
- STO-3G* - Polarized version of STO-3G

***1.5.5.2. Split-valence basis sets***

During most molecular bonding, it is the valence electrons which principally take part in the bonding. In recognition of this fact, it is common to represent valence orbitals by more than one basis function. Basis sets in which there are multiple basis functions corresponding to each valence atomic orbital are called valence double, triple, quadruple-zeta, and so on, basis sets. Since the different orbitals of the split have different spatial extents, the combination allows the electron density to adjust its spatial extent appropriate to the particular molecular environment. Minimum basis sets are fixed and are unable to adjust to different molecular environments.



The notation for the split-valence basis sets arising from the group of John-pople is typically X-YZg. In this case, X represents the number of primitive Gaussians comprising each core atomic orbital basis function. The Y and Z indicate that the valence orbitals are composed of two basis functions each, the first one composed of a linear combination of Y primitive Gaussian functions, the other composed of a linear combination of Z primitive Gaussian functions. In this case, the presence of two numbers after the hyphens implies that this basis set is a split-valence

double-zeta basis set. Split-valence triple- and quadruple-zeta basis sets are also used, denoted as X-YZWg, X-YZWVg, etc. Here is a list of

commonly used split-valence basis sets of this type:

- STO-3G
- 3-21G
- 3-21G* - Polarized
- 3-21+G - Diffuse functions
- 3-21+G* - With polarization *and* diffuse functions
- 4-21G
- 4-31G
- 6-21G
- 6-31G
- 6-31G*
- 6-31+G*
- 6-31G(3df, 3pd)
- 6-311G
- 6-311G*
- 6-311+G*



Basis sets in which there are multiple basis functions corresponding to each atomic orbital, including both valence orbitals and core orbitals or just the valence orbitals, are called double, triple or quadruple-zeta basis sets. Commonly used multiple zeta basis sets are:

- cc-pVDZ - Double-zeta
- cc-pVTZ - Triple-zeta
- cc-pVQZ - Quadruple-zeta
- cc-pV5Z - Quintuple-zeta, etc.

- aug-cc-pVDZ, etc. - Augmented versions of the preceding basis sets with added diffuse functions.
- TZVPP- Triple –zeta
- QZVPP-Quadruple-zeta

The 'cc-p' stands for 'correlation-consistent polarized' and the 'V' indicate they are valence only basis sets. They include successively larger shells of polarization (correlating) functions (*d*, *f*, *g*, etc.). More recently these 'correlation-consistent polarized' basis sets have become widely used and are the current state of the art for correlated or Post- Hartree-Fock calculations.

***1.4.5.3. Polarised basis sets***

Polarisation functions can be added to basis sets to allow for non-uniform displacement of charge away from atomic nuclei, therby improving descriptions of chemical bonding. Polarisation functions describe orbitals of higher angular momentum quantum number than those required for the isolated atom (e.g.,p-type functions for H and He, and d-type functions for atoms with Z>2), and are added to the valence electron shells. For example, the 6-31G (d) basis set is constructed by adding six d-type Gaussian primitives to the 6-31G description of each non-hydrogen atom. The 6-31G (d,p) is identical to 6-31G(d) for heavy atoms, but adds a set of Gaussian p type functions to hydrogen and helium atoms. The addition of p-orbitals to hydrogen is particularly important in systems where hydrogen is a bridging atom.



***1.4.5.4. Diffuse basis sets***

Species with significant electron density far removed from the nuclear centres (e.g., anions, lone pairs and excited states) require diffuse

functions to account for the outermost weakly bound electrons. Diffuse basis sets are recommended for calculations of electron affinities, proton affinities, inversion barriers and bond angles in anions. The addition of diffuse s- and p- type Gaussian functions to non-hydrogen atoms is denoted by a plus sign as in 3-21G. Further addition of diffuse functions to both hydrogen and larger atoms is indicated by a double plus.

***1.4.5.5. High angular momentum basis sets***

Basis sets with multiple polarization functions are now practical for many systems and although not generally required for Hartree-Fock calculations, are useful for describing the interactions between electrons in electron correlation methods. Examples of high angular momentum basis sets include: 6-31G (2d) –two d-functions are added to heavy atoms;



6-311G (2df, pd) - besides the (311) valence functions, two d functions and one f function are added to heavy atoms, and p and d functions to hydrogen; 6-311G (3df, 2df, p) - three d functions and one f function are added to atoms with Z>11, 2d functions and one f functions to first-row atoms (Li to Ne) and one p function to hydrogen;

High angular momentum basis sets augmented with diffuse functions represent the most sophisticated basis sets available. The most accurate ab initio studies of energetic materials would be produced by reasonable sophisticated polarized split-valence basis sets augmented with high angular momentum and diffuse atomic orbitals. However, the size of the optimum basis set, especially when used with electron correlation methods will ultimately be determined by the size of the energetic molecule, the amount computing power available, and the time allotted for the studies.

## 1.5. Computational details

### 1.5.1. GAUSSIAN

GAUSSIAN is a computational chemistry software program. It is a general purpose electronic structure package capable of predicting many properties of atoms, molecules and reactive systems. The Gaussian package was first written by John pople and the name originates from Pople's use of Gaussian orbital to speed calculations over those using Slater-type orbital.

Capabilities of Gaussian are:

- Determine most stable (optimum) molecular geometry and energy.
- Define a potential energy surface by stepping through a range of values for a geometry coordinate, such as bond distance or torsion angle.
- Predict IR, Raman, UV, NMR, and other spectra
- Optimize transition states
- Solvate molecules using the 'polarized continuum (PCM)' or other models.
- Special tools for optimizing transition metal complexes, and other molecules containing large atoms.
- "ONIOM" technique for defining layers within one molecule where higher and lower accuracy methods can be applied.
- Model surfaces using a 2D periodic boundary condition (PBC) method, or crystals using 3D PBC



### 1.5.2. Gauss view

Gaussview is a graphical user interface (GUI) designed to be used with Gaussian to make calculation preparation and output analysis easier,

quicker and more efficient. With the help of Gaussview, one can prepare input for submission to Gaussian and to examine graphically the output that Gaussian produces. Gaussview incorporates an excellent molecule builder. One can use it to rapidly sketch in molecules and examine them in three dimensions. Molecules can be built by atom, ring, group, amino acid and nucleoside. Gaussview can graphically display a variety of Gaussian calculation results, including the following:

- Optimize transition states
- Molecular orbitals
- Atomic charges
- Surfaces from the electron density, electrostatic potential, NMR shielding density and other properties. Surfaces may be displayed in solid, translucent and wire mesh modes.
- Surfaces can be coloured by a separate property.
- Animation of the normal modes corresponding to vibrational frequencies.
- Animation of the steps in geometry optimizations, potential energy surface scans, intrinsic reaction coordinate (IRC) paths and molecular dynamics trajectories from BOMD and ADMP calculations.



### 1.6. Vibrational energy distribution analysis

Vibrational spectroscopy is one of the powerful spectroscopes. Absorption of infra-red light by organic molecules was studiedalready at the end of XIX century by Abney and by Festing, while the Raman scattering was theoretically predicted and experimentally measured in 1920s by Smekal, Raman, Landsberg and Mandelstam. Nowadays, IR and Raman spectroscopes are developing dynamically and a variety of techniques such as Vibrational Circular Dichroism, Raman Optical

Activity, 2D spectroscopes combining the classical spectra with the chiroptical methods, resonance Raman techniques, and numerous Surface Enhanced Raman Spectroscopy methods are being extensively exploited. Most of these experimental measurements require a computational support. This is because numerous finger-print bands are not easily assignable based on sole experimental knowledge.

Calculation of theoretical vibrational spectra is now possible by using a variety of quantum mechanical software enabling use of a variety of quantum chemical approaches based on variational, perturbational, density functional, and coupled clusters methods. The most of vibrational spectra are still calculated within the harmonic approximation generating some systematical errors. Generally, there are two ways to interpret a theoretical vibrational spectrum of a molecule: a visualization of the atom movement, and PotentialEnergy Distribution (PED) analysis [44–49]. The first is simple yet trivial and deceptive. First of all because of overestimation of hydrogen atoms movements which are visible but often engage negligible energy of the mode. This is especially striking for large molecules in which some normal modes are extended over entire molecule. The PED analysis is more accurate and enables to quantitatively describe the contribution of movement of a given group of atoms in a normal mode. Nevertheless, the PED analysis has a limitation originating from ambiguity of the solutions discussed latter. Therefore, a correct PED interpretation requires spectroscopic knowledge and thoroughness of the interpreter.



The PED analysis results in presentation of a normal mode coordinate as a superposition of local mode coordinates. In consequence, the interpreter finds contributions of local mode energy in overall energy of the normal mode. In 1970s, a program for PED analysis was written by

Balga and next modified by Lapinski [50, 51]. This program requires the set of local mode coordinates to be defined by user. The coordinates must be linearly independent. This condition is difficult to be satisfied manually even for 16-atomic molecules for which 42 coordinates must be defined. Moreover, quality of the PED analysis is strongly depended on the introduced set of local coordinates. As the number of normal coordinates increases with 3N-6, for N equal to ca. 50 atoms, the PED analysis was hardly possible. Therefore, in the end of 1990s J.Cz. Dobrowolski et al., the VEDA program which made possible automatic generation of the set of linearly independent local coordinates, first applied in analysis of 9-atomic diformate anion vibrations [52]. Since then, the VEDA program has been continuously developed and has received over 130 independent citations from laboratories all over the world. Wide interest in use of the VEDA program prompted me to describe its possibilities. Now, there are available two versions of the VEDA program enabling analysis of molecules constituted from up to 120 and (in an extended version, up to 240 atoms). The VEDA program is a freeware available from http://www.smmg.pl/ web page.



## 1.7. HOMO-LUMO

Highest occupied molecular orbital energy (EHOMO) and lowest unoccupied molecular orbital energy (ELUMO) are very popular quantum chemical parameters. These orbitals, determine the way molecule interacts with other species. HOMO is the orbital that could act as an electron donor, since it is the outermost (highest energy) orbital containing electrons. LUMO is the orbital that could act as the electron acceptor; since it is the innermost (lowest energy) orbital that has room to accept electrons. According to the frontier molecular orbital theory, formation of a transition state is due to interaction between frontier orbitals of reactants [53]. The

energy of HOMO is directly related to ionization potential and LUMO is directly related to electron affinity and HOMO-LUMO gap is the important stability index [54].

### 1.8. Molecular Electrostatic Potential

Molecular electrostatic potential (MEP) at a point in space around a molecule gives information about the net electrostatic effect produced at that point by total charge distribution (electron + proton) of the molecule and correlates with dipole moments, electro-negativity, partial charges and chemical reactivity of the molecules. It provides a visual method to understand the relative polarity of the molecule [55, 56]. An electron density isosurface mapped with electrostatic potential surface depicts the size, shape, charge density and site of chemical reactivity of the molecules. MEP has been found to be a very useful tool in the investigation of correlation between molecular structures with its physiochemical property relationship including biomolecules and drugs [57, 58].



### 1.9. Molecular Docking Analysis

Protein-ligand interactions play a critical role in the distribution, metabolism and transport of small molecules in biological systems and processes [59]. Molecular docking technique is an attractive scaffold to understand the ligand-protein interactions which can substantiate the experimental results. AutoDock4 (version 4.2) with the Lamarckian genetic algorithm was used to perform docking studies [60]. Lamarckian genetic algorithm(LGA) for ligand conformational searching, which is a hybrid of a genetic algorithm and a local search algorithm. AutoDock was run several times to get various docked conformations, and used to analyze the predicted docking energy. The binding sites for these molecules were selected based on the ligand-binding pocket of the templates [61].

## 1.10. Importance of Semicarbazide derivative materials

Semicarbazide is the one of the urea derivatives. Clinical use of semicarbazide gives the evidence that an inflammatory reaction can be reduced by blocking the enzymatic activity of the enzyme semicarbazide-sensitive amine oxidase (SSAO). SSAO activity was found significantly increased in blood and tissues in some pathological conditions. The enzyme activity has been reported to be elevated in diabetes and cancer. The mean specific activity of SSAO was significantly elevated in the group of patients having prostate cancer with skeletal metastases. Semicarbazide can reduce inflammatory response and can protect against the progressive vascular complications caused by oxidative stress. It also can reduce pain. The SSAO inhibitor also appears able to protect endothelial cells against toxic effects of free radicals. Semicarbazide itself is a standard enzyme inhibitor and new SSAO inhibitors are in development. SSAO inhibitors significantly blocked the catalytic activity of VAP-1 in tumor, attenuated tumor progression, and reduced neo-angiogenesis.



Semicarbazones derivatives have been investigated due to interest in their coordination behavior, analytical applications [62] and biological properties such as antimalarial [63], antibacterial [64], antifungal [65] and antitumor activity [66]. Because of their ease of preparation and rich and varies complexing abilities, Semicarbazones represent a very interesting group of ligands to several main group metals of d and f-block elements [67–69]. The semicarbazones of aromatic and unsaturated carbonyl compounds have anticonvulsant properties and their advantage over the analogous thiosemicarbazones is their lower neurotoxicity [70]. Vanadium (V) complexes with salisilaldehyde semicarbazones derivatives show in vitro anti-tumor activity toward kidney tumor cells [71]. Leovac et al. [72], reported the physicochemical and structural characteristics of Ni(II)

complexes with pyridoxal semicarbazones. Dimmock and Baker [73] reported the anticonvulsant activities of 4-bromo benzaldehyde semicarbazone. The photochromic study of (E)-4-phenyl-(pyridine-2-ylmethylene)semicarbazide was carried out in both solution and solid state by Lin et al. [74]. In these thesis structural studies have been carried out for the following important samicarbazide derivatives

1. (E)-1-(3-bromobenzylidene)semicarbazide
2. (E)-1-(4-bromobenzylidene)semicarbazide
3. (E)-1-(5-chloro-2-hydroxybenzylidene)semicarbazide
4. (E)-1-(5-bromo-2-hydroxybenzylidene)semicarbazide
5. (E)-1-(2-hydroxy-5-nitrobenzylidene)semicarbazide

## References


[1] N.B. Colthup, L.H. Daly, S.E. Wiberely, Introduction to Infrared and Raman spectroscopy, Academic Press, Newyork, 1964.

[2] G.F. Dyke, A.J. Floyd, M.Sainsburg, R.S. Theobald, Organic Spectroscopy: An Introduction, Longman Inc., Newyork, 1981.

[3] J.M. Chalmers, P.R. Griffiths, Handbook of Vib. Spectrosc., Vol.1, Wiley and sons, Chishester Baffins Lane, UK, 2002.

[4] J.M. Hollas, Modern spectroscopy, 2nd Ed., Wiley and Sons, Baffins Lane 1992.

[5] A.J. Barnes, W.J. Orville, Vib. Spectrosc. Modern Trends, Elsevier Scientific Publishing Company, Amsterdam, Netherlands, 1977.

[6] W.Demtroder, Laser Spectroscopy, Basic concepts and instrumentation, Springer –Verlag Berlin, Heidelberg, 1981.

[7] P.R. Bunker, Molecular symmetry and Spectroscopy, Academic Press Inc., Newyork, 1979.

[8] H.J.Jodl, J.R.Durig (Ed.), Vibrational spectra and structure. A series of advances, Vol.13, Elsevier Science Publishers BV, Amsterdam, The Netherlands, 1984.

[9] R.A .Niquist, Interpreting infrared, Raman and nuclear magnetic resonance spectra, Vol.1, Academic Press, San Diego, 2001.

[10] D.A. Long, Raman Spectroscopy, McGraw Hill, Grat Britain, 1977.

[11] B. Schrader, Infrared & Raman Spectroscopy, VCH publishers, Inc.,New York,1995.

[12] E.S. Brandt, T.M. Cotton, In: Rossiter B.W, Baetzold R.C.(ed). Physical methods of Chemistry Series, 2nd Ed., Vol. IXB, Wiley, 1993.

[13] A.G. Marshall, F.R. Verdun, Fourier Transforms in NMR, Optical and Mass spectroscopy, Elsevier, Amsterdam, 1990.

[14] P.B.Fellget, Three concepts make a million points, Infrared Phys. 24 (1984) 95-98.

[15] P.J. Jacquinot, the Luminosity of Spectrometers with Prisms, Gratings, or Fabry-Perot Etalons, J. Opt.Soc. Am. 44B (1954) 761-765.

[16] J.R.Durig, S.M. Craven and W.C. Harris, Vibrational Spectra and Structure, Ed. James R. Durig, Marcel Dekker, Inc., Newyork, 1972.

[17] D.N.Sathyanarayanan, Vibrational spectroscopy theory and applications, New Age International publishers, New Delhi, 2004.

[18] B.K. Sharma, Spectroscopy, Goel Publishing House, Meerut, Eleventh editions, 1995.

[19] H.H.Willard, L.L Merritt, J.A.Dean, F.A.Settle, Instrumental methods of Analysis, Sixth Edition, CBS publishers and Distributors, Delhi,1986.

[20] R.S. Khandpur, Handbook of Analytical Instruments, Tata McGraw-Hill Publishing Company Limited, New Delhi, 2002.

[21] K.A. Rubinson, J.F. Rubinson, Contemporary Instrumental Analysis, Prentice Hall International, New Jersey, 2000.

[22] D.A. Skoog, F.J. Holler, T.A. Nieman, Principles of Instrumental analysis, Fifth Edition, Harcourt Asia PTE Ltd., Singapore, 1998.

[23] H.Kaur, Instrumental Methods of Chemical Analysis, Second Edition, Pragathi Prakashan, India, 2003.

[24] C.N. Banwell, Fundamentals of Molecular Spectroscopy, Tata McGraw Hill, 1972.

[25] C.V.Raman, Nature 108 (1921) 367.

[26] C.V. Raman and K.S. Krishnan, Raman Spectroscopy: The Principles Nature 121(1928) 501-502.

[27] J.R.Ferraro and K. Nakamoto, Introductory Raman Spectroscopy, Academic Press Ltd.,1994.

[28] R.L. McCreery, Raman Spectroscopy for Chemical Analysis, Wiley Interscience, 2000.

[29] J.J.Laserna, Modern Techniques in Raman Spectroscopy, Wiley, 1996.

[30] G.Aruldhas, Molecular Structure and Spectroscopy, Prentice Hall of India Pvt Ltd, New Delhi, 2007

[31] B. K. Sharma, Instrumental Methods of Chemical Analysis, Goel Publishing House, Meerut, 2007.

[32] I.Notingher and L.L.Hench, Raman microspectroscopy: a non-invasive tool for studies of individual living cells in vitro, Expert Rev.Med.Devic.3 (2006)1-20.

[33] E.B.Hanlon, R. Manoharan, T.W. Koo, K.E.Shafer, J.T.Motz, M.Fitzmaurice, J.R.Kramer,I.Itzkan, R.R.Dasari and M.S.Feld, Prospects for in vivo Raman spectroscopy, Phys.Med.Biol.45 (2000) 1-59.

[34] J.B.Foresman, C.Frisch, Exploring Chemistry with Electronic structure methods, 2nd ed., Gaussian Inc., Pittsburgh, PA, 1996.

[35] Ira N.Levine, Quantum Chemistry, Englewood cliffs, New Jersey: Prentice Hall, 1991.

[36] G.Robert Parr, D.P.Craig and I.G.Ross, Molecular orbital calculations of the lower excited electronic levels of benzene, configuration interaction included, J.Chem.Phys, 18 (1950)1561-1563.

[37] I.N.Levine,Quantum Chemsitry, Boston: Allyn and Bacon, Inc.,1983.

[38] D.B.Cook, Handbook of Computational Quantum Chemistry, Oxford University Press, 1998.

[39] R.G.Parr, W.Wang, Density functional theory of atoms and molecules, Oxford University Press, Newyork, 1989.

[40] F.Jenson, Introduction to Computational Chemistry, Wiley and Sons, Baffins Lane, United Kingdom, 1999.

[41] T.Zieglar, Approximate density functional theory as a practical tool in molecular energetics and dynamics, Chem.Rev.91 (1991) 651-667.

[42] P.Hohenberg, W. Kohn, Inhomegenous electron gas, Phys. Rev. 136B (1964)8 64-871.

[43] W.Kohn L.J. Sham, Self consistent equations including exchange and correlation effects, Phys. Rev. 140A (1965)1133- 1138.

[44] Y. Morino, K. Kuchitsu, A note on the classification of normal vibrations of molecules, J. Chem. Phys. 20 (1952) 1809–1810.

[45] W.J. Taylor, Distribution of kinetic and potential energy in vibrating molecules, J. Chem. Phys. 22 (1954) 1780–1781.

[46] T. Miyazawa, T. Shimanouchi, S. Mizushima, Normal vibrations of n-methylacetamide, J. Chem. Phys. 29 (1958) 611–616.

[47] G. Zerbi, J. Overend, B. Crawford, Urey-Bradley force constants of methanol, J. Chem. Phys. 38 (1963) 122–127.

[48] G. Keresztury, G. Jalsovszky, Alternative calculation of vibrational potential energy distribution, J. Mol. Struct. 10 (1971) 304.

[49] P. Pulay, G. Fogarasi, F. Pang, J.E. Boggs, Systematic ab initio gradient calculation of molecular geometries, force constants, and dipole moment derivatives, J. Am. Chem. Soc. 101 (1979) 2550–2560.

[50] L. Lapinski, P. Pongor, PED-program, Warsaw, 1994.

[51] L. Lapinski, M.J. Nowak, BALGA –-Computer Program for PED Calculation, Institute of Physics Polish Academy of Sciences, Warsaw.

[52] J.Cz. Dobrowolski, M.H. Jamroz, J.K. Kazimirski, K. Bajdor, M.A. Borowiak, R. Larsson, Theoretical vibrational spectra of diformates: diformate anion, J. Mol. Struct. 482-483 (1999) 183–187.

[53] K.Fukui, Theory of Orientation and Stereoselection, Springer-Verlag, New York, 1975.

[54] D.F.V. Lewis, C. Ioannides, D.V. Parke, Interaction of a series of nitriles with the alcohol-inducible isoform of P450: Computer analysis of structure—activity relationships, Xenobiotica 24 (1994) 401-408.

[55] S. Chidangil, M.K. Shukla, P.C. Mishra, A molecular electrostatic potential mapping study of some fluoroquinolone anti-bacterial agents, J. Mol. Model 4 (1998) 250-258.

[56] F.J. Luque, J.M. Lopez, M. Orozco, Perspective on "Electrostatic interactions of a solute with a continuum. A direct utilization of ab initio molecular potentials for the prevision of solvent effects, Theor. Chem. Acc. 103 (2000) 343.

[57] J.S. Murray, K. Sen, Molecular Electrostatic Potentials Concepts and Applications, Elsevier, Amsterdam, 1996.

[58] E. Scrocco, J. Tomasi, Electronic molecular structure, reactivity and intermolecular forces: an euristic interpretation by means of electrostatic molecular potentials, Adv. Quantum Chem. 11 (1978) 115-193.

[59] U. Kragh-Hansen, Molecular aspects of ligand binding to serum albumin, Pharmacol. Rev., 33 (1981) 17-46.

[60] G.M. Morris, R. Huey, W. Lindstrom, M.F. Sanner, R.K. Belew, D.S. Goodsell, A.J.Olson, AutoDock4 and AutoDockTools4: Automated docking with selective receptor flexibility, J. Comput. Chem. 16 (2009) 2785-2791.

[61] M.W.Chang, C.Ayeni, S. Breuer, Virtual Screening for HIV Protease Inhibitors: A Comparison of AutoDock 4 and Vina, PLoS One. 5 (2010) 1-9.

[62] J.S. Casas, M.S.G. Tasende, Main group metal complexes of semicarbazones and thiosemicarbazones. A structural review, Coord. Chem. Rev. 209 (2000) 197–261.

[63] J.P. Scovill, D.L. Klaymam, C. Lambros, G.E. Childs, J.D. Notsch, 2-Acetylpyridine thiosemicarbazones. 9. Derivatives of 2-acetylpyridine 1-oxide as potential antimalarial agents, J. Med. Chem. 27 (1984) 87–91.

[64] M.T. Cocco, C. Congiu, V. Onnis, M.L. Pellerano, A. De Logu, Synthesis and antimycobacterial activity of new S-alkylisothiosemicarbazone derivatives, Med. Chem. 10 (2002) 501–506.

[65] M.C.R. Arguelles, E.C.L. Silva, J. Sanmartin, P. Pelagatti, F. Zani, Copper complexes of imidazole-2-, pyrrole-2- and indol-3-carbaldehyde thiosemicarbazones: Inhibitory activity against fungi and bacteria, J. Inorg. Biochem. 99 (2005) 2231–2239.

[66] W. Hu, W. Zhou, C. Xia, X. Wen, Synthesis and anticancer activity of thiosemicarbazones, Bioorg. Med. Chem. Lett. 16 (2006) 2213–2218.

[67] S.P. Mital, R.V. Singh, J.P. Tandon, Synthesis and Studies of Semicarbazonato Lantianum (III) and Samarium (III) Coordination Complexes, Synth. React. Inorg. Met. Org. Chem. 12 (1982) 269–286.

[68] S.B. Padhye, G.B. Kaufman, Transition metal complexes of semicarbazones and thiosemicarbazones, Coord. Chem. Rev. 63 (1985) 127–160.

[69] N.C. Kasuga, K. Sekino, C. Koumo, N. Shimada, M. Ishikawa, K. Nomiya, Synthesis, structural characterization and antimicrobial activities of 4-and 6-coordinate nickel (II) complexes with three thiosemicarbazones and semicarbazone, J. Inorg. Biochem. 84 (2001) 55–65.

[70] J.R. Dimmock, S.C. Vashishta, J.P. Stables, Anticonvulsant properties of various acetylhydrazones, oxamoylhydrazones and semicarbazones derived from aromatic and unsaturated carbonyl compounds, Eur. J. Med. Chem. 35 (2000) 241–249.

[71] P. Noblia, E.J. Baran, L. Otero, P. Darper, H. Cerecetto, M. Gonzalez, O.E. Piro, E.E. Castellano, T. Inohora, Y. Adachi, H. Sakurai, New Vanadium(V) Complexes with Salicylaldehyde Semicarbazone Derivatives: Synthesis, Characterization, and in vitro Insulin-Mimetic Activity − Crystal Structure of [VvO2(salicylaldehyde semicarbazone)], Eur. J. Inorg. Chem. 2 (2004) 322– 328.

[72] V.M. Leovac, L.S. Jovanoic, V. Divjakovic, A. Pevec, I. Leban, T. Armbruster, Transition metal complexes with thiosemicarbazide-based ligands. Part LIV. Nickel(II) complexes with pyridoxal semi-(PLSC) and thiosemicarbazone (PLTSC). Crystal and molecular structure of [Ni(PLSC)(H2O)3](NO3)2 and [Ni(PLTSC-H)py]NO3, Polyhedron 26 (2007) 49–58.

[73] L. Lin, W. Fan, S. Chen, J. Ma, W. Hu, Y. Lin, H. Zhang, R. Huang, Photochromism of (E)-4-phenyl-1-(pyridine-2-ylmethylene) semicarbazide, New J. Chem. 36 (2012) 2562–2567.

[74] N. Ramesh Babu, S. Subashchandrabose, M.S.A. Padusha, H. Saleem, V. Manivannan, Y. Erdogdu, Synthesis and structural characterization of (E)-N′-((Pyridin-2-yl) methylene) benzohydrazide by X-ray diffraction, FT-IR, FT-Raman and DFT methods, J. Mol. Struct. 1072 (2014) 84–93.

# CHAPTER – II

## Synthesis, Spectroscopic (FT-IR, FT-Raman, NMR, UV-Visible), Fukui Function, Antimicrobial and Molecular Docking Study of (E)-1-(3-Bromobenzylidene) Semicarbazide by Dft Method

### 2.1. Introduction

Semicarbazones and its derivatives have been a large number of applications in the field of synthetic chemistry widely used such as starting materials in a vast amount of medicinal chemistry, organometallics, polymers [1-3] and herbicides and many other industrial processes. Particularly, Semicarbazones and its derivatives of (E)-1-(3-bromobenzylidene)semicarbazide (3BSC) have exhibit interesting biological activities, such as antifungal, antibacterial, antimalarial, anti-cancer, anticonvulsant, antiproliferative, anti-inflammatory, antitumor and antiviral activity [4-6].



V.M. Kolb et al. [7] reported Abnormally High IR Frequencies for the Carbonyl Group of Semicarbazones of the Benzaldehyde and Acetophenone Series. J.R. Dimmock et al. [8] reported some aryl semicarbazones possessing anticonvulsant activities. A. Dhandapani et al. [9] reported synthesis, structural, spectroscopic studies, NLO, NBO and HOMO-LUMO of (E)-1-(3-methyl-2,6-diphenyl piperidin-4-ylidene) semicarbazide with experimental and theoretical approaches. S. Subashchandrabose et al. [10] reported Vibrational studies on (E)-1-((pyridine-2-yl) methylene) semicarbazide using experimental and theoretical method.

Structural and bonding features reveal that this 3BSC molecule has several reactive groups which participate in both intra and intermolecular

hydrogen bonding instigating interactions with biological targets. Literature survey reveals that so far there is no experimental and theoretical study of the title compound. In the previous literature motivate us to make this computed and observed vibrational spectroscopic investigate based on the molecule to give a detailed assignment of the fundamental bands in FT-IR and FT-Raman spectra on the basis of calculated PED.

In this present study, we report the synthesis and detailed spectroscopic investigation of (E)-1-(3-bromobenzylidene) semicarbazide (3BSC) using B3LYP/6-311++G(d,p) level of the theory. The FT-IR and FT-Raman spectral analysis of 3BSC are performed using density functional theory. The redistribution of electron density(ED) in various bonding, antibonding orbitals and E(2) energies are calculated by the natural bond orbital(NBO) investigation to give limpid proof of stabilization originating from the hyperconjugation of diverse intra-molecular interactions. The local reactivity descriptors like the local softness and electrophilicity indices are obtained with the help of Fukui function calculation. Several properties like molecular geometry, Nonlinear Optical (NLO) property, Highest Occupied Molecular Orbital (HOMO) and Lowest Unoccupied Molecular Orbital (LUMO) energies, Nuclear Magnetic Resonance (NMR), UV-Visible, Molecular Electrostatic Potential (MEP) analysis of the 3BSC are carry out to clear the information about charge transfer within the molecule. Antimicrobial activity together with Molecular docking of 3BSC was also analyzed.



## 2.2. Synthesis

For the preparation of (E)-1-(3-bromobenzylidene)semicarbazide compound, the aqueous solution of semicarbazide hydrochloride (1.1 g,

0.01 mol), taken in a round bottom flask, 3- bromobenzaldehyde (1.8 mL, 0.01 mol) in 1:1 molar ratio. The reaction mixture was kept over a magnetic stirrer and stirred well at a room temperature for 1 h. The colourless solid was formed, filtered and washed with petroleum ether (40-60%). The crude solid obtained was dried and recrystallized using absolute alcohol. The recrystallized product was dried in a vacuum desiccator over fused Calcium Chloride. The purity of the ligand was checked by thin layer chromatography (TLC). The scheme of the synthesis is shown in Fig. 2.1.

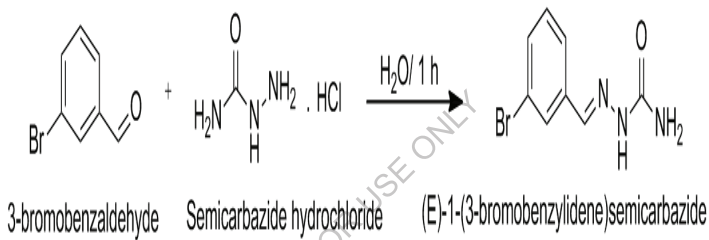




**Fig. 2.1. The scheme of the synthesis of 3BSC**

## 2.3. Experimental details

The FT-IR spectrum of the synthesis compound 3BSC was recorded in the region 4000-450 $cm^{-1}$ in evacuation mode using a KBr pellet technique with 1.0 $cm^{-1}$ resolution on a PERKIN ELMER FT-IR spectrophotometer. The FT-Raman spectrum of the title molecule was recorded in the region 4000-100 $cm^{-1}$ in a pure mode using Nd: YAG Laser of 100 mW with 2 $cm^{-1}$ resolution on a BRUCKER RFS 27 at SAIF, IIT, Chennai, India. Carbon($^{13}C$) NMR and Proton ($^{1}H$) NMR spectra were recorded in DMSO-$d_6$ using TMS as an internal standard on a Bruker high-resolution NMR spectrometer at 400 MHz at CAS in Crystallography & Biophysics, University of Madras, Chennai, India. The ultraviolet

absorption spectrum of the sample is examined in the range 200-600 nm using UV-1700 series recording spectrometer.

### 2.4. Computational methods

Quantum chemical density functional computations were carried out at the Becke3-Lee-Yang-parr (B3LYP) level with 6-311++G(d,p) basis set using Gaussian 09W program package [11] to get a clear knowledge of optimized parameters. The optimized molecular structure (Fig. 2) is used for the computation of vibrational frequencies, Raman activities and IR intensities with the Gaussian 09W software system and GaussView 5.0 [12] molecular visualization program at the same level of theory and basis set. The theoretical vibrational assignments of the 3BSC molecule using percentage potential energy distribution (PED) have been done with the VEDA program [13]. In order to understand the electronic properties, the theoretical UV-Vis spectra have been investigated by TD-DFT method with 6-311++G(d,p) basis set for the gas phase. The proton and carbon NMR chemical shift were calculated with gauge-including atomic orbital (GIAO) approach [14] by applying B3LYP/6-311++G(d,p) method of the title molecule and compared with the experimental NMR spectra. Molecular docking (ligand-protein) simulations have been performed by using autoDock 4.2.6 free software package. The calculated Raman activities ($S_i$) with Gaussian 09W program have been converted to relative Raman Intensities ($I_i$) using the following relationship obtained from the basic theory of Raman scattering [15],



$$I_i = \frac{f(\nu_0 - \nu_i)^4 s_i}{\nu_i[1-\exp(-hc\nu_i)]/kT} \quad (2.1)$$

Where is the laser exciting frequency in $cm^{-1}$, is the vibrational frequency of the ith normal mode, *h*, c and *k* are universal constants and f is a suitably chosen common scaling factor for all peak intensities.

## 2.5. Results and discussion

### 2.5.1. Molecular geometry

The bond parameters (bond length and bond angles) of the 3BSC molecules are listed in Table 1 using DFT/B3LYP method with 6-311++G(d,p) basis set. The optimized molecular structure of title compound is obtained from Gaussian 09W and GaussView 5.0 programs are shown in Fig.2. To the best of our knowledge, exact experimental data on the geometrical parameters of 3BSC are not available in the literature. Therefore, the crystal data of a closely related molecule such as (E)-2-(4-Methylbenzylidene) hydrazinecarboxamide [16] is compared with that of the title compound. From the calculated values, it is found that most of the optimized molecular bond lengths are slightly higher than the experimental values due to the fact that the theoretical calculations were carried out isolated molecule in the gas phase and the experimental XRD results were carried out in the solid state.



The homonuclear bond lengths (C6-C7, C7-C12, C7-C8, C10-C11, C9-C10, C11-C12 and N1-N2) are higher and heteronuclear bond lengths (C6-H17, C8-H18, C11-H20, C10-H19, C12-H21 and N6-H14) are lower. The important reason for the like charges (electron-electron, nucleus-nucleus) is repulsive and the forces of unlike charges (electrons and nucleus) are attractive.

**Table 2.1**

**Geometrical parameters optimized in (E)-1-(3-bromobenzylidene)**

| Parameters | Experimental[a] | B3LYP/ 6-311++G(d,p) | Parameters | Experimental[a] | B3LYP/ 6-311++G(d,p) |
|---|---|---|---|---|---|
| **Bond length(Å)** | | | **Bond angle(°)** | | |
| N1-N2 | 1.376 | 1.349 | N1-C3-N5 | 117.37 | 114.8 |
| N1-C3 | 1.363 | 1.397 | N2-C6-C7 | 122.12 | 122.4 |
| N1-H14 | 0.97 | 1.016 | N2-C6-H17 | 118.9 | 120.8 |
| N2-C6 | 1.275 | 1.282 | O4-C3-N5 | 123.5 | 125.3 |
| C3-O4 | - | 1.219 | C3-N5-H15 | - | 121.0 |
| C3-N5 | - | 1.359 | C3-N5-H16 | - | 117.7 |
| N5-H15 | - | 1.006 | H15-N5-H16 | - | 121.3 |
| N5-H16 | - | 1.005 | C7-C6-H17 | 118.9 | 116.7 |
| C6-C7 | 1.461 | 1.464 | C6-C7-C8 | 118.08 | 118.4 |
| C6-H17 | 0.960 | 1.095 | C6-C7-C12 | 122.3 | 122.6 |
| C7-C8 | 1.388 | 1.403 | C8-C7-H12 | 119.5 | 119.1 |
| C7-C12 | 1.388 | 1.404 | C7-C8-C9 | 119.61 | 119.8 |
| C8-C9 | 1.386 | 1.390 | C7-C8-H18 | 119.5 | 120.2 |
| C8-H18 | 0.960 | 1.083 | C7-C12-C11 | 120.9 | 120.2 |
| C9-C10 | 1.388 | 1.390 | C7-C12-H21 | 119.5 | 119.3 |
| C9-Br13 | - | 1.918 | C9-C8-H18 | 119.5 | 120.0 |
| C10-C11 | 1.388 | 1.397 | C8-C9-H10 | 119.9 | 121.4 |
| C10-H19 | 0.960 | 1.082 | C8-C9-Br13 | - | 119.1 |
| C11-C12 | 1.386 | 1.387 | C10-C9-Br13 | - | 119.4 |
| C11-H20 | 0.960 | 1.084 | C9-C10-C11 | 118.8 | 118.6 |
| C12-H21 | 0.960 | 1.082 | C9-C10-H19 | 119.5 | 120.6 |
| **Bond angle(°)** | | | C11-C10-H19 | 199.9 | 120.8 |
| N2-N1-C3 | 119.98 | 122.7 | C10-C11-C12 | 120.9 | 120.9 |
| N2-N1-H14 | - | 121.9 | C10-C11-H20 | 119.5 | 119.2 |
| N1-N2-C6 | 115.78 | 118.5 | C12-C11-H20 | 119.9 | 119.9 |
| C3-N1-H14 | - | 115.4 | C11-C12-H21 | 119.9 | 120.5 |
| N1-C3-O4 | 119.12 | 119.9 | | | |

[a] Taken from Ref [16].

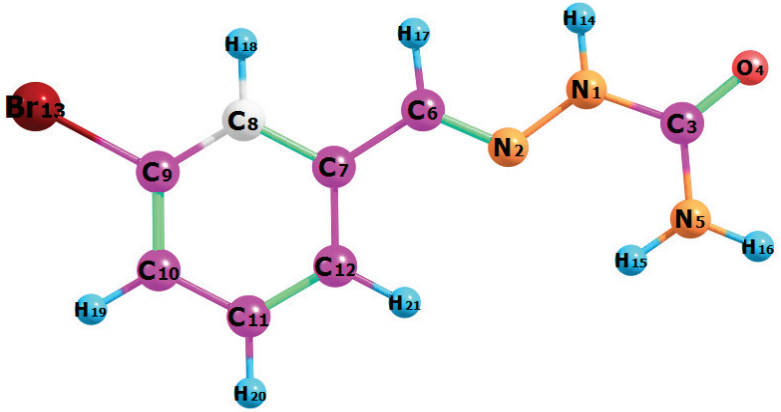


**Fig. 2.2.** Optimized geometric structure with atoms numbering of 3BSC

### 2.5.2. Vibrational analysis

The maximum number of potentially active observable fundamentals of the non-linear molecule, which contains N atoms, is equal to (3N-6) apart from the translational and three rotational degrees of freedom. The 3BSC molecule consists of 21 atoms, which has 57 normal modes of vibration. The comparative theoretical and experimental FT-IR and FT-Raman spectra are shown in Fig. 2.3 and 2.4. The calculated vibrational frequencies (Unscaled and Scaled), IR intensity, Raman activity are tabulated in Table 2.2.



#### *2.5.2.1. C-H vibrations*

In the aromatic compounds, the C-H stretching wavenumbers appear in the range 3000-3100 $cm^{-1}$ which are the characteristic region for the ready identification of C-H stretching vibrations [17]. The C-H stretching and bending regions are of the most difficult regions to interpret in infrared spectra. The nature and position of the substituent cannot affect these vibrations. Most of the aromatic compounds have almost four infrared

peaks in the region 3080-3010 $cm^{-1}$ due to ring C-H stretching bands [18]. In this present study, the C-H stretching vibrations are observed at 3082, 3078, 3062, 3052 and 2926 $cm^{-1}$[mode nos 54-50] by B3LYP/6-311++G(d,P) method show excellent agreements with experimental vibrations. The bands observed in the recorded FT-IR spectrum 3063(m), 3015(m), 2926(m) $cm^{-1}$ and with the FT-Raman spectrum bands at 3063(s), 3013(w), 2941(w) $cm^{-1}$. The PED corresponding to this pure mode of title molecule contributed 99, 100, 99, 87 and 100% is shown in Table 2.2.

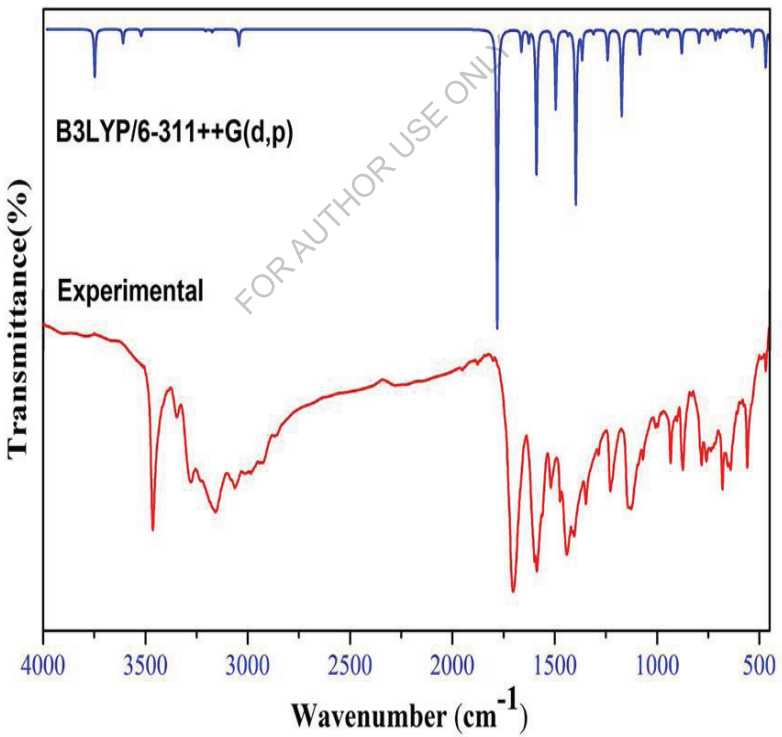



**Fig. 2.3.** FT- IR spectra of 3BSC (Experimental, B3LYP/6-311++G(d,p))

**Table 2.2**

Observed and calculated vibrational frequency of 3BSC at B3LYP method with 6-311++G(d,P) basis set.

| Experimental wave number ($cm^{-1}$) | | Theoretical wave number($cm^{-1}$) | | Assignments (PED)[a] |
|---|---|---|---|---|
| **FTIR** | **FT-Raman** | **Unscaled** | **Scaled** | |
| - | 3616(vw) | 3749 | 3603 | $\gamma_{as}$ $NH_2$(60) |
| 3463(s) | 3470(vw) | 3611 | 3470 | $\gamma_a$ $NH_2$(100) |
| 3347(w) | 3395(vw) | 3522 | 3385 | γ NH(100) |
| - | 3110(vw) | 3207 | 3082 | γ CH(99) |
| - | - | 3203 | 3078 | γ CH(100) |
| 3063(m) | 3063(s) | 3187 | 3062 | γ CH(99) |
| 3015(m) | 3013(w) | 3175 | 3052 | γ CH(87) |
| 2926(m) | 2941(w) | 3045 | 2926 | γ CH(100) |
| 1703(vs) | 1724(w) | 1782 | 1713 | γ OC(69)+γ NC(30) |
| 1598(vs) | 1609(vs) | 1664 | 1600 | γ NC(67) |
| 1587(vs) | 1560(m) | 1628 | 1565 | γ CC(32) |
| 1561(s) | - | 1595 | 1533 | γ CC(42) |
| 1519(s) | 1524(m) | 1591 | 1529 | β HNH(75) |
| 1473(s) | 1475(s) | 1515 | 1456 | γ CC(10)+β HNN(18)+β HCC(19) |
| 1440(s) | 1417(w) | 1496 | 1438 | β HCC(32)+β HNN(32) |
| 1414(s) | - | 1437 | 1381 | γ CC(29)+β HCC(27) |
| 1404(s) | 1354(w) | 1398 | 1344 | β HNN(17)+γ NC(36)+β OCN(15)+β HNH(12) |
| 1348(s) | 1301(w) | 1368 | 1314 | β HCN(54) |
| 1286(m) | 1286(s) | 1338 | 1286 | γ CC(27)+β HCC(54) |
| - | - | 1313 | 1261 | β HCC(16)+γ CC(33) |
| 1228(s) | - | 1243 | 1195 | β HCC(19)+β HCN(11)+γ CC(26) |
| - | 1144(s) | 1190 | 1144 | β HCC(54)+γ CC(11) |
| 1126(s) | 1106(vw) | 1174 | 1128 | γ NN(55) |
| 1068(m) | 1070(vw) | 1117 | 1073 | γ CC(12)+β HCC(36) |
| - | 1039(vw) | 1087 | 1044 | γ CC(22) |
| 1007(w) | 1012(w) | 1084 | 1042 | β HNC(54) |

| | | | | |
|---|---|---|---|---|
| 995(w) | 994(s) | 1010 | 970 | β CCC(69)+γ CC(10) |
| - | 962(vw) | 994 | 955 | γ NC(61)+β NNC(11) |
| 933(s) | 947(vw) | 992 | 953 | τ HCCC(61)+τ CCCC(22) |
| 902(w) | 900(w) | 950 | 913 | τ HCNN(75) |
| 873(m) | 880(w) | 918 | 882 | τ HCCC(87) |
| - | - | 884 | 850 | τ HCCC(70)+τ CCCC(10)+τ HCNN(11) |
| 830(vw) | - | 881 | 846 | γ CC(14)+β CCC(30) |
| 758(m) | 783(w) | 796 | 765 | τ HCCC(81) |
| 737(m) | 711(w) | 753 | 724 | Out ONNC(87) |
| 680(s) | - | 716 | 688 | β CCC(24)+γ BrC(45)+β NCC(17) |
| 653(m) | 653(w) | 694 | 667 | τ CCCC(64)+τ HCCC(13) |
| 640(m) | 628(w) | 662 | 636 | γ CC(13)+β CCC(44)+β NCC(11)+β NCC(11) |
| 607(w) | - | 613 | 589 | γ NC(42)+β NCN(14)+β CNN(21)+β HNC(10) |
| 559(m) | 552(w) | 575 | 552 | τ HNCN(73)+τ HNNC(12)+ |
| - | - | 563 | 541 | Out BrCC(22)+out CCCC(31) |
| 494(vw) | 522(vw) | 536 | 515 | β OCN(61)+β OCN(10) |
| 468(vw) | 489(vw) | 471 | 453 | τ HNNC(78)+τ HNCN(10) |
| - | 438(vw) | 450 | 433 | β NCN(53)+β CCC(24) |
| - | - | 441 | 424 | τ CCCC(34)+τ HCCC(24)+out BrCC(19) |
| - | 335(w) | 336 | 323 | β NNC(11)+γ BrC(34)+β CCC(12) |
| - | 299(m) | 316 | 304 | τ CCCC(10)+τ NCNN(11)+τ NNCC(41)+τ CCCC(27) |
| - | - | 291 | 280 | γ BrC(20)+β BrCC(43) |
| - | 267(w) | 263 | 253 | τ CCCC(17)+τ NCCC(20)+τ CNNC(23)+τ NCNN(17)+out CCCC(10) |
| - | 230(vw) | 243 | 234 | β NCC(23)+β CCC(12)+β NCN(11)+β CNN(10)+γ CC(11)+ |
| - | 177(m) | 172 | 165 | out BrCC+τ CCCC(45) |

| | | | | |
|---|---|---|---|---|
| - | 158(m) | 147 | 141 | β CNN(20)+β CCC(11)+β BrCC(32) |
| - | 104(s) | 111 | 106 | out CCCC(16)+τ CNNC(37)+τ NNCC(12)+τ CCCC(16) |
| - | - | 62 | 60 | τ NCNN(39)+τ NNCC(25)+out CCCC(12)+ |
| - | - | 61 | 59 | β NCC(28)+β CNN(10)+β NNC(22)+β CCC(25) |
| - | - | 23 | 22 | τ CNNC(30)+τ NCCC(62) |
| - | - | 16 | 15 | τ HCCC(43)+τ HNCN(31)+τ NCNN(16) |

[a]γ-stretching,$\gamma_a$-Symmetrical stretching,$\gamma_{as}$-asymmetrical stretching, β-inplane bending ,ω- outplane bending, τ-torsion, vs-very strong, s- strong, m-medium, w-weak, vw-very weak.

[b]scaling factor : 0.961 for B3LYP/6-311+G(d,p)

[c]Relative absorption intensities normalized with highest peak absorption equal to 100.

[d]Relative Raman intensities normalized to 100.



***2.5.2.2. $NH_2$ vibrations***

The $NH_2$ group has two (N-H) stretching vibrations, first one asymmetric and another one symmetric. The asymmetric stretching for the $NH_2$, $CH_2$ and $CH_3$ has a magnitude higher than the symmetric stretching [19].The aromatic structure shows the presence of C-H and N-H stretching vibrations above 3000 $cm^{-1}$ which is the characteristic region for ready identification of this structure [20, 21]. The title compound has only one $NH_2$ group and hence one symmetric and one asymmetric N-H stretching vibrations in $NH_2$ group are expected. The symmetric $NH_2$ stretching vibrations appear from 3420 to 3500 $cm^{-1}$ [22]. The theoretical wavenumbers computed using the B3LYP/6-311++G(d,p) method

identified at 3603 and 3470 $cm^{-1}$ [mode no 57, 56] are assigned to $NH_2$ asymmetric and symmetric stretching vibrations contributing 60 and 100% to the PED. In this work, the FT-Raman band at 3616(vw) $cm^{-1}$ has been assigned to $NH_2$ asymmetric stretching vibrations. The $NH_2$ symmetric stretching vibrations observed in the FT-IR and FT-Raman have strong and very weak intensity bands. The experimental FT-IR and FT-Raman symmetric stretching bands found at 3463(s) $cm^{-1}$ and 3470(vw) $cm^{-1}$.

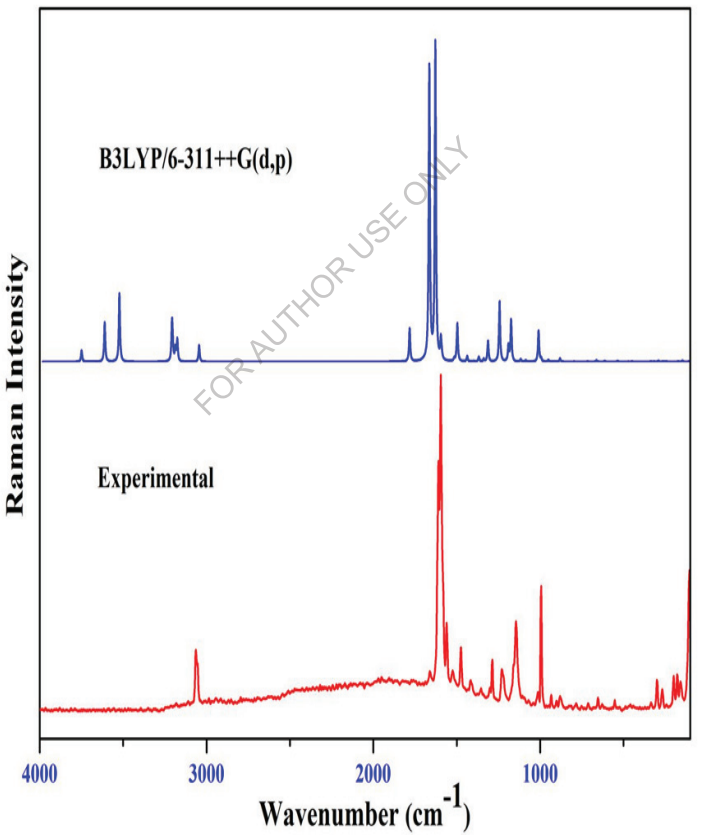



**Fig. 2.4.** FT-Raman spectra of 3BSC

### *2.5.2.3. C-C ring vibrations*

The C-C stretching vibrations are expected in the range from 1650 to 1100 $cm^{-1}$ which are not significantly influenced by the nature of the substituents [23]. The C-C stretching vibrations of the 3BSC compound were observed from1590 to 625 $cm^{-1}$. In this present study , the C-C stretching vibrations are found at 1587(vs), 1561(s), 1473(s), 1414(s), 1286(m), 1228(s), 1068(m), 995(w), 830(vw), 640(m) $cm^{-1}$ in FT-IR and 1560(m), 1475(s), 1286(s), 1144(s), 1070(vw), 1039(vw), 994(s), 628(w) $cm^{-1}$ in FT-Raman respectively. The theoretical wavenumbers at 1565, 1533, 1546, 1381, 1286, 1195, 1144, 1073, 1044, 970, 846 and 636 $cm^{-1}$ (mode no 47, 46, 44, 42, 39, 37, 36, 34, 33, 31, 25, 20) are assigned as C-C stretching vibrations.



### *2.5.2.4. C-Br Vibrations*

The most aromatic bromo compounds C-Br stretching vibrations occur in the region 650-395 $cm^{-1}$ [24]. The vibration belonging to the bond between the ring and the Bromine atom is salient as a combination of vibrations is possible owing to the presence of heavy atom [25]. The C-Br stretching vibrations for title molecule is assigned at 688, 323 $cm^{-1}$ (mode no 22, 12) in B3LYP/6-311++G(d,p) and 680(s) $cm^{-1}$ in FT-IR and 335(w) $cm^{-1}$ in FT-Raman with a PED of 45 and 34%.

### *2.5.2.5. C-N vibrations*

The C-N stretching frequency is a very tough task since it falls in a composite region of the vibrational spectrum, i.e., mixing of several bands are possible in this region [20] assigned C-N stretching absorption in the region 1386-1266 $cm^{-1}$ for the aromatic compound. The bands observed at 1703(vs), 1598(vs), 1404(s), 607(w) $cm^{-1}$ in FT-IR and 1724(w), 1609(vs), 1354(w), 962(vw) $cm^{-1}$ in FT-Raman are assigned as N-C stretching

vibrations. The theoretically scaled wavenumbers calculated at 1713, 1600, 1344, 955 and 589 $cm^{-1}$ (mode no 49, 48, 41, 30, 19) are assigned as C-N stretching vibrations with PED contribution of 30, 67, 36, 61 and 42% respectively.

**2.6. NMR spectral analysis**

The experimental and theoretical values for carbon ($^{13}C$) and proton ($^{1}H$) NMR of the title compound are given in Table 2.3. The experimental $^{13}C$ and $^{1}H$ NMR spectra were recorded in a DMSO-$d_6$ solvent are shown in Figs. 2.5, 2.6 and the theoretical NMR spectra were calculated in the gas phase are shown in Figs. 2.7, 2.8. The theoretical $^{13}C$ and $^{1}H$ chemical shifts are calculated for the optimized geometry to obtain from B3LYP/6-311++G(d,p) using GIAO method [26]. The result in Table 2.3 shows that the range carbon ($^{13}C$) NMR chemical shifts of the typical organic molecule usually > 100 [27-29]. In most cases, highly shielded electrons appear at downfield and vice versa. The calculated chemical shift values by the DFT theoretical method values well coincides with the experimental values. In this work, aromatic carbons are observed from 122.32 to 137.38 ppm in carbon ($^{13}C$) NMR spectrum for the 3BSC molecule. The nitrogen (N) atom's high electronegative property polarizes the electron distribution in its bond to the adjacent carbon atom and decreases the electron density at the bridge for the title molecule. Therefore, the chemical shift value seems to be moderately high for the title molecule under study at 131.57 and 156.74 ppm ($C_6$, $C_3$).

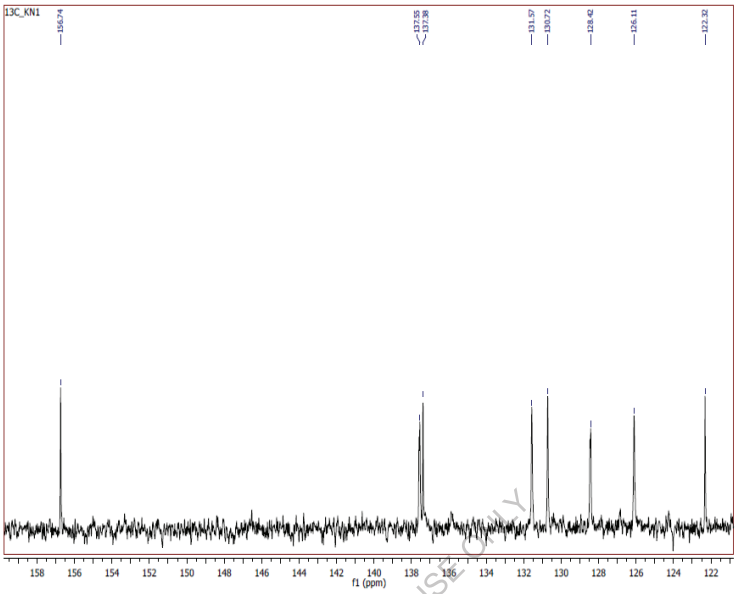


**Fig. 2.5.** $^{13}$C NMR spectrum of 3BSC (Experimental)



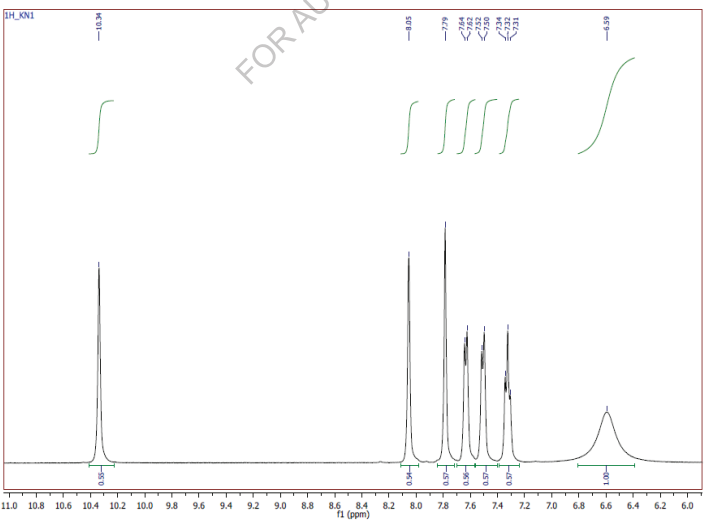


**Fig. 2.6**. $^{1}$H NMR spectrum of 3BSC (Experimental)

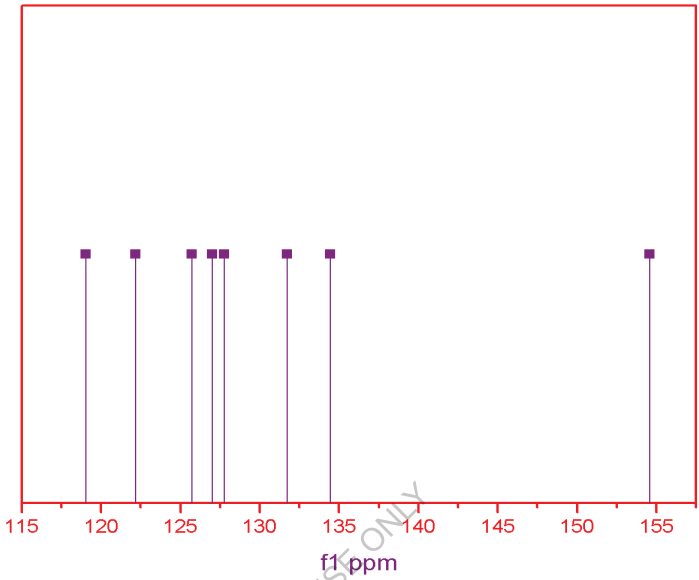


**Fig. 2.7**. $^{13}$C NMR spectrum of 3BSC (Theoretical)



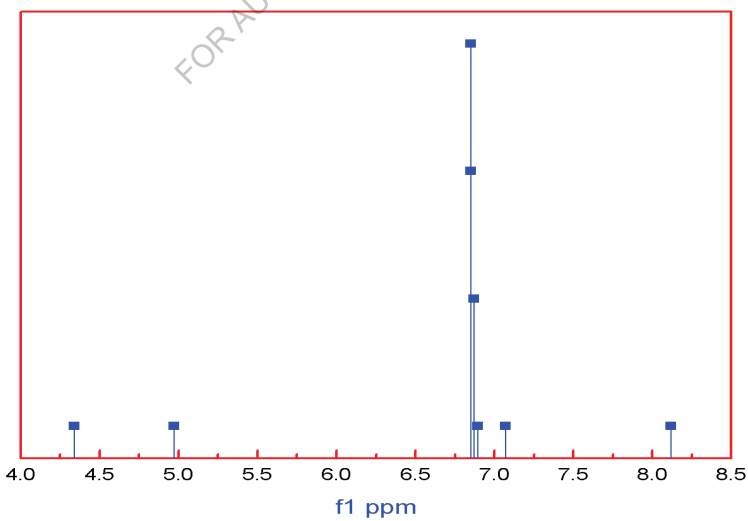


**Fig. 2.8**. $^{1}$H NMR spectrum of 3BSC (Theoretical)

**Table 2.3**

Theoretical and experimental 13C and 1H isotropic chemical shifts [with respect to TMS, all values in ppm] for 3BSC molecule

| Atom | Experimental | Calculated chemical shifts (ppm) |
|---|---|---|
| C3 | 156.74 | 154.56 |
| C6 | 131.57 | 131.73 |
| C7 | 122.32 | 122.18 |
| C8 | 128.42 | 126.99 |
| C9 | 137.38 | 134.43 |
| C10 | 130.72 | 127.76 |
| C11 | 126.11 | 125.71 |
| C12 | 122.32 | 119.02 |
| H14 | 6.59 | 6.84 |
| H15 | 3.37 | 4.97 |
| H16 | 2.5 | 4.33 |
| H17 | 7.32 | 6.86 |
| H18 | 7.31 | 6.85 |
| H19 | 7.5 | 7.06 |
| H20 | 7.34 | 6.89 |
| H21 | 8.05 | 8.11 |



The computed and recorded $^{1}H$ chemical shift values also complement with experimental finding at 3.37, 2.5ppm with computed chemical shifts at 4.9702, 4.3396 ppm for $H_{15}$ and $H_{16}$. It is evident from Table 2.3 the theoretical chemical shift evaluation slightly deviated from the experimental assessment are due to the theoretical calculations were carried out in the isolated gas phase.

## 2.7. Electronic properties

The observed and computed UV-Visible spectrum of 3BSC molecule is shown in Fig. 2.9. Absorption maximum ($\lambda_{max}$) of our title molecule is calculated by TD-DFT/B3LYP method with 6-311++G(d,p) basis set. The calculation of molecular orbital geometry shows that the visible absorption maxima of the 3BSC resemble the electronic transition from HOMO to LUMO. The experimental UV-Vis spectra of 3BSC molecule were used to DMSO solvent and theoretical calculations were carried out in the DMSO and gas phase. The $\lambda_{max}$ is a function of substitution, the more electrons pushed into the ring, the larger $\lambda_{max}$ [30]. The electronic transition amid frontier orbitals such as transformation from HOMO to LUMO as can be seen through the UV-Vis spectra absorption values 294 (Experimental), 295 (DMSO) and 290 nm (Theoretical) are listed in Table 2.4. The calculated results involving the wavelength, and oscillating strength and band gap energy are carried out compared with experimental data. The band gap energy was calculated using the formula, $E = hc/\lambda$. Here h and c are constant; $\lambda$ is the cut off wavelength. HOMO and LUMO is related to the ionization potential and electron affinity. The energy difference between HOMO and LUMO orbits is called as band gap that is important stability for structure [31]. The electronic absorption corresponds that is mainly described by one electron excitation from HOMO to LUMO for these values increase molecular becomes more stable and decreases the intermolecular charge transfer which makes the compound be NLO active. The HOMO and LUMO energies, the energy gap ($\Delta E$), the ionization potential (I), the electron affinity (A), the absolute electronegativity ($\chi$), the absolute hardness ($\eta$) and softness (S) for the 3BSC molecule have been calculated at B3LYP/6-311++G(d,P) basis set (Fig 2.10) and the result are given in the Table 2.5.

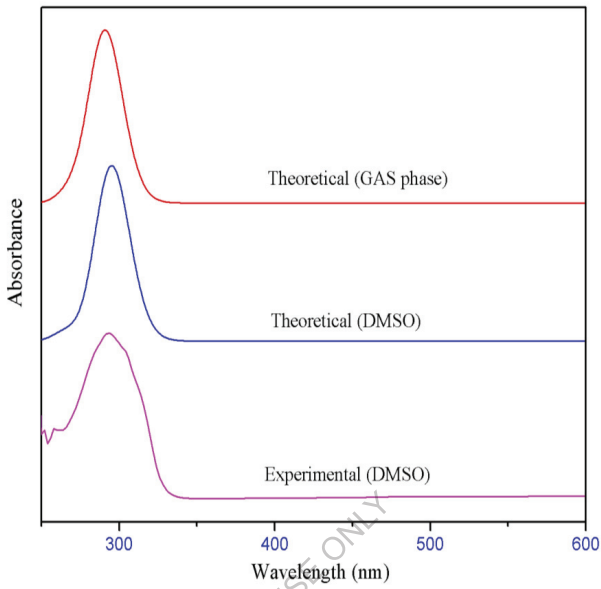


Fig. 2.9. UV–Vis spectra of 3BSC



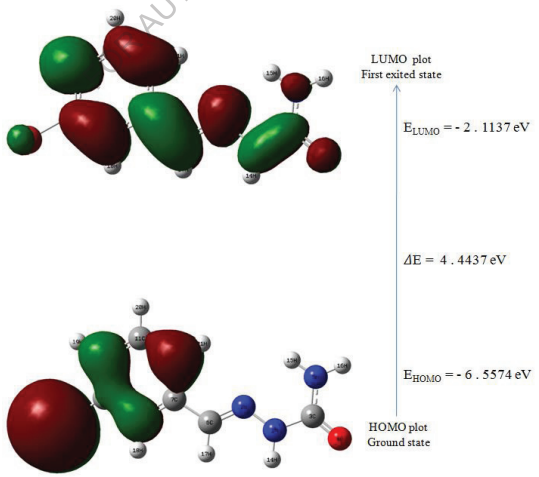


**Fig. 2.10.** Atomic orbital HOMO – LUMO composition of the frontier molecular orbital for 3BSC

**Table 2.5**

Calculated energy values of title compound by B3LYP/6-311++G(d,p).

| Basis set | B3LYP/6-311++G(d,p) |
|---|---|
| $E_{Homo}$(eV) | -6.5574 |
| $E_{Lumo}$(eV) | -2.1137 |
| Ionization potential | 6.5574 |
| Electron affinity | 2.1137 |
| Energy gap(eV) | 4.4437 |
| Electronegativity | 4.3355 |
| Chemical potential | -4.3355 |
| Chemical hardness | 2.2218 |
| Chemical softness | 0.2250 |
| Electrophilicity index | 4.2300 |



**Table 2.4** The UV–vis band gap energy E (eV) and oscillator strength (f) for 3BSC calculated by TD-DFT/B3LYP method

| **Experimental** | | **TD-DFT/B3LYP-311++G(d,p)** | | | | | | | |
|---|---|---|---|---|---|---|---|---|---|
| **$\lambda_{max}$ (nm)** | **Band gap (ev)** | **DMSO** | | | | **Gas phase** | | | |
| | | **$\lambda_{cal}$ (nm)** | **Band gap (eV)** | **Energy ($cm^{-1}$)** | ***f*** | **$\lambda_{cal}$ (nm)** | **Band gap (eV)** | **Energy ($cm^{-1}$)** | ***f*** |
| **294** | 4.228 | 295 | 4.214 | 33898 | 0.663 | 290 | 4.286 | 34373 | 0.512 |
| | | 267 | 4.655 | 37428 | 0.042 | 270 | 4.604 | 36945 | 0.049 |
| | | 238 | 5.223 | 41967 | 0.0001 | 260 | 4.781 | 38412 | 0 |

By using HOMO and LUMO energy values for a molecule, electronegativity and chemical hardness can be calculated as follow:

$$\chi = \frac{I+A}{2} \text{ (Electronegativity)} \quad (2.2)$$

$$\mu = -\frac{(I+A)}{2} \text{ (Chemical potential)} \quad (2.3)$$

$\eta = \frac{}{}$ (Chemical hardness)

(2.4)

s=1/2η (chemical softness), $\omega=\mu^2/2\eta$ (Electrophilicity index)

Where I and A are ionization potential and electron affinity; $I = -E_{HOMO}$ and $A = -E_{LUMO}$ respectively [32]. Energy gap of title molecule is calculated experimentally by UV-Visible spectrum is 4.2283 eV, Energy gap is calculated theoretically by TD-DFT (DMSO and gas) method is 4.2141, 4.2866 eV and from HOMO-LUMO diagram is 4.4437 eV. All are very well executed which are listed in Table 2.4 and 2.5.

**2.8. Other molecular properties**

**2.8.1. Local reactivity descriptors**

Local quantities such as Fukui function and local softness describe the reactivity/ selectivity of the specific site in a molecule. The Fukui function is defined as

$$f(\vec{r})=(\partial\rho/\partial N)\,\upsilon(\vec{r})=\left(\frac{}{\delta\upsilon(\vec{r})}\right)N$$



Kolandaival et al.[33] introduced the atomic descriptor to determine the local reactive sites of the molecular system. The individual atomic charges calculated by Mulliken population analysis (MPA) have been used to calculated the Fukui function. Fukui function $(f^+(\vec{r}),\ f^-(\vec{r}),\ f^0(\vec{r}))$, $(s_r^+, s_r^-, s_r^0)$ [34] for all atomic sites in 3BSC have been listed in Table 2.6. Weitao Yang and Wilfried J. Mortier [35] have given a simple procedure to calculate the atomic condensed Fukui function indices based on MPA and on three possible forward, backward, and central finite difference approximations to the derivatives [36]. Fukui functions are calculated using the following equation,

$$f^{+}(\vec{r}) = q_r(N+1) - q_r(N) \quad \text{for nucleophilic attack} \tag{2.5}$$

$$f^{-}(\vec{r}) = q_r(N) - q_r(N-1) \quad \text{for electrophilic attack} \tag{2.6}$$

$$f^{0}(\vec{r}) = (q_r(N+1) - q_r(N-1))/2 \quad \text{for radical attack} \tag{2.7}$$

In these equations, $q_r$ is the atomic charge (evaluated from Mulliken population analysis, electrostatic derived charge, etc.) at the $r^{th}$ atomic site is the neutral (N), anionic (N+1), cationic (N-1) chemical species.

**Table 2.6** Condensed fukui function $f_r$ and new descriptor $(sf)_r$ for 3BSC.

| Atoms | $f_r^+$ | $f_r^-$ | $f_r^0$ | $s_r^+ f_r^+$ | $s_r^- f_r^-$ | $s_r^0 f_r^0$ |
|---|---|---|---|---|---|---|
| N1 | 0.0270 | -0.0989 | -0.0360 | 0.0061 | -0.0223 | -0.0081 |
| N2 | -0.1322 | -0.0489 | -0.0905 | -0.0297 | -0.0110 | -0.0204 |
| C3 | -0.0022 | 0.0154 | 0.0066 | -0.0005 | 0.0035 | 0.0015 |
| O4 | -0.0852 | -0.1310 | -0.1081 | -0.0192 | -0.0295 | -0.0243 |
| N5 | -0.0197 | -0.0265 | -0.0231 | -0.0044 | -0.0060 | -0.0052 |
| C6 | -0.0518 | -0.0107 | -0.0313 | -0.0117 | -0.0024 | -0.0070 |
| C7 | 0.0126 | -0.0528 | -0.0201 | 0.0028 | -0.0119 | -0.0045 |
| C8 | 0.0217 | 0.0158 | 0.0188 | 0.0049 | 0.0035 | 0.0042 |
| C9 | -0.0790 | -0.1060 | -0.0925 | -0.0178 | -0.0239 | -0.0208 |
| C10 | -0.0913 | -0.0276 | -0.0595 | -0.0206 | -0.0062 | -0.0134 |
| C11 | -0.0127 | -0.0061 | -0.0094 | -0.0029 | -0.0014 | -0.0021 |
| C12 | -0.0752 | 0.0010 | -0.0371 | -0.0169 | 0.0002 | -0.0083 |



The local softness is related to Fukui function as follows:

$$s(\vec{r}) = \left(\frac{\rho(\vec{r})}{}\right) \upsilon(\vec{r}) = \left(\frac{\rho(\vec{r})}{}\right) \upsilon(\vec{r}) \left(\frac{N}{}\right) \upsilon(\vec{r}) = f(\vec{r})S \quad (2.8)$$

where S is the global softness given as

$$s = \left(\frac{}{}\right) = \int s(\vec{r}) d\vec{r} \quad (2.9)$$

The local softness can be represented as

for nucleophilic attack (2.10)

for electrophilic attack (2.11)

for radical attack (2.12)

Where +, -, 0 signs show nucleophilic, electrophilic and radical attack respectively.



Fukui functions and local softness for selected atomic sites in 3BSC have been listed in Table 2.6. It has been found that MPA schemes predict $O_4$ has lower $f_r^-$ value indicates the possible site for electrophilic attack. From Table 2.6 shows, MPA schemes predict the reactivity order for the electrophilic case as $O_4 > C_9 > N_1 > C_7 > N_2 > C_{10} > N_5 > C_8 > C_3 > C_{11}$. The calculated $f_r^+$ values predicts that the possible sites for nucleophilic attack is $N_1$ , $C_8$ *and* $C_7$ site and the radical attack was predicted at $C_8$ and $C_3$ site. The title compound more electrophilic attack than nucleophilic attack and radical attack. These results show 3BSC compound act as more biological activity.

### 2.8.2. Molecular electrostatic potentials (MEP)

Molecular electrostatic potential (MEP) simultaneously displays molecular shape, size, and electrostatic potential in terms of colour

grading. MEPs map and contour plot has been found to be a very helpful tool in the analysis of the correlation amid molecular structures with its physiochemical property relationship, including biomolecules and drugs [37]. It generally provides information regarding the chemical reactivity of a molecule. The electrostatic potential generated in space around a molecule by the charge distribution is useful to comprehend electrophilic or nucleophilic properties [38].

MEPs map and contour plot of the (E)-1-(3-bromobenzylidene)semicarbazide (3BSC) generated at the optimized geometry of the title molecule using GaussView 5.0 program is shown in Fig 2.11 and 2.12. The various values of the electrostatic potential are represented by various colours; red represented the regions of the most negative electrostatic potential, blue represents the regions of the most positive electrostatic potential and green presents the region of zero potential. The potential increases in the order red < orange < yellow < green < cyan < blue. It can be seen that the negative regions are mainly over the $O_4$ atoms. Negative (red colour) and positive (blue) regions of electrostatic potential are associated with electrophilic and nucleophilic reactivity. The majority of light green region MEP surface resemble a potential halfway between two extremes red and dark blue colour. The negative molecular electrostatic potential resembles to an attraction of the proton by the evaluate electron density in the molecule (shades of red), the positive electrostatic potential corresponds to the repulsion of the protons by the atomic nuclei (shades of blue). According to these calculated results, the MEP map illustrates that the negative potential sites are on oxygen and nitrogen atoms and the positive potential sites as well are

around the hydrogen atoms. These active sites found to be clear evidence of biological activity in the title compound.

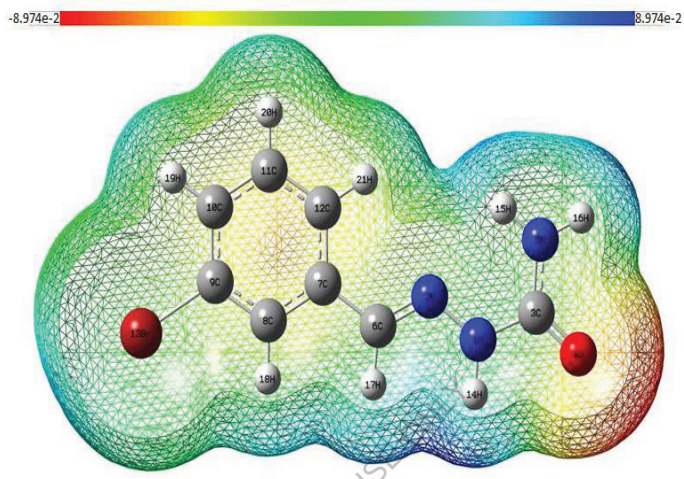


**Fig. 2.11**. Total electron density mapped with molecular electrostatic potential surface of 3BSC

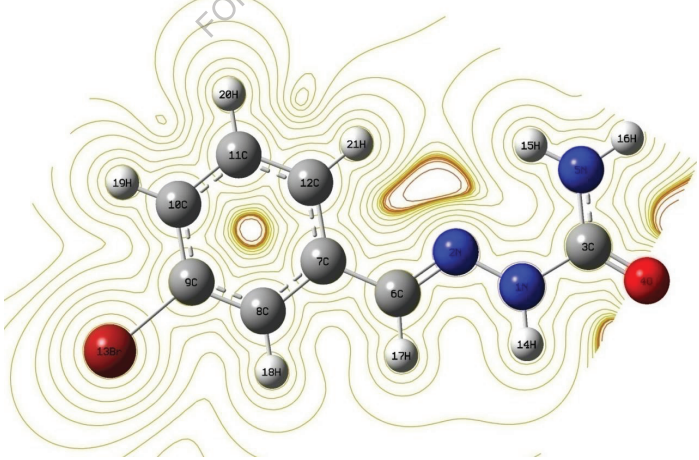


**Fig. 2.12.** The contour map of electrostatic potential of the total density of 3BSC.

### 2.8.3. NBO analysis

The NBO analyzes grant and more efficient method for studying intra and inter molecular bonding and interaction among bonds, and also provides a convenient basis for inspecting charge transfer or conjugative interactions in the molecular system. Some electron donor orbital, acceptor orbital and the overlap stabilization energy resulting from the second-order micro-disturbance theory are reported [39-41]. The higher the E(2) value, the molecular interaction between electron donors and electron acceptors is more intensive and the greater the extent of conjugation of the entire system . Delocalization of electron density amid occupied Lewis-type (bond or lone pair) NBO orbitals and properly unoccupied (antibond or Rydgberg) non-Lewis NBO orbitals resemble to a stabilizing donor-acceptor interaction. NBO analysis has been performed on the title molecule at the B3LYP/6-311++G(d,p) level in order to elucidate the intra molecular, rehybridization and delocalization of electron density within the molecule.



The second order fock matrix was carried out to evaluate the donor-acceptor interactions in the NBO analysis [42]. NBO studies provide the most precise possible 'natural Lewis structure' picture of ϕ because all orbital details are mathematically chosen to include the highest possible percentage of the electron density. For each donor (I) and acceptor (j), the stabilization energy E(2) associated with the delocalization i, j estimated as:

**Table 2.7** Second order perturbation theory analysis of Fock matrix in NBO basis for 3BSC

| Donor (i) | Type | Acceptor (i) | Type | [a]E(2) (kJ mol$^{-1}$) | [b]E(J)-E(i) (a.u.) | [c]F(I,j) (a.u.) |
|---|---|---|---|---|---|---|
| $N_2$-$C_6$ | π | $C_7$-$C_8$ | π* | 13.39 | 0.39 | 0.07 |
| $N_5$-$H_{15}$ | σ | $C_3$-$O_4$ | σ* | 4.11 | 1.31 | 0.06 |
| $N_5$-$H_{16}$ | σ | $N_1$-$C_3$ | σ* | 4.34 | 1.11 | 0.06 |
| $C_6$-$C_7$ | σ | $N_1$-$N_2$ | σ* | 4.58 | 1.13 | 0.06 |
| | | $N_2$-$C_6$ | σ* | 4.59 | 1.39 | 0.07 |
| | | $C_7$-$C_8$ | σ* | 5.82 | 1.40 | 0.08 |
| | | $C_7$-$C_{12}$ | σ* | 6.00 | 1.40 | 0.08 |
| $C_6$-$H_{17}$ | σ | $C_7$-$C_{12}$ | σ* | 5.04 | 1.20 | 0.07 |
| $C_7$-$C_8$ | π | $N_2$-$C_6$ | π* | 27.74 | 0.28 | 0.08 |
| | | $C_9$-$C_{10}$ | π* | 22.52 | 0.30 | 0.07 |
| | | $C_{11}$-$C_{12}$ | π* | 20.16 | 0.32 | 0.07 |
| $C_7$-$C_{12}$ | σ | $C_6$-$C_7$ | σ* | 6.58 | 1.37 | 0.08 |
| | | $C_7$-$C_8$ | σ* | 7.30 | 1.38 | 0.09 |
| $C_9$-$C_{10}$ | π | $C_7$-$C_8$ | π* | 21.01 | 0.33 | 0.07 |
| | | $C_{11}$-$C_{12}$ | π* | 18.96 | 0.33 | 0.07 |
| $C_{11}$-$C_{12}$ | π | $C_7$-$C_8$ | π* | 23.10 | 0.31 | 0.07 |
| | | $C_9$-$C_{10}$ | π* | 24.25 | 0.29 | 0.07 |
| $N_1$ | LP(1) | $N_2$-$C_6$ | π* | 30.96 | 0.29 | 0.08 |
| | | $C_3$-$O_4$ | π* | 52.45 | 0.30 | 0.11 |
| $N_2$ | LP(1) | $C_6$-$H_{17}$ | σ* | 10.23 | 0.76 | 0.07 |
| $O_4$ | LP(2) | $N_1$-$C_3$ | σ* | 24.35 | 0.68 | 0.11 |
| | | $C_3$-$N_5$ | σ* | 23.55 | 0.69 | 0.11 |
| $N_5$ | LP(1) | $C_3$-$O_4$ | π* | 54.86 | 0.28 | 0.11 |
| $Br_{13}$ | LP(3) | $C_9$-$C_{10}$ | π* | 10.36 | 0.32 | 0.05 |
| $N_2$-$C_6$ | π* | $C_7$-$C_8$ | π* | 75.26 | 0.04 | 0.08 |
| $C_9$-$C_{10}$ | π* | $C_7$-$C_8$ | π* | 249.40 | 0.02 | 0.09 |
| | | $C_{11}$-$C_{12}$ | π* | 194.85 | 0.02 | 0.09 |

$$E_2 = \Delta E_{ij} = q_i \frac{F(i,j)^2}{E_i - E_j} \quad (2.13)$$

Where $q_i$ is the donor orbital occupancy, $E_i$ and Ej are diagonal elements and F(i,j) is the off diagonal NBO Fock matrix elements.

The strong intramolecular hyper conjugative interaction of the $\sigma$ and $\pi$ electrons of C-C to the anti C - C bond of the ring leads to stabilization of some part of the ring as evident from Table 2.7. The strong intramolecular hyperconjugative interaction of σ ($C_7 - C_8$) distributes to σ * ($C_6 - C_7$, $C_7 - C_{12}$, $C_8 - C_9$ and $C_9 - B_{13}$) of the ring. On the other hand, side the π($C_7 - C_8$) in the ring conjugate to the anti-bonding orbital of π*($N_2 - C_6$), π*($C_9 - C_{10}$) and π*($C_{11} - C_{12}$) which leads to strong delocalization of 22.74, 22.52 and 20.16 kJ/mol respectively. The σ system shows some contribution to the delocalization corresponds to the donor - acceptor interactions are ($N_1 - N_2$) → ($C_6 - C_7$), ($N_1 - C_3$) → ($N_2 - C_6$), ($N_1 - H_{14}$) → ($C_3 - C_5$), ($N_2 - C_6$) → ($C_6 - C_7$), ($C_7 - C_{12}$) → ($C_6 - C_7$), ($C_{10} - C_{11}$) → ($C_9 - C_{10}$) bondings are shown in the Table 2.7. LP (1) $N_1$ antibonding acceptor π*($N_2 - C_6$), π*($C_3 - O_4$) of the 3BSC energy of 30.96 and 52.45 kJ/mol. The most important interaction energy, related to the resonance in the molecule is electrons donating from antibonding donor π*($C_9 - C_{10}$) to the antibonding acceptor π*($C_7 - C_8$), π*($C_{11} - C_{12}$) with large stabilization energy of 249.40, 194.85 kJ/mol as shown in Table 2.7.



### 2.8.5. NLO property

Non-linear optical (NLO) is the forefront of present research because of its significance in grants the key functions of frequency shifting, optical modulation, optical switching, optical logic, and optical

memory for the emerging technologies in areas such as telecommunications, signal processing, and optical interconnections [43]. Hyperpolarizability are very sensitive to the basis sets and level of theoretical approach employed [44-46], that the electron correlation can change the value of hyperpolarizability. The NLO activities of the 3BSC compound were calculated by Density Functional Theory (DFT) using B3LYP method with 6-311++G(d,p) basis set using Gaussian 09W program package.

**Table 2.8**

The values of calculated dipole moment μ (D), polarizability ($\alpha_0$), first order hyperpolarizability (βtot) components of 3BSC.



| **Parameters** | **B3LYP/6-311++G(d,p)** | **Parameters** | **B3LYP/6-311++G(d,p)** |
|---|---|---|---|
| $\mu_x$ | -0.89 | $\beta_{xxx}$ | -1019.90 |
| $\mu_y$ | 0.71 | $\beta_{xxy}$ | 434.20 |
| $\mu_z$ | 0 | $\beta_{xyy}$ | -47.78 |
| μ(D) | 1.14 | $\beta_{yyy}$ | -107.22 |
| $\alpha_{xx}$ | 252.54 | $\beta_{zxx}$ | 24.50 |
| $\alpha_{xy}$ | 1.53 | $\beta_{xyz}$ | 9.66 |
| $\alpha_{yy}$ | 136.79 | $\beta_{zyy}$ | -5.76 |
| $\alpha_{xz}$ | 0 | $\beta_{xzz}$ | -86.80 |
| $\alpha_{yz}$ | 0 | $\beta_{yzz}$ | 42.81 |
| $\alpha_{zz}$ | 74.79 | $\beta_{zzz}$ | 0 |
| $\alpha_0$ (e.s.u) | $2.29X10^{-23}$ | βtot (e.s.u) | $1.047X10^{-30}$ |
| Δα (e.s.u) | $6.88X10^{-23}$ | | |

Urea is the prototypical molecule utilized in investigating of the NLO properties of the compound. For this reason, urea was used often as a threshold value for comparative purpose. The calculated dipole moment and hyperpolarizability values of 3BSC are given in Table 2.8. The computed first order hyperpolarizability of 3BSC molecule is $1.0475X10^{-30}$ esu and 2.8 times more than the value of urea ($\beta_o = 0.372 \times 10^{-30}$ esu).

### 2.8.6. Thermodynamic properties

The thermodynamic parameters provide very helpful information for the further study of the title molecule. On the basis of vibrational analysis, the statistical thermodynamics and the standard thermodynamic function, heat capacity $\left(C^{\,0}_{p,m}\right)$, entropy $\left(S^{\,0}_{m}\right)$ and enthalpy changes $\left(H^{\,0}_{m}\right)$ were computed at B3LYP/6-311++G(d,p) basis set by using perl script THERMO.PL [47] and are listed in Table 2.9. Thermodynamic functions are all values increasing with the temperature ranging from 100 to 1000K due to the fact that the molecular vibrations intensities increase with temperature. The correlation equation among heat capacities, entropies, enthalpy changes with temperatures were fitted by quadratic formulas and the corresponding fitting factors ($R^2$) these thermodynamic properties are 0.9999, 0.9995 and 0.9994 respectively. The correlations plot of those shown in Fig 2.13. The thermodynamic correlation fitting equation is follows:



$$\left(C^{\,0}_{p,m}\right) = 26.3182 + 0.6430T - 2.8301 \times 10^{-4}T^2 \quad (R^2 = 0.9995) \qquad (2.14)$$

$$\left(S^{\,0}_{m}\right) = 259.025 + 0.7814T - 2.1282 \times 10^{-4}T^2 \quad (R^2 = 0.9998) \qquad (2.15)$$

$$\left(H^{\,0}_{m}\right) = -8.3301 + 0.0989T - 1.6560 \times 10^{-4}T^2 \quad (R^2 = 0.9993) \qquad (2.16)$$

They can be used to compute the other thermodynamic energy according to the relationship of thermodynamic functions and evaluate directions of chemical behavior according to the second law of thermodynamics in the thermochemical field [48].

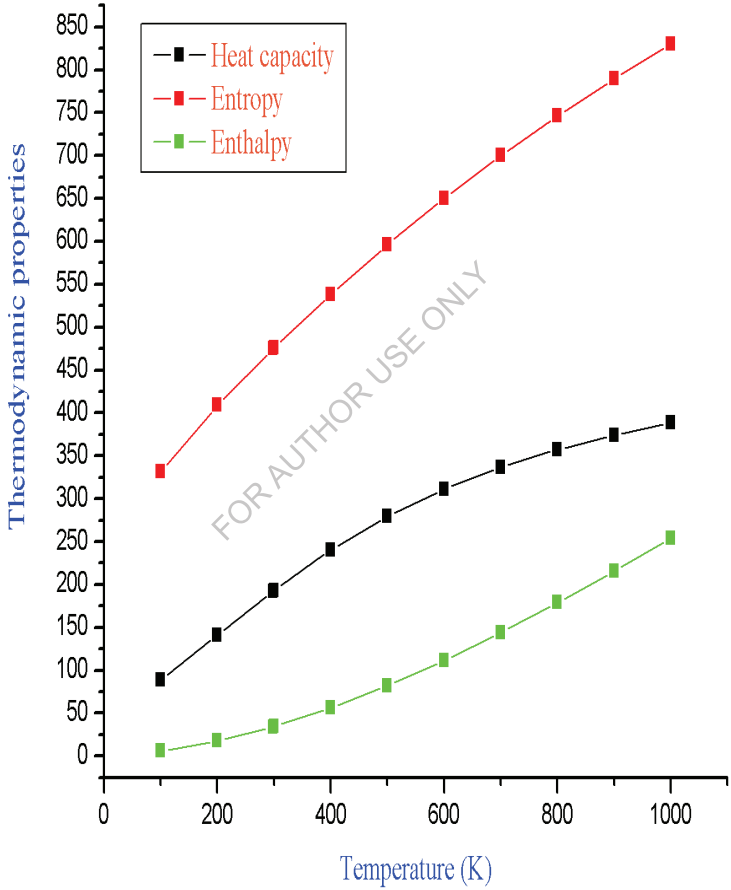


**Fig . 2.13.** Correlation plot of thermodynamic properties at different temperature of the title compound.

**Table 2.9**

Temperature dependence of thermodynamic properties of 3BSC at B3LYP /6-311++G(d,P)

| T(K) | $C^{0}_{p,m}$ (J/ mol K) | $S^{0}_{m}$ (J/ mol K) | $H^{0}_{m}$ (kJ/ mol) |
|---|---|---|---|
| 100 | 88.92 | 331.34 | 6.15 |
| 200 | 141.13 | 408.95 | 17.65 |
| 298 | 192.19 | 474.89 | 34.02 |
| 300 | 193.12 | 476.08 | 34.38 |
| 400 | 240.31 | 538.27 | 56.11 |
| 500 | 279.62 | 596.27 | 82.17 |
| 600 | 311.20 | 650.15 | 111.77 |
| 700 | 336.54 | 700.09 | 144.21 |
| 800 | 357.19 | 746.42 | 178.93 |
| 900 | 374.30 | 789.51 | 215.53 |
| 1000 | 388.67 | 829.71 | 253.70 |



### 2.8.7. Antimicrobial activity

The title compound was screened for its antimicrobial activity against bacterial and fungal strains by Kirby-Bauer agar well diffusion method [49]. The activity was determined by measuring the inhibition zone diameter values (mm) of the investigated compound and antimicrobial activity of 3BSC against bacterial and fungal pathogens are photographed and it is shown in Fig. 2.14 and 2.15. The antimicrobial and solvent sensitivity tests for both bacterial and fungal strains were observed and listed in Table 2.10(a) and 2.10(b) respectively. It is noted that the DMSO solvent, it has no activity on the microbes. 3BSC dissolved at two concentrations (100 µl and 200 µl ) were screened for their antibacterial activity against four bacterial strains such as, *Enterobacter*, *Bacillus*

*subtillis*, *Escherichia coli* and *K. pneumoniae* and three fungal strains such as, *Candida albicans*, *A.niger* and *A.fumicatus* which were selected for the present investigation by the agar well diffusion method. From Tables 2.10(a) and 2.10(b) shows a good activity of 3BSC against the three fungal strains *Candida albicans*, *A.niger* and *A.fumicatus*. Moreover, it is found that synthesized compound exhibits higher antifungal activity than antibacterial activity and the highest activity is against *Candida albicans* where C. albicans is the most commonly isolated species which can cause infections (Candidiasis or thrush) in humans and other animals.

**2.8.10. Molecular docking study**

AutoDock suite 4.2.6 is a recently been used as a convenient tool to get insights into the molecular mechanism of protein-ligand interactions, bind to a receptor of known three-dimensional structure. With the aim to investigate the binding mode, a molecular modeling study was performed using AutoDock Tools for docking. 3BSC was selected to be docked into the active site of three receptors 3GFX [50], 4HOE [51] and 3EQA [52] of antimicrobial proteins which was downloaded from RCSB protein data bank (http://www.rcsb.org/pdb/home/home.do). In order to examine more comprehensive visualization of potentially fit ligands, Accelrys, Discovery Studio Visualizer 4.1 was utilize for the evaluation of hydrogen bonds in protein- ligand interaction. The ligand was docked into the functional sites of the respective proteins individually and the docking energy was examined to achieve a minimum value. AutoDock results indicate the binding position and bound conformation of the peptide, together with a rough estimate of its interaction. Docked conformation which had the lowest binding energy was chosen to investigate the mode of binding. The molecular docking binding energies (kcal/mol) and inhibition constants

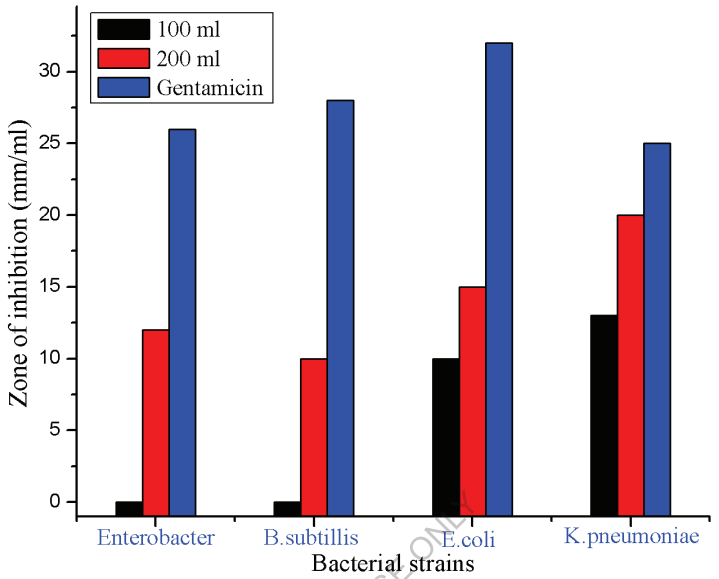


**Fig. 2.14.** A bar diagram for the antibacterial activity of 3BSC.



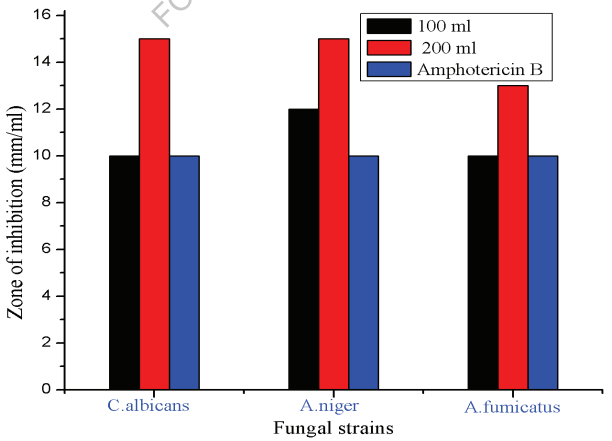


**Fig. 2.15.** A bar diagram for the antifungal activity of 3BSC.

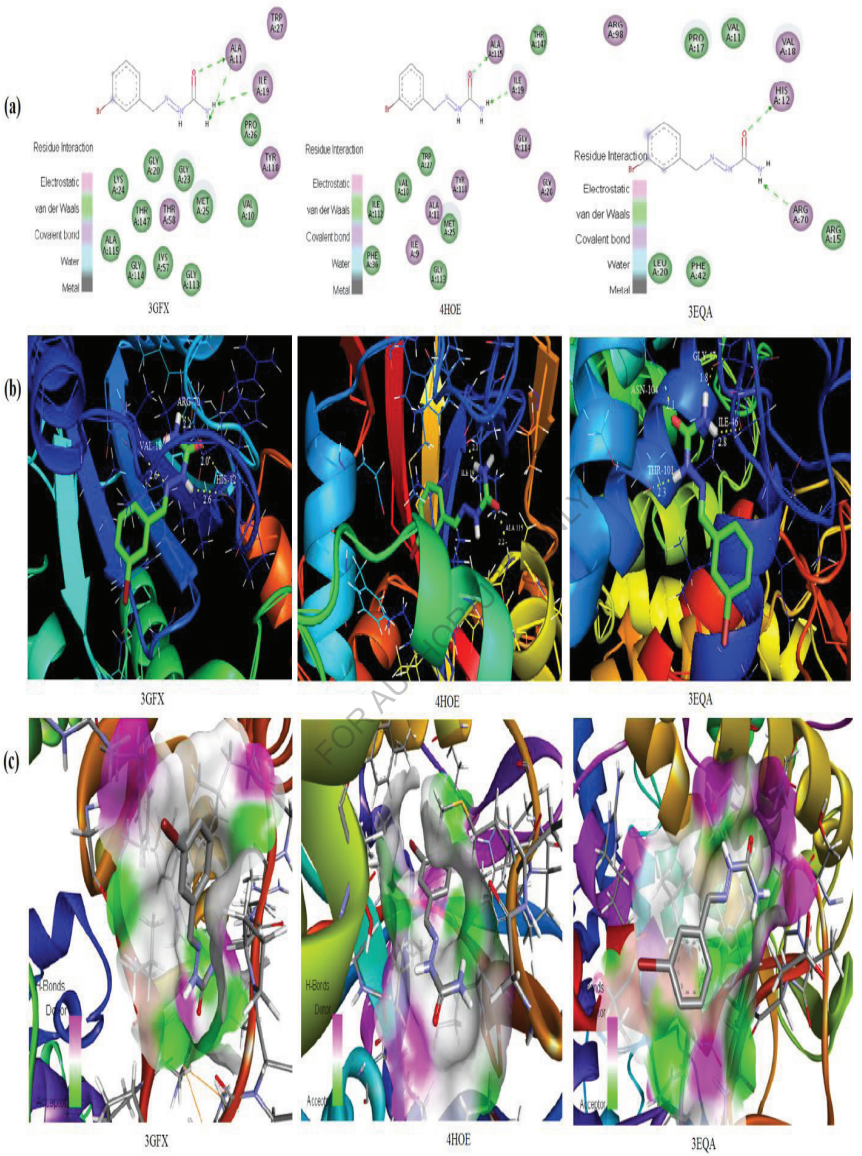


**Fig .2.16.** (a) 3BSC interaction (2D), (b) and (c) 3BSC docked into the binding site (3D) of 3GFX, 4HOE and 3EQA

(μm) were also obtained and listed in Table 2.11. Among them, 3GFX exhibited the lowest free energy at −5.23 kcal/mol and most docked inhibitors interacted with the ligand within the 3GFX binding site. They exhibited up to four N H· · ·O hydrogen bonds involving VAL 18, HIS 12, HIS 12 and ARG 70 with RMSD being 53.2˚A. The docking simulation shows the binding mode of the 3BSC into 3GFX. The 3BSC ligand interacts with different receptors are shown in Fig. 2.16.

**Table 2.10(a)** Antibacterial activity of DMSO extracts

| S. no | Bacterial pathogen | DMSO Extract added and Zone of inhibition (mm/ml) | | | |
|---|---|---|---|---|---|
| | | 100 µl | 200 µl | DMSO | Gentamicin |
| 1 | *Enterobacter* | - | 12 | - | 26 |
| 2 | *Bacillus subtillis* | - | 10 | - | 28 |
| 3 | *E.coli* | 10 | 15 | - | 32 |
| 4 | *K. pneumoniae* | 13 | 20 | - | 25 |



**Table 2.10(b)** Antifungal activity of DMSO extracts

| S. no | Fungal pathogen | DMSO Extract added and Zone of inhibition (mm/ml) | | | |
|---|---|---|---|---|---|
| | | 100 µl | 200 µl | DMSO | Amphotericin B |
| 1 | *Candida albicans* | 10 | 15 | - | 10 |
| 2 | *A.niger* | 12 | 15 | - | 10 |
| 3 | *A.fumicatus* | 10 | 13 | - | 10 |

**Table 2.11**

Hydrogen bonding and molecular docking with antimicrobial protein targets

| Protein (PDB ID) | Bonded residues | Bond distance (Å) | EIC (µm) | Binding energy (kcal/mol) | Reference RMSD (Å) |
|---|---|---|---|---|---|
| 3GFX | VAL 18 | 2.6 | 146.28 | -5.23 | 53.2 |
| | HIS 12 | 2.6 | | | |
| | HIS 12 | 2.0 | | | |
| | ARG 70 | 2.2 | | | |
| 4HOE | ALA 115 | 2.2 | 247.10 | -4.92 | 27.01 |
| | ILE 19 | 2.1 | | | |
| 3EQA | ILE 46 | 2.8 | 1.24 | -3.97 | 38.43 |
| | GLY 47 | 1.8 | | | |
| | ASN 104 | 2.1 | | | |
| | THR 101 | 2.3 | | | |

## Reference


[1] J.D. Warren, D.L. Woodward, R.T. Hargreaves, 4-Substituted semicarbazones of mono- and dichlorobenzaldehydes as antihypertensive agents, J. Med. Chem. 20(11) (1977) 1520-1521.

[2] S. Chandra , L.K. Gupta, Spectroscopic and biological studies on newly synthesized nickel(II) complexes of semicarbazones and thiosemicarbazones, Spectrochim. Acta A 62 (2005) 1089-1094.

[3] V.K. Jain, A. Handa, R. Pandya, P. Shrivastav, Y.K. Agrawal, Polymer supported calix[4]arene-semicarbazone derivative for separation and preconcentration of La(III), Ce(III), Th(IV) and U(VI). React. Funct. Polym. 51 (2012) 101–110.

[4] R. Sharma, S. Mudgal, B. Shrivastava, P. Sharma, Synthesis, characterization & biological evaluation of newer 4-(4-substituted aryl) semicarbazones as anticonvulsant and anti-microbial agents, Indo American. J. Pharm Rech. 3 (2013) 5522-5540.

[5] G. Saravanan, V. Alagarsamy, C. Rajaram Prakash, Synthesis, characterization and in vitro antimicrobial activity of some 1-(substitutedbenzylidene)-4-(4-(2-(methyl/phenyl)-4-oxoquinazolin-3(4H) yl)phenyl)semicarbazide derivatives, J. Saudi Chem. Soc. 19 (2015) 3-11.

[6] A.P. Martinez, W.W. Lee, Some Semicarbazones and Thiosemicarbazones, *J. Med. Chem.* 10 (1967) 1192.

[7] V.M. Kolb, J.W. Stupar, T.E. Janota, and W. L. Duaxl, Abnormally High IR Frequencies for the Carbonyl Group of Semicarbazones of the Benzaldehyde and Acetophenone Series, J. Org. Chem. 54 (1989) 2341-2346.

[8] J.R. Dimmock, K.K Sidhu, S.D. Tumber, S.K. Basranl, M. Chen, J.W. Quail, J. Yang, I. Rozas, D.F. Weaver, Some aryl

semicarbazones possessing anticonvulsant activities, Eur. J. Med. Chem. 30 (1995) 287-301.

[9] A. Dhandapani, S. Manivarman, S. Subashchandrabose, H. Saleem, Molecular structure and vibrational analysis on (E)-1-(3-methyl-2,6-diphenyl piperidin-4-ylidene) semicarbazide, J. Mol. Struct. 1058 (2014) 41-50.

[10] S. Subashchandrabose, N. Ramesh Babu, H. Saleem, M. Syed Ali Padusha, Vibrational studies on (E)-1-((pyridine-2-yl)methylene)semicarbazide using experimental and theoretical method, J. Mol. Struct. 1094 (2015) 254–263.

[11] M. J. Frisch, G. W. Trucks, H. B. Schlegel, G. E. Scuseria, M. A. Robb, Gaussian 09, Revision **E.01,** Gaussian, Inc., Wallingford CT, 2009.

[12] GaussView, Version 5, Roy Dennington, Todd Keith, and John Millam, *Semichem Inc.,* Shawnee Mission, KS, 2009.

[13] M. H. Jomroz, Vibrational Energy Distribution Analysis, VEDA4, Warsaw, 2004.

[14] K. Wolinski, R. Haacke, J.F. Hinton, P. Pulay, Methods for parallel computation of SCF NMR chemical shifts by GIAO method: Efficient integral calculation, multi-Fock algorithm, and pseudodiagonalization, J.Comp. Chem. 18 (6) (1997) 816-825.

[15] G. Keresztury, S. Holly, J. Varga, G. Besenyei, A.Y. Wang, J.R. During, Vibrational spectra of monothiocarbamates-II. IR and Raman spectra, vibrational assignment, conformational analysis and *ab* initio calculations of S-methyl-N,N-dimethylthiocarbamate, Spectrochim. Acta A 49 (1993) 2007-2026.

[16] Y. Kia, H. Osman, Vikneswaran, Murugaiyah, Madhukar Hemamalinic, Hoong-Kun Fun, Acta Cryst. E67 (2011) o242.

[17] N. Swarnalatha, S.Gunasekaran, S. Muthu, M. Nagarajan, Molecular structure analysis and spectroscopic characterization of 9-methoxy-2H-furo[3,2-g]chromen-2-one with experimental (FT-IR and FT-Raman) techniques and quantum chemical calculations, spectrochim. Acta part A 137 (2015) 721-729.

[18] L.G. Wade (Ed), Advanced Organic Chemistry, 4th ed., Wiley, New York,1992. p.723.

[19] D. Lin-Vien, N.B. Colthup, W.G. Fately, J.G. Grasselli, The Handbook of Infrared and Raman Characteristic Frequencies of Organic Molecules, Academic Press Boston, MA, 1991.

[20] M. Silverstein, G.C. Basseler, C. Morill, Spectrometric Identification of Organic Compounds, Wiley, New York, 1981.

[21] V. Krishnakumar, R. Ramasamy, Scaled quantum chemical studies of the structure and vibrational spectra of 2-(methylthio) benzimidazole, Spectrochim. Acta Part A 62 (2005) 570-577.

[22] L.J. Bellamy, The Infrared Spectra of Complex Molecules, vol. 2, Chapman and Hall, London, 1980.

[23] N. Sundaraganesan, S.Illakiamani, C. Meganathan, B.D. Joshua, Vibrational spectroscopy investigation using ab initio and density functional theory analysis on the structure of 3-aminobenzotrifluoride, Spectrochim. Acta A 67 (2007) 214-224.

[24] G. Varsanyi, Aassignments for vibrational Spectra of Seven Hundred Benzene Derivatives, vol. 1, Adam Hilger, London, 1974.

[25] V. Udayakumar, S. Periandy, S. Ramalingam, Experimental (FT-IR and FT-Raman) and theoretical (HF and DFT) investigation, IR intensity, Raman activity and frequency estimation analyses on 1-bromo-4-chlorobenzene, Spectrochim. Acta A 79 (2011) 920-927.

[26] R.Ditchfield, Molecular Orbital Theory of Magnetic Shielding and Magnetic Susceptibility, J.Chem. Phys. 56 (1972) 5688-5692.

[27] G. Varsanyi, Vibrational spectra of Benzene Derivatives, Academic press, New York, 1969.

[28] G. Socrates, Infrared Characteristic Group Frequencies, John Wiley Interscience, New York, 1980

[29] B.T. Gowda, K. Jyothi, J.D. D'Souza, Infrared and NMR Spectra of Arylsulphonamides, 4-X-C6H4SO2NH2 and i-X, j-YC6H3SO2NH2 (X¼H; CH3; C2H5; F; Cl; Br; I or NO2 and i-X, j-Y¼2,3-(CH3)2; 2,4-(CH3)2; 2,5- (CH3)2; 2-CH3, 4-Cl; 2-CH3, 5-Cl; 3-CH3, 4-Cl; 2,4-Cl2 or 3,4-Cl2), Z. Naturforsch. 57a (2002) 967-973.

[30] N. Subramanian, N. Sundaraganesan, J.Jayabharathi, Molecular structure, spectroscopic (FT-IR, FT-Raman, NMR, UV) studies and first-order molecular hyperpolarizabilities of 1,2-bis(3-methoxy-4-hydroxybenzylidene)hydrazine by density functional method, Spectrochim. Acta A 76 (2010) 259-269.

[31] D.F.V. Lewis, C. Ioannides, D.V. Parke, Interaction of a series of nitriles with the alcohol-inducible isoform of P450: computer analysis of structure-activity relationships, Xenobiotica 24 (1994) 401-408.

[32] R. G. Pearson, Absolute electronegativity and hardness correlated with molecular orbital theory, Proc. Natl. Acad. Sci. 83 (1986) 8440-8441.

[33] P. Kolandaivel, G. Praveen, P. Selvarengan, Study of atomic and condensed atomic indices for reactive sites of molecules, J. Chem. Sci. 117 (2005) 591-598.

[34] S. Muthu, E. Isac Paulraj, Spectroscopic and molecular structure (monomeric and dimeric structure) investigation of 2-[(2-

hydroxyphenyl) carbonyloxy] benzoic acid by DFT method: A combined experimental and theoretical study, J. Mol. Struct. 1038 (2013) 145-162.

[35] Weitao Yang and Wilfried J. Mortier , The use of global and local molecular parameters for the analysis of the gas-phase basicity of amines, J. Am. Chem. Soc. 108 (1986) 5708-5711.

[36] Y. X. Sun, Q. L. Hao, W. X. Wei, Z. X. Yu, L. D. Lu, X. Wang, Y. S. Wang, Experimental and density functional studies on 4-(3, 4-dihydroxybenzylideneamino) antipyrine, and 4-(2,3,4-trihydroxy benzylideneamino) antipyrine, J. Mol. Struct. THEOCHEM 904 (2009) 74-82.

[37] S.K. Pathak, R. Srivastava, A.K. sachan, O. Prasad, L. Sinha, A.M. Asiri, M. Karabacak, Experimental (FT-IR, FT-Raman, UV and NMR) and quantum chemical studies on molecular structure, spectroscopic analysis, NLO, NBO and reactivity descriptors of 3,5-Difluoroaniline, Spectrochim.Acta A 135 (2015) 283-295.

[38] Zeynep Demircioğlu, Ciğdem Albayrak, Orhan Büyükgüngör, Theoretical and experimental investigation of (E)-2-([3,4-dimethylphenyl)imino]methyl)-3-methoxyphenol: Enol–keto tauto merism, spectroscopic properties, NLO, NBO and NPA analysis, J. mol. Struct. 1065-1066 (2014) 210-222.

[39] R. Srinivasaraghavan, S. Thamaraikannan, S. Seshadri, T. gnanasambandan, Molecular conformational stability and Spectroscopic analysis of Parared with experimental techniques and quantum chemical calculations, Spectrochim. Acta A 137 (2015) 1194-1205.

[40] C. James, A. Amal Raj, R. Reghunathan, V.S. Jayakumar, I.Hubert Joe, Structural conformation and vibrational spectroscopic studies of

2,6-bis(*p*-*N*,*N*-dimethyl benzylidene) cyclohexanone using density functional theory, J. Raman Spectrosc. 37 (2006) 1381-1392.

[41] J. Liu, Z. Chen, S. Yuan, Study on the prediction of visible absorption maxima of azobenzene compounds, J. Zhejing Univ. Sci B. 6 (2005) 584-589.

[42] M. Szafran, A. komasa, E.B. Adamska, Crystal and molecular structure of 4-carboxypiperidinium chloride (4-piperidinecarboxylic acid hydrochloride), J. Mol. Struct. THEOCHEM 827 (2007) 101-107.

[43] G. Velraj, S. Soundharam, C.Sridevi, Structure, vibrational, electronic, NBO and NMR analyses of 3-methyl-2,6-diphenylpiperidin-4-one (MDPO) by experimental and theoretical approach, Journal of Molecular Structure 1060 (2014) 156-165.

[44] A.E. Reed, L.A. Curtiss, F. Weinheld, Intermolecular Interactions from a Natural Bond Orbital, Donor-Acceptor Viewpoint, Chem.Soc. 102 (1988) 899-926.

[45] J.P. Foster, F.Weinhold, Natural Hybrid Orbitals, J. AM. Chem. Soc. 102 (1980) 7211-7218.

[46] H. Sekino, R.J. Bartlett, Hyperpolarizabilities of the hydrogen fluoride molecule: A discrepancy between theory and experiment?, J. Chem. Phys. 84 (1986) 2726-2733.

[47] K.K. Irikura, THERMO. PL (National Institute of Standards and Technology), Gaithersburg, MD, 2002.

[48] Leena Sinha, Mehmet Karabacak, V. Narayan, Mehmet Cinar, Onkar Prasad, Molecular structure, electronic properties, NLO, NBO analysis and spectroscopic characterization of Gabapentin with experimental (FT-IR and FT-Raman) techniques

and quantum chemical calculations, Spectrochim. Acta A 109 (2013) 298-307.

[49] T. Abdel-Ghani , M.F. Abo El-Ghar, A.M. Mansour, Novel Ni(II) and Zn(II) complexes coordinated by 2-arylaminomethyl-1H-benzimidazole: Molecular structures, spectral, DFT studies and evaluation of biological activity, Acta Spectrochimica Acta A 104 (2013) 134-142.

[50] A. Ravi Kumar, G Sathaiah, A. Chandra Shekhar, K. Raju, P. Shanthan Rao, B. Narsaiah, Y. Kanaka Raju, U. S. N. Murthy, V. Srimai, M. Ramesh, and T. Parthasarathy, Synthesis of 6-Fluoro-7-cyclic Amino-substituted Dicarboxylic Acid Quinolones and their Antibacterial Activity, J. Hetercycl Chem. 51 (2014) 114-122.

[51] N. G. Dayanandan, L. Paulsen, K.Viswanathan, S. Keshipeddy, N. Lombardo, W. Zhou, M. Lamb, E. Sochia, J B. Alverson, D. Priestley, L. Wright and C. Anderson, Propargyl-Linked Antifolates are Dual Inhibitors of Candida albicans andCandida glabrata, J. Med. Chem, 57 (2014) 2643- 2656.

[52] Jaeyong Lee and Mark Paetzel, Structure of the catalytic domain of glucoamylase from Aspergillus niger, Acta Cryst. F67 (2011) 188–192.

# CHAPTER – III

## Synthesis, Spectroscopic (FT-IR, FT-Raman, NMR, UV-Visible), First Order Hyperpolarizability, NBO and Molecular Docking Study of (E)-1-(4-Bromobenzylidene) Semicarbazide

### 3.1. Introduction

The synthesis of Semicarbazones derivative has generated vast interest to organics as well as for medicinal chemistry, organometallics, polymers [1-3] and herbicides and many other industrial processes. Several semicarbazones and its derivatives have proved the efficiency and efficacy in combating various diseases [4, 5]. Particularly, Semicarbazones and its derivatives of (E)-1-(4-bromobenzylidene) semicarbazide (4BSC) wide variety of biological activities such as antifungal, antibacterial, antimalarial, anti-cancer, anticonvulsant, antiproliferative, anti-inflammatory, antitumor and antiviral activity [6-8]. Its chemical formula is $C_8H_8BrN_3O$. A density functional theory (DFT) investigation has a potential significance towards the design and enlargement of organic inhibitors in the organic synthesis field. Vibrational spectroscopy (FT-IR, FT-Raman and NMR) and UV-Vis techniques are widely used to study the structural conformation and electronic transition of the molecular system. The combination of theoretical and experimental work could solve many problems in several areas of research [9,10]. The search for new materials with nonlinear optical (NLO) properties has been the subject of intense research due to their application in a wide range of technologies such as optical computing and communications [11,12] and much attention has been paid to organic NLO materials due to their promising applications in optoelectronic technology [13,14].

To our knowledge, Literature survey reveals that the DFT/B3LYP frequency calculations of (E)-1-(4-bromobenzylidene)semicarbazide (4BSC) have not been carried out so far. In this present work, we report the synthesis and comprehensive spectroscopic investigation of 4BSC using B3LYP/6-311++G(d,p) level of the theory. The experimental spectral data (FT-TR, FT-Raman, UV and NMR) of the 4BSC is compared by means of the theoretical spectral data obtain by DFT/B3LYP method 6-311++G(d,p) basis set. The molecular properties like dipole moment, polarizability, first order hyperpolarizability, molecular electrostatic potential and thermodynamic parameters have been calculated. Global reactivity descriptors such as chemical potential, electronegativity, hardness, softness and electrophilicity index have been computed. HOMO-LUMO analysis has been performed which help to elucidate charge transfer occurring in the molecule. UV–Vis experimental band gap value of the title compound is compared with theoretical UV band gap and HOMO-LUMO diagram band gap values measured by TD-DFT approach. The natural bond orbital (NBO) investigation has been useful to the stability of the molecule arising from charge delocalization. Molecular docking of 4BSC was also analyzed.



### 3.2. Synthesis

For the synthesis of (E)-1-(4-bromobenzylidene)semicarbazide compound, solution of 4-bromobenzaldehyde (1.8 ml, 0.01 mol) in ethanol (15 mL), semicarbazide hydrochloride (1.1 g, 0.01 mol) was added followed by the reaction mixture was kept in magnetic stirrer and stirred well for 1 hour. The progress of the reaction was continuously monitored by thin layer chromatography (TLC). The reaction mixture was diluted with ethyl acetate and washed with water. The crude solid obtained was

dried and recrystallized using absolute alcohol. The recrystallized product was dried in a vacuum desiccator over fused Calcium Chloride. The scheme of the synthesis is shown in Fig. 3.1.

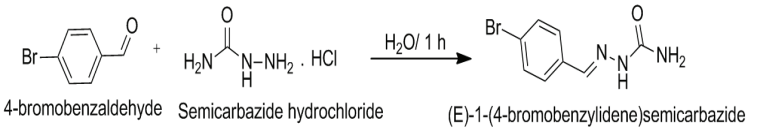


**Fig. 3.1.** The scheme of the synthesis of 4BSC

### 3.3. Experimental details

The FT-IR spectrum of the synthesis compound (E)-1-(4-bromobenzylidene)semicarbazide (4BSC) was recorded in the region 4000-450 $cm^{-1}$ in evacuation mode using a KBr pellet technique with 1.0 $cm^{-1}$ resolution on a PERKIN ELMER FT-IR spectrophotometer. The FT-Raman spectrum of the 4BSC compound was recorded in the region 4000-100 $cm^{-1}$ in a pure mode using Nd: YAG Laser excitation wavelength of Raman 100 mW with 2 $cm^{-1}$ resolution on a BRUCKER RFS 27 at SAIF, IIT, Chennai, India. Carbon($^{13}C$) NMR and Proton ($^{1}H$) NMR spectra were recorded in DMSO-$d_6$ using TMS as an internal standard on a Bruker high-resolution NMR spectrometer at 400 MHz at CAS in Crystallography & Biophysics, University of Madras, Chennai, India. The ultraviolet absorption spectrum of the sample is examined in the range 250-600 nm using UV-1700 series recording spectrometer.



### 3.4. Computational details

Initial atomic coordinates for molecular geometry optimization have been performed by using GaussView 5.0 software package [15]. The molecular structure of 4BSC the ground state (in the gas phase) was

optimized by DFT/B3LYP methods with 6-311++G(d,p) basis set level, and the optimized structure was used in the vibrational frequency calculations. The calculated harmonic vibrational frequencies were scaled by 0.961 for B3LYP/6-311++G(d,p) level [16,17]. The entire calculations (vibrational wavenumbers, geometric parameters, and other molecular properties) were implemented by using GaussView 5.0 program [18] and Gaussian 09W program package on a computing system [19]. Additionally, the calculated vibrational frequencies were explained by means of the potential energy distribution (PED) analysis of all the fundamental vibration modes by using VEDA 4 program [20] used in previous studies by many researchers [21–23]. In order to understand the electronic properties, the theoretical UV-Vis spectra have been investigated by TD-DFT method with 6-311++G(d,p) basis set for the DMSO and gas phase. The proton and carbon NMR chemical shift were calculated with the gauge-including atomic orbital (GIAO) approach by applying B3LYP/6-311++G(d,p) method of the title molecule and compared with the experimental NMR spectra. Molecular docking (ligand-protein) simulations have been performed by using autoDock 4.2.6 software package.



### 3.5. Results and discussion

#### 3.5.1. Molecular geometry

The geometrical parameters (bond length and bond angles) of the synthesis 4BSC compound are listed in Table 3.1 using DFT/B3LYP method with 6-311++G(d,p) basis set. The optimized molecular structure of title compound is obtained from Gaussian 09W and GaussView 5.0 programs are shown in Fig. 3.2. To the best of our knowledge, exact experimental data on the geometrical parameters of 4BSC are not available

in the literature. Therefore, the crystal data of a closely related molecule such as (E)-2-(4-Methylbenzylidene)hydrazinecarboxamide [24] is compared with that of the title compound. From the calculated values, it is found that most of the optimized molecular bond lengths are slightly higher than the experimental values owing to the fact that the theoretical calculations were carried out isolated molecule in the gas phase and the experimental XRD results were carried out in the solid state.

This title molecule has seven C - C bond lengths, five C - H bond lengths, three (C - N, N - H) bond lengths and one (N - N, C - O, C - Br) bond lengths respectively. The highest bond length was calculated for $C_6$ - $C_7$ found to be 1.461 Å (experimental) and 1.462 Å (theoretical) respectively. The calculated bond length values for C-C and C-H in the benzene ring vary from 1.388-1.462 Å and 1.082-1.096 Å by B3LYP/6-311++G(d,p) basis set and well agreed with experimental values [24]. The homonuclear bond lengths (C-C and N-N) are higher than the heteronuclear bond lengths (C-H and N-H). The important reasons for the same charges are repulsive and opposite charges are attractive.



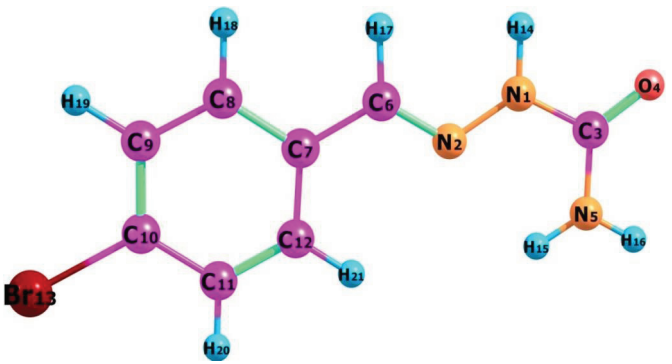


**Fig.3.2.** Optimized geometric structure with atoms numbering of 4BSC

**Table 3.1**

Geometrical parameters optimized in (E)-1-(4-bromobenzylidene) semicarbazide bond length (Å) and bond angle (°).

| **Bond length (Å)** | **Experimental[a]** | **B3LYP/6-311++G(d,p)** | **Bond angle (°)** | **Experimental[a]** | **B3LYP/6-311++G(d,p)** |
|---|---|---|---|---|---|
| N1-N2 | 1.376 | 1.35 | C3-N1-H14 | - | 115.4 |
| N1-C3 | 1.363 | 1.397 | N1-C3-O4 | 119.12 | 119.9 |
| N1-H14 | 0.97 | 1.016 | N1-C3-N5 | 117.37 | 114.8 |
| N2-C6 | 1.275 | 1.283 | N2-C6-C7 | 122.12 | 122.7 |
| C3-O4 | - | 1.219 | N2-C6-H17 | 118.9 | 120.7 |
| C3-N5 | - | 1.359 | O4-C3-N5 | 123.5 | 125.3 |
| N5-H15 | - | 1.006 | C3-N5-H15 | - | 121 |
| N5-H16 | - | 1.005 | C3-N5-H16 | - | 117.7 |
| C6-C7 | 1.461 | 1.462 | H15-N5-H16 | - | 121.3 |
| C6-H17 | 0.96 | 1.096 | C7-C6-H17 | 118.9 | 116.6 |
| C7-C8 | 1.388 | 1.402 | C6-C7-C8 | 118.08 | 119 |
| C7-C12 | 1.388 | 1.405 | C6-C7-C12 | 122.3 | 122.6 |
| C8-C9 | 1.386 | 1.392 | C8-C7-C12 | 119.5 | 118.4 |
| C8--H18 | 0.96 | 1.085 | C7-C8-C9 | 119.61 | 121.2 |
| C9-C10 | 1.388 | 1.39 | C7-C8-H18 | 119.5 | 119.7 |
| C9-H19 | - | 1.082 | C7-C12-C11 | 120.9 | 120.9 |
| C10-C11 | 1.388 | 1.395 | C7-H12-H21 | 119.5 | 119.3 |
| C10-Br13 | - | 1.915 | C9-C8-H18 | 119.5 | 119.1 |
| C11-C12 | 1.386 | 1.388 | C8-C9-C10 | - | 119 |
| C11-H20 | 0.96 | 1.082 | C8-C9-H19 | - | 120.5 |
| C12-H21 | 0.96 | 1.083 | C10-C9-H19 | - | 120.5 |
| **Bond angle (°)** | **Experimental[a]** | **B3LYP/6-311++G(d,p)** | C9-C10-C11 | 118.8 | 121 |
| N2-N1-C3 | 119.98 | 122.8 | C9-C10-Br13 | - | 119.6 |
| N2-N1-H14 | - | 121.9 | C11-C10-Br13 | - | 119.4 |
| N1-N2-C6 | 115.78 | 118.4 | C10-C11-C12 | 120.9 | 119.4 |

### 3.5.2. Vibrational analysis

The maximum number of potentially active observable fundamentals of the non-linear molecule, which contains N atoms, is equal to (3N-6) apart from the translational and three rotational degrees of freedom. The 4BSC molecule consists of 21 atoms, which has 57 normal modes of vibration. The vibrational band assignments were made by the aid of potential energy distribution (PED) using VEDA program. The comparative observed and simulated FT-IR and FT-Raman spectra are shown in Fig. 3.3 and 3.4. The calculated vibrational frequencies (Unscaled and Scaled), IR intensity, Raman activity are tabulated in Table 3.2.

#### *3.5.2.1. C-H vibrations*

In the aromatic compounds, the C-H stretching wavenumbers appear in the range 3000-3100 $cm^{-1}$ which are the characteristic region for the ready identification of C-H stretching vibrations [25]. The C-H stretching and bending regions are of the most difficult regions to interpret in infrared spectra. The nature and position of the substituent cannot affect these vibrations. Most of the aromatic compounds have almost four infrared peaks in the region 3080-3010 $cm^{-1}$ due to ring C-H stretching bands [26]. In this present study, the C-H stretching vibrations are observed at 3077, 30774, 3063, 3049 and 2920 $cm^{-1}$ [mode nos 54-50] by B3LYP/6-311++G(d,P) method show good agreements with experimental vibrations. The band observed in the recorded FT-IR spectrum 3065(s) and with the FT-Raman spectrum bands at 3092(s), 3086(w), 3059(s), 2933(w) $cm^{-1}$. The PED corresponding to this pure mode of title molecule contributed 94, 90, 99, 95 and 100% is shown in Table 3.2.

### *3.5.2.2. $NH_2$ vibrations*

The $NH_2$ group has two (N-H) stretching vibrations, first one asymmetric and another one symmetric. The asymmetric stretching for the $NH_2$, $CH_2$ and $CH_3$ has a magnitude higher than the symmetric stretching [27]. The aromatic structure shows the presence of C-H and N-H stretching vibrations above 3000 $cm^{-1}$ which are the characteristic region for ready identification of this structure [28, 29]. The title compound has only one $NH_2$ group and hence one symmetric and one asymmetric N-H stretching vibrations in $NH_2$ group are expected. The symmetric $NH_2$ stretching vibrations appear from 3420 to 3500 $cm^{-1}$ [30]. In this work, the FT-Raman band at 3598(w) $cm^{-1}$ has been assigned to $NH_2$ asymmetric stretching vibrations. The $NH_2$ symmetric stretching vibrations observed in the FT-IR and FT-Raman has very strong and weak intensity bands. The experimental FT-IR and FT-Raman symmetric stretching bands found at 3463(vs) $cm^{-1}$ and 3477(w) $cm^{-1}$. The theoretical wavenumbers calculated at 3600 and 3467 $cm^{-1}$ [mode no 57, 56] are assigned as $NH_2$ asymmetric and symmetric stretching vibrations. The PED contributions are 99% for each asymmetric and symmetric stretching mode.



### *3.5.2.3. C-C ring vibrations*

The C-C stretching vibrations are expected in the range from 1650 to 1100 $cm^{-1}$ which are not significantly influenced by the nature of the substituents [31]. The C-C stretching vibrations of the 4BSC compound were observed from1591 to 231 $cm^{-1}$. In this present study , the C-C stretching vibrations are found at 1591(vs), 1399(s), 1100(s), 1009(w), 820(m), 626(w) $cm^{-1}$ in FT-IR and 1561(vs), 1529(w), 1399(m), 1230(s), 1100(m), 1010(m), 826(w), 622(m), 231(m) $cm^{-1}$ in FT-Raman respectively. The theoretical wavenumbers at 1564, 1534, 1372, 1244,

1086, 1040, 827, 622 and 202 $cm^{-1}$ (mode no 47, 46, 42, 38, 34, 32, 26, 20, 8) are assigned as C-C stretching vibrations with PED contributions of 41, 47, 35, 58, 16, 47, 36, 21 and 15% respectively.

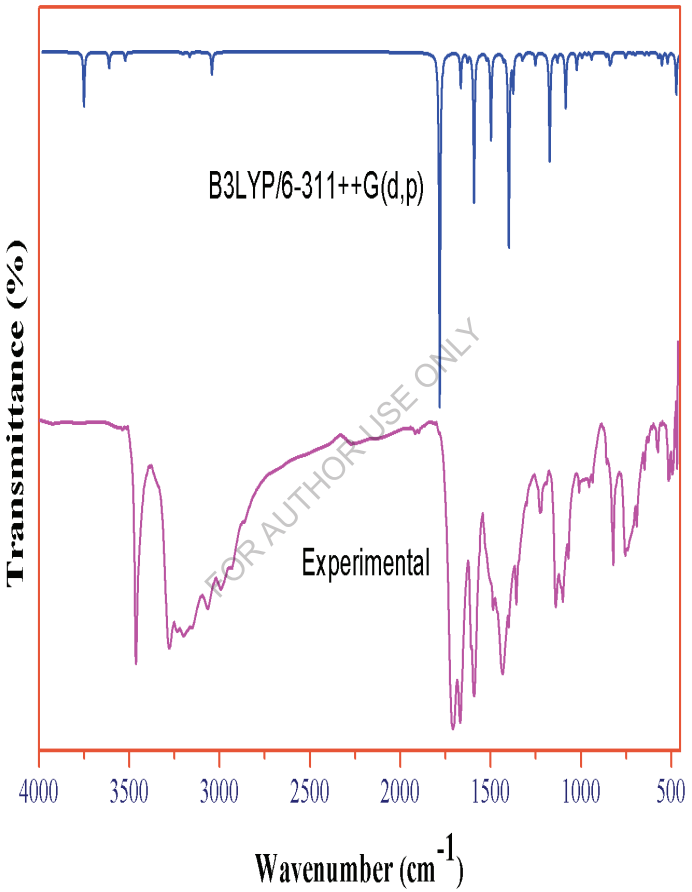



**Fig. 3.3.** FT- IR spectra of 4BSC

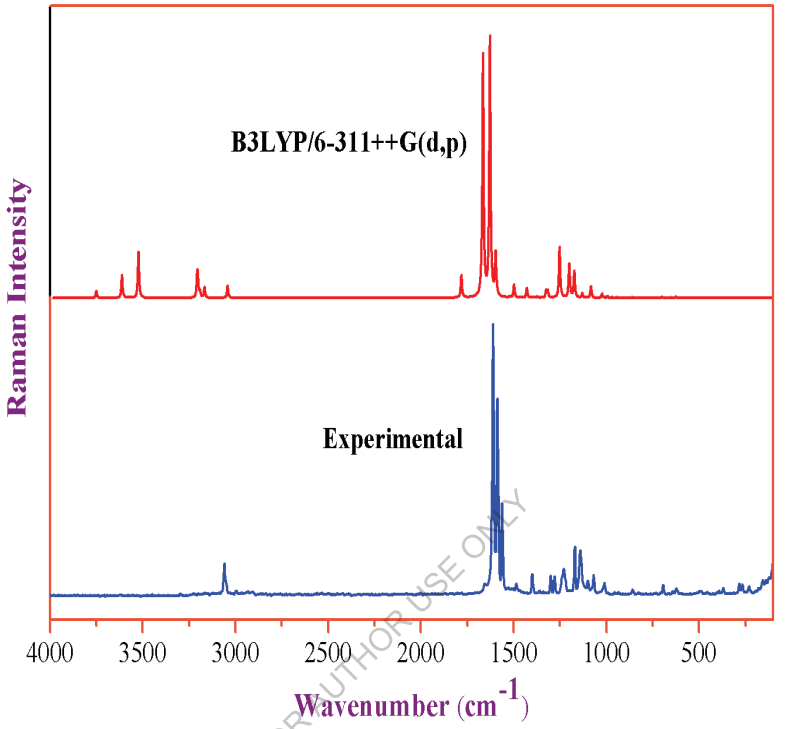



**Fig. 3.4.** FT-Raman spectra of 4BSC

### *3.5.2.4. C-Br Vibrations*

The most aromatic bromo compounds C-Br stretching vibrations occur in the region 650-395 $cm^{-1}$ [32]. The vibration belonging to the bond between the ring and the Bromine atom is salient as a combination of vibrations is possible owing to the presence of heavy atom [33]. The C-Br stretching vibrations for 4BSC molecule is assigned at 672, 364, 202 $cm^{-1}$ (mode no 21, 12, 8) in B3LYP/6-311++G(d,p) and 648(w) $cm^{-1}$ in FT-IR and 369(m), 231(m) $cm^{-1}$ in FT-Raman with a PED of 26, 36 and 26%.

**Table 3.2**

Observed and calculated vibrational frequency of 4BSC at B3LYP method with 6-311++G(d,P) basis set.

| Experimental wave number ($cm^{-1}$) | | Theoretical wave number($cm^{-1}$) | | Assignments (PED)[a] |
|---|---|---|---|---|
| **FTIR** | **FT-Raman** | **Unscaled** | **Scaled[b]** | |
| - | 3598(w) | 3750 | 3600 | $\gamma_{as}$ $NH_2$(99) |
| 3463(vs) | 3477(w) | 3611 | 3467 | $\gamma_s$ $NH_2$(99) |
| - | 3391(w) | 3522 | 3381 | γ NH(100) |
| - | 3092(w) | 3205 | 3077 | γ CH(94) |
| - | 3086(w) | 3202 | 3074 | γ CH(90) |
| 3065(s) | - | 3191 | 3063 | γ CH(99) |
| - | 3059(s) | 3176 | 3049 | γ CH(95) |
| - | 2933(w) | 3042 | 2920 | γ CH(100) |
| 1708(vs) | 1707(w) | 1781 | 1712 | γ OC(43)+γ NC(38) |
| 1607(s) | 1610(vs) | 1665 | 1600 | γ NC(68) |
| 1591(vs) | 1561(vs) | 1627 | 1564 | γ CC(41) |
| - | 1529(w) | 1597 | 1534 | γ CC(47)+β CCC(12) |
| - | 1501(w) | 1591 | 1529 | β HNH(76) |
| 1486(s) | 1486(m) | 1522 | 1463 | β HCC(30) |
| 1434(vs) | - | 1497 | 1439 | β HNN(39)+β HCN(13) |
| 1399(s) | 1399(m) | 1428 | 1372 | γ CC(35)+β HCC(24) |
| 1356(s) | 1359(w) | 1399 | 1344 | γ NC(38)+β OCN(-14)+β HNH(-12)+β HNN(18) |
| 1300(m) | 1300(m) | 1374 | 1321 | β HCN(49)+β HNN(11) |
| - | 1278(m) | 1324 | 1273 | β HCC(71) |
| - | 1230(s) | 1294 | 1244 | γ CC(58) |
| 1226(m) | - | 1252 | 1203 | β HCN(14) |
| - | 1170(s) | 1199 | 1153 | β HCC(76) |
| 1138(s) | 1140(s) | 1172 | 1127 | γ NN(54) |
| 1100(s) | 1100(m) | 1130 | 1086 | γ CC(16)+β HCC(11) |
| 1069(s) | 1068(m) | 1084 | 1042 | β HNC(49) |
| 1009(w) | 1010(m) | 1082 | 1040 | γ CC(47)+β HNC(12) |

| | | | | |
|---|---|---|---|---|
| - | - | 1023 | 983 | β CCC(64) |
| 955(w) | 956(w) | 994 | 955 | γ NC(62)+β NNC(10) |
| - | 936(w) | 984 | 945 | τ HCCC(64)+τ CCCC(14) |
| 935(w) | - | 968 | 930 | τ HCCC(53)+τ HCNN(20) |
| - | 900(w) | 941 | 904 | τ HCCC(12)+τ HCNN(67) |
| 820(m) | 826(w) | 860 | 827 | γ CC(36)+β CCC(40) |
| - | - | 839 | 807 | τ HCCC(50) |
| - | - | 832 | 800 | τ HCCC(85) |
| 754(m) | 733(w) | 753 | 723 | OUT ONNC(88) |
| 691(m) | 693(m) | 717 | 689 | τ CCCC(56) |
| 648(w) | - | 700 | 672 | γ BrC(26)+β NCC(19)+β CCC(11) |
| 626(w) | 622(m) | 648 | 622 | γ CC(21)+β CCC(24) |
| - | 598(w) | 625 | 600 | β NCN(-18)+β CNN(17) |
| 573(w) | - | 571 | 549 | τ HNCN(80)+τ HNNC(15) |
| 515(w) | 549(w) | 551 | 530 | β OCN(59) |
| 510(w) | 515(w) | 520 | 500 | τ NNCC (12)+ BrCCC (-14) + τ CCCC(34)+τ CCCC(12)+τ HCCC(13) |
| 467(w) | 458(w) | 472 | 453 | τ HNNC(76)+τ HNCN(11) |
| - | 421(w) | 443 | 426 | β CCC(24)+β NCN(32) |
| - | 392(w) | 417 | 400 | τ CCCC(63) |
| - | 369(m) | 379 | 364 | γ BrC(36)+β NNC(14) |
| - | 332(w) | 359 | 345 | τ NNCC(-27)+OUT BrCCC(30)+τ CCCC(20) |
| - | 283(m) | 278 | 267 | τ NCCC(11)+τ NCNN(-29)+τ CNNC(-11)+OUT CCCC(13)+τ NNCC(14) |
| - | 266(m) | 277 | 266 | β BrCC(49)+β CCC(-10)+β CNN(12)+β NCN(11) |

| | | | | |
|---|---|---|---|---|
| - | 231(m) | 211 | 202 | γ CC(15)+γ BrC(26)+β NNC(11)+β CCC(12) |
| - | 177(w) | 181 | 174 | τ NCCC(15)+τ CNNC(-16)+OUT BrCCC(26)+τ NNCC(20) |
| - | 157(m) | 179 | 172 | β BrCC(-30)+β CNN(26)+β CCC(-17)+β NCN(10) |
| - | - | 80 | 77 | τ NCNN(14)+τ CNNC(33)+τ CCCC(18)+ BrCCC(10) |
| - | - | 58 | 56 | β NCC(32)+β CNN(11)+β NNC(21)+β CCC(23) |

[a]γ-stretching,$\gamma_a$-Symmetrical stretching,$\gamma_{as}$-asymmetrical stretching, β-inplane bending ,ω- outplane bending, τ-torsion, vs-very strong, s- strong, m-medium, w-weak.



***3.5.2.5. C-N vibrations***

The C-N stretching frequency is a very tough task since it falls in a composite region of the vibrational spectrum, i.e., mixing of several bands are possible in this region [28] assigned C-N stretching absorption in the region 1386-1266 $cm^{-1}$ for the aromatic compound. The bands observed at 1708(vs), 1607(s), 1356(s), 955(w) $cm^{-1}$ in FT-IR and 1707(w), 1610(vs), 1359(w), 956(w) $cm^{-1}$ in FT-Raman are assigned as N-C stretching vibrations. The theoretically scaled wavenumbers calculated at 1712, 1600, 1344 and 955$cm^{-1}$ (mode no 49, 48, 41, 30) are assigned as C-N stretching vibrations with PED contribution of 38, 68, 38 and 62% respectively.

**3.6. Electronic properties**

The observed and computed UV-Visible comparison spectrum of title molecule is shown in Fig. 3.5. Absorption maximum ( $\lambda_{max}$) of our title molecule is calculated by TD-DFT/B3LYP method with 6-311++G(d,p)

basis set. The calculation of molecular orbital geometry shows that the visible absorption maxima of the 4BSC resemble the electronic transition from HOMO to LUMO. The experimental UV-Vis spectra of 4BSC molecule were used to DMSO solvent and theoretical calculations were carried out in the DMSO and gas phase. The electronic transition amid frontier orbitals such as transformation from HOMO to LUMO as can be seen through the UV-Vis spectra absorption values 294 (Experimental), 302.26 (DMSO) and 298.99 nm (gas phase) are listed in Table 3.3. The $\lambda_{max}$ is a function of substitution, the more electrons pushed into the ring, the larger $\lambda_{max}$ [34].

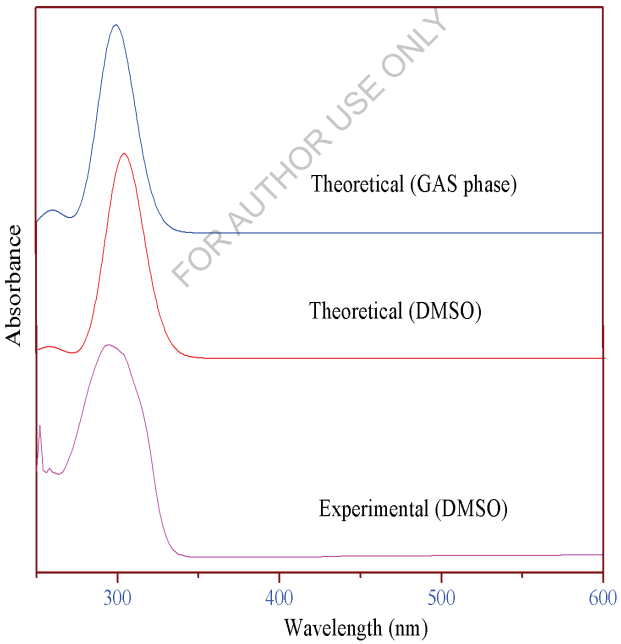



**Fig. 3.5.** UV–Vis spectra of 4BSC (Experimental, Theoretical (DMSO, GAS phase))

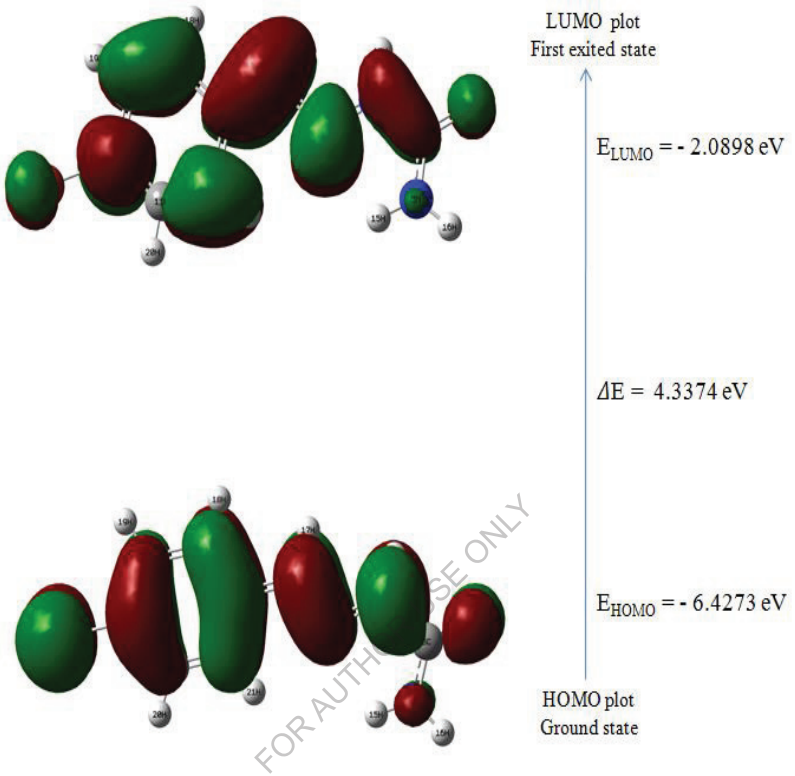



**Fig. 3.6.** Atomic orbital HOMO – LUMO composition of the frontier molecular orbital for 4BSC

The calculated results involving the wavelength, and oscillating strength and band gap energy are carried out compared with experimental data. The band gap energy was calculated using the formula, $E = hc/\lambda$. Here h and c are constant; λ is the cut off wavelength. The energy difference between HOMO and LUMO orbits is called as band gap that is important stability for structure [35]. HOMO and LUMO is related to the ionization potential and electron affinity.

**Table 3.3**

The UV–vis wavelength (λ), band gap energy (ΔE), and oscillator strength (f) for 4BSC calculated by TD-DFT/B3LYP method

| **Experimental** | | **TD-DFT/B3LYP-311++G(d,p)** | | | | | |
|---|---|---|---|---|---|---|---|
| **$\lambda_{max}$ (nm)** | **Band gap (ev)** | **DMSO** | | | **Gas phase** | | |
| | | **$\lambda_{cal}$ (nm)** | **Energy ($cm^{-1}$)** | ***f*** | **$\lambda_{cal}$ (nm)** | **Energy ($cm^{-1}$)** | ***f*** |
| 294 | 4.228 | 302.26 | 33037 | 0.859 | 298.99 | 33445 | 0.699 |
| | | 257.14 | 38889 | 0.048 | 259.87 | 38480 | 0 |
| | | 245.94 | 40659 | 0 | 259.67 | 38510 | 0.076 |



**Table 3.4**

Calculated energy values of title compound by B3LYP/6-311++G(d,p) method.

| **Basis set** | **B3LYP/6-311++G(d, p)** |
|---|---|
| $E_{HOMO}$ (eV) | -6.4273 |
| $E_{LUMO}$ (eV) | -2.0898 |
| Ionization potential | 6.4273 |
| Electron affinity | 2.0898 |
| Energy gap (eV) | 4.3374 |
| Electronegativity | 4.2585 |
| Chemical potential | -4.2585 |
| Chemical hardness | 2.1687 |
| Chemical softness | 0.2305 |
| Electrophilicity index | 4.1811 |

The HOMO and LUMO energies, the energy gap (ΔE), the ionization potential (I), the electron affinity (A), the absolute electronegativity (χ), the absolute hardness (η) and softness (S) for the 4BSC molecule have been calculated at B3LYP/6-311++G(d,P) basis set(Fig 3.6) and the result are given in the Table 3.4. By using HOMO and LUMO energy values for a molecule, electronegativity and chemical hardness can be calculated as follow:

$\chi =$ —— (Electronegativity)

(3.1)

$\mu =$ $\frac{(I \quad A)}{}$ (Chemical potential)

(3.2)

$\eta =$ —— (Chemical hardness)

(3.3)

s=1/2η (chemical softness), $\omega=\mu^2/2\eta$ (Electrophilicity index)



Where I and A are ionization potential and electron affinity; $I= - E_{HOMO}$ and $A= - E_{LUMO}$ respectively [36]. The energy gap of title molecule is calculated experimentally by UV-Visible spectrum is 4.2283 eV, the Energy gap is calculated theoretically by TD-DFT (DMSO and gas phase) method is 4.1069, 4.1577 eV and from HOMO-LUMO diagram is 4.3374 eV. All energy gap values are very well executed which are listed in Table 3.3 and 3.4.

### 3.7. NMR spectra

The NMR spectroscopy is one of the most important techniques for the structural conformational analysis for the organic compounds. We used this technique ($^1$H and $^{13}$C NMR) due to the useful, common to have more

information about the studied molecule. The theoretical $^{1}H$ and $^{13}C$ chemical shifts in calculated by using gauge invariant atomic orbital (GIAO) and 6-311++G(d,p) basis set. The GIAO [37, 38] method was one of the most common approaches for calculating isotropic nuclear magnetic shielding tensors. The experimental and theoretical values for carbon ($^{13}C$) and proton ($^{1}H$) NMR of the title compound are given in Table 3.5. The experimental and theoretical $^{13}C$ and $^{1}H$ NMR spectra in DMSO solvent are shown in Figs. 3.7-3.10.

There are eight carbon atoms (in the ring) in the 4BSC molecule. Organic molecules, the $^{13}C$ NMR chemical shift appear in the range > 100 ppm [39-41]. The calculated chemical shift values by the DFT theoretical method values well coincides with the experimental values. In this work, aromatic carbons are observed from 122.15 to 156.78 ppm in carbon ($^{13}C$) NMR spectrum for the 4BSC molecule. The nitrogen (N) atom's high electronegative property polarizes the electron distribution in its bond to the adjacent carbon atom and decreases the electron density at the bridge for the title molecule. Therefore, the chemical shift value seems to be moderately high for the title molecule under study at 138.07 and 156.78 ppm ($C_6$, $C_3$). There are also eight hydrogen atoms (ring, NH and $NH_2$ group) in the title molecule. The $^{1}H$ NMR observed chemical shift values at 10.33, 7.8, 7.69, 7.67, 7.57, 7.55, 6.55, 6.55ppm with the theoretical chemical shift values at 8.4615, 7.2658, 7.2646, 7.2417, 7.2005, 6.9458, 5.4653, 4.6595 ppm for $H_{21}$, $H_{20}$, $H_{17}$, $H_{19}$, $H_{14}$, $H_{18}$, $H_{15}$ and $H_{16}$. The predicted all chemical shift values are in good agreement with the experimental values.

### 3.8. Hyperpolarizability calculations

The first order hyperpolarizability ($\beta_{total}$) of the 4BSC along with related properties (μ, α and Δα) are investigated by DFT/ Becke-3-Lee-Yang-Parr method with 6-311++G(d,P) basis set, is based on the finite-field approach.

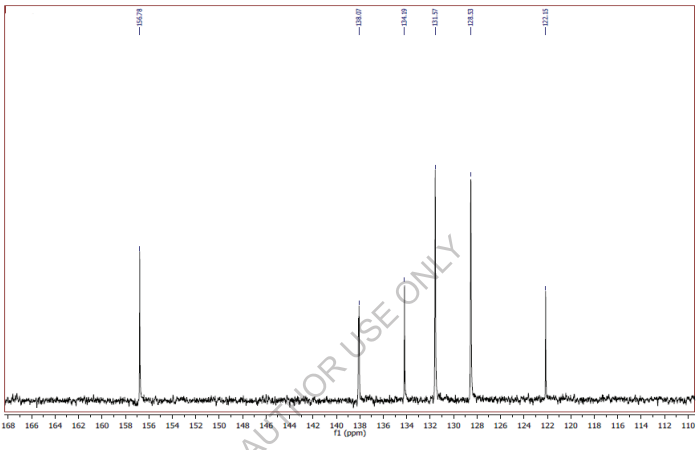



**Fig. 3.7.** $^{13}$C NMR spectrum of 4BSC (Experimental)

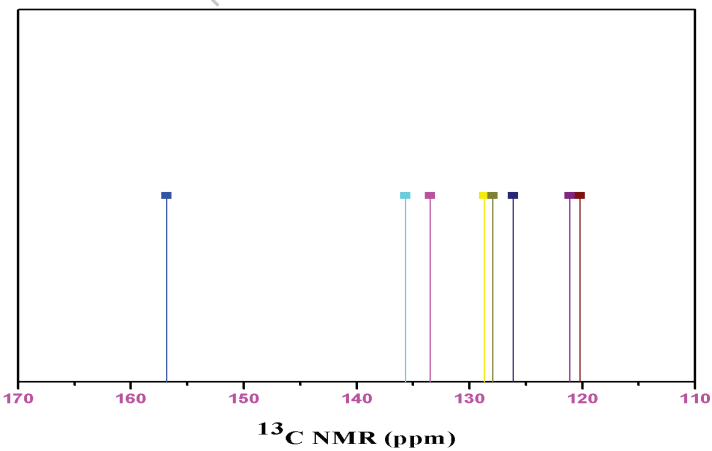


**Fig. 3.8.** $^{13}$C NMR spectrum of 4BSC (Theoretical)

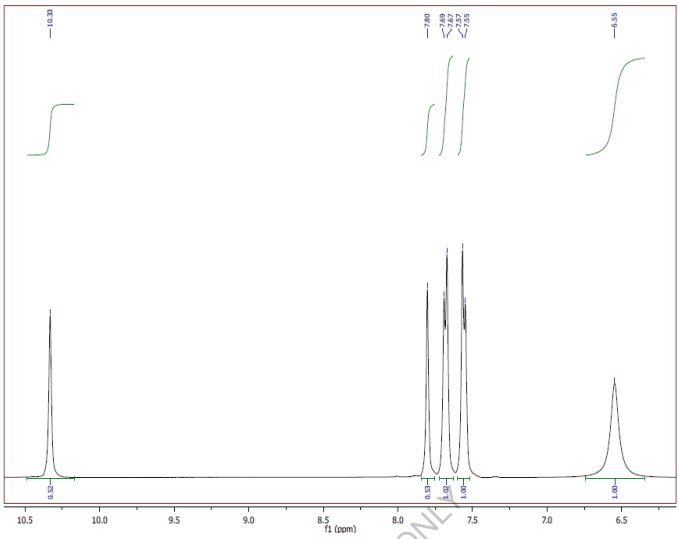


**Fig. 3.9**. $^{1}$H NMR spectrum of 4BSC (Experimental)



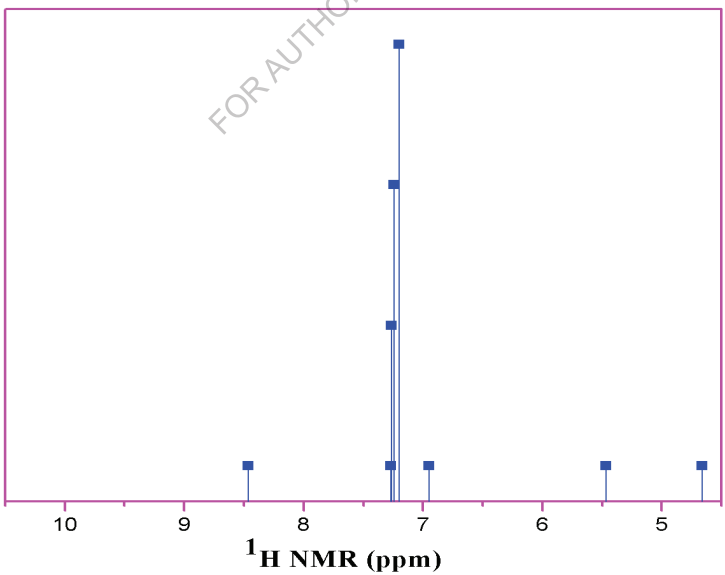


**Fig. 3.10.** $^{1}$H NMR spectrum of 4BSC (Theoretical)

**Table 3.5**

Theoretical and experimental $^{13}C$ and $^{1}H$ isotropic chemical shifts [with respect to TMS, all values in ppm] for 4BSC molecule

| Atom | Chemical shifts (ppm) | |
|---|---|---|
| | Experimental | B3LYP/6-311++G(d,p) |
| $C_3$ | 156.78 | 156.8014 |
| $C_6$ | 138.07 | 135.6601 |
| $C_{10}$ | 134.19 | 133.4618 |
| $C_{11}$ | 131.57 | 128.6918 |
| $C_9$ | 128.53 | 127.9113 |
| $C_8$ | 128.53 | 126.1072 |
| $C_{12}$ | 122.15 | 121.0872 |
| $C_7$ | 122.15 | 120.2149 |
| $H_{21}$ | 10.33 | 8.4615 |
| $H_{20}$ | 7.8 | 7.2658 |
| $H_{17}$ | 7.69 | 7.2646 |
| $H_{19}$ | 7.67 | 7.2417 |
| $H_{14}$ | 7.57 | 7.2005 |
| $H_{18}$ | 7.55 | 6.9458 |
| $H_{15}$ | 6.55 | 5.4653 |
| $H_{16}$ | 6.55 | 4.6595 |



NLO activity arises from the interactions of electromagnetic fields in different media to produce latest fields changed in phase, frequency, amplitude or other propagation characteristics' from the incident fields. Nonlinear optical effects (NLO) is at the forefront of the recent investigation because of its significance in bestowing the key functions of optical modulation, optical logic, optical memory, optical switching and frequency shifting for the presently growing technologies in areas such as telecommunications, signal processing, and optical interconnections

[42,43]. The non-linear optical response of an isolated molecule in an electric field $E_i$ (ω) can be represented as a Taylor series enlargement of the total dipole moment, $\mu_{tot}$, induced by the field:

$$\mu_{tot} = \mu_0 + \alpha_{ij}E_j + \beta_{ijk}E_jE_k + \ldots, \quad (3.4)$$

Where α is the linear polarizability, $\mu_0$ is the permanent dipole moment and $\beta_{ijk}$ are the first hyperpolarizability tensor components. The isotropic (or average) linear polarizability is defined as:

$$\alpha = \frac{\alpha_{xx} + \alpha_{yy} + \alpha_{zz}}{3} \quad (3.5)$$

The first order hyperpolarizability is a third rank tensor that can be described by 3×3×3 matrix. The 27 components of 3D matrix can be abridged to 10 components owing to the Kleinman symmetry [44]

Components of the first hyperpolarizability can be reckoned using the following equation:

$$\beta_i = \beta_{iii} + \sum_{i \neq j}(\beta_{ijj} + \beta_{jij} + \beta_{jji}) \quad (3.6)$$

Using the x, y and z components of β, the magnitude of the first hyperpolarizability tensor can be calculated by:

$$\beta_{tot} = \sqrt{(\beta_x^2 + \beta_y^2 + \beta_z^2)} \quad (3.7)$$

The entire equation for reckoning the magnitude of β from Gaussian 09W program output is given a follows:

$$\beta_{tot} = \sqrt{(\beta_{xxx} + \beta_{xyy} + \beta_{xzz})^2 + (\beta_{yyy} + \beta_{yzz} + \beta_{xxy})^2 + (\beta_{zzz} + \beta_{xxz} + \beta_{yyz})^2} \quad (3.8)$$

The calculations of the total molecular dipole moment (μ), linear polarizability (α) and first-order hyperpolarizability (β) from the Gaussian output have been explained in detail previously [45], and DFT has been widely used as an efficient method to investigate the organic NLO materials [46,47]. In addition, the polar properties of the 4BSC were computed at the DFT (B3LYP)/6-311++G(d,p) level using Gaussian 09W program package.

**Table 3.6**

The values of calculated dipole moment μ (D), polarizability ($\alpha_0$), first order hyperpolarizability (βtot) components of 4BSC.

| **Parameters** | **B3LYP/6-311++G(d,p)** | **Parameters** | **B3LYP/6-311++G(d,p)** |
|---|---|---|---|
| $\mu_x$ | -0.9513 | $\beta_{xxx}$ | -638.6300 |
| $\mu_y$ | 0.0589 | $\beta_{xxy}$ | -5.0377 |
| μz | 0 | $\beta_{xyy}$ | -33.1800 |
| μ(D) | 0.9532 | $\beta_{yyy}$ | -186.7300 |
| $\alpha_{xx}$ | 259.2700 | $\beta_{zxx}$ | -71.1250 |
| $\alpha_{xy}$ | -32.6840 | $\beta_{xyz}$ | 32.0000 |
| $\alpha_{yy}$ | 139.8800 | $\beta_{zyy}$ | 7.0182 |
| $\alpha_{xz}$ | 0 | $\beta_{xzz}$ | -135.2300 |
| $\alpha_{yz}$ | 0 | $\beta_{yzz}$ | 36.1870 |
| $\alpha_{zz}$ | 74.7110 | $\beta_{zzz}$ | 0 |
| $\alpha_0$ (e.s.u) | $2.3409X10^{-23}$ | βtot (e.s.u) | $7.1223X10^{-30}$ |
| α (e.s.u) | $7.0759X10^{-23}$ | | |



Urea is the prototypical molecule utilized in investigating of the NLO properties of the compound. For this reason, urea was used often as a threshold value for comparative purpose. The calculated dipole moment

and hyperpolarizability values obtained from B3LYP/6-311++G(d,p) methods are collected in Table 3.6. The first order hyperpolarizability of 4BSC with B3LYP/6-311++G(d,p) basis set is 7.1223 x $10^{-30}$ nineteen times greater than the value of urea ($\beta_o$ = 0.372 x $10^{-30}$ esu). From the computation, the high values of the hyperpolarizabilities of 4BSC are probably attributed to the charge transfer existing amid the benzene rings within the molecular skeleton. This is evidence for the nonlinear optical (NLO) property of the molecule.

### 3.9. Donor- acceptor interactions

The NBO analyzes aid and more efficient method for studying intra and inter molecular bonding and interaction among bonds, and also provides a convenient basis for inspecting charge transfer or conjugative interactions in the molecular system. Some electron donor orbital, acceptor orbital and the overlap stabilization energy resulting from the second-order micro-disturbance theory are reported [48-50]. NBO studies provide the most precise possible 'natural Lewis structure' picture of ϕ because all orbital details are mathematically chosen to include the highest possible percentage of the electron density. For each donor (I) and acceptor (j), the stabilization energy E(2) associated with the delocalization i, j estimated as:



$$E_2 = \Delta E_{ij} = q_i \frac{F(i,j)^2}{E_i - E_j} \quad (3.9)$$

Where $q_i$ is the donor orbital occupancy, $E_i$ and Ej are diagonal elements and F(i,j) is the off diagonal NBO Fock matrix elements.

**Table 3.7**

Second order perturbation theory analysis of Fock matrix in NBO basis for 4BSC

| Donor (i) | Type | ED/e | Acceptor (i) | ED/e | [a]E(2)(KJ mol$^{-1}$) | [b]E(J)-E(i) (a.u.) | [c]F(I,j) (a.u.) |
|---|---|---|---|---|---|---|---|
| $N_2$-$C_6$ | σ | 1.985 | $N_1$-$C_3$ | 0.0720 | 1.84 | 1.37 | 0.045 |
| | | | $C_6$-$C_7$ | 0.0315 | 4.37 | 1.57 | 0.074 |
| | | | $C_7$-$C_8$ | 0.0299 | 2.75 | 1.58 | 0.059 |
| $N_2$-$C_6$ | π | 1.921 | $C_7$-$C_8$ | 0.3950 | 13.20 | 0.39 | 0.070 |
| $C_7$-$C_8$ | π | 1.622 | $N_2$-$C_6$ | 0.2276 | 27.97 | 0.28 | 0.082 |
| | | | $C_9$-$C_{10}$ | 0.3848 | 24.32 | 0.30 | 0.076 |
| | | | $C_{11}$-$C_{12}$ | 0.2814 | 20.70 | 0.31 | 0.074 |
| $C_8$-$C_9$ | σ | 1.965 | $C_9$-$C_{10}$ | 0.0302 | 6.12 | 1.39 | 0.082 |
| | | | $C_{10}$-$Br_{13}$ | 0.0385 | 6.06 | 0.85 | 0.064 |
| $C_8$-$H_{18}$ | σ | 1.976 | $C_7$-$C_{12}$ | 0.0339 | 5.07 | 1.17 | 0.069 |
| $C_9$-$C_{10}$ | π | 1.676 | $C_7$-$C_8$ | 0.3950 | 18.95 | 0.33 | 0.072 |
| | | | $C_{11}$-$C_{12}$ | 0.2814 | 20.82 | 0.33 | 0.075 |
| $C_{11}$-$C_{12}$ | π | 1.673 | $C_7$-$C_8$ | 0.3950 | 22.21 | 0.31 | 0.076 |
| | | | $C_9$-$C_{10}$ | 0.3848 | 22.27 | 0.30 | 0.074 |
| $N_1$ | LP(1) | 1.692 | $N_2$-$C_6$ | 0.2276 | 30.86 | 0.29 | 0.086 |
| | | | $C_3$-$O_4$ | 0.3721 | 52.50 | 0.30 | 0.114 |
| $N_2$ | LP(1) | 1.914 | $C_6$-$H_{17}$ | 0.0410 | 10.27 | 0.76 | 0.080 |
| $O_4$ | LP(2) | 1.855 | $N_1$-$C_3$ | 0.0720 | 24.33 | 0.68 | 0.117 |
| | | | $C_3$-$N_5$ | 1.0644 | 23.56 | 0.69 | 0.116 |
| $N_5$ | LP(1) | 1.789 | $C_3$-$O_4$ | 0.3721 | 54.81 | 0.28 | 0.116 |
| $Br_{13}$ | LP(3) | 1.931 | $C_9$-$C_{10}$ | 0.3848 | 10.49 | 0.32 | 0.057 |
| $N_2$-$C_6$ | π* | 0.227 | $C_7$-$C_8$ | 0.3950 | 76.16 | 0.04 | 0.083 |
| $C_9$-$C_{10}$ | π* | 0.384 | $C_7$-$C_8$ | 0.3950 | 250.04 | 0.02 | 0.094 |
| | | | $C_{11}$-$C_{12}$ | 0.2814 | 204.06 | 0.02 | 0.090 |

[a]$E^{(2)}$ means energy of hyper conjugative interaction (stabilization energy)

[b]Energy difference between donor and acceptor i and j NBO orbitals.

[c]F(i,j) is the Fock matrix element between i and j NBO orbitals

The second order fock matrix was carried out to evaluate the donor-acceptor interactions in the NBO analysis [51]. The higher the E(2) value, the molecular interaction between electron donors and electron acceptors is more intensive and the greater the extent of conjugation of the entire system. Delocalization of electron density amid occupied Lewis-type (bond or lone pair) NBO orbitals and properly unoccupied (antibond or Rydgberg) non-Lewis NBO orbitals resemble to a stabilizing donor-acceptor interaction. NBO analysis has been performed on the title molecule at the B3LYP/6-311++G(d,p) level in order to elucidate the intra molecular, rehybridization and delocalization of electron density within the molecule. The strong intramolecular hyper conjugative interaction of the $\sigma$ and $\pi$ electrons of C - C to the anti C - C bond of the ring leads to stabilization of some part of the ring as evident from Table 3.7. The strong intramolecular hyperconjugative interaction of $\sigma$ ($C_7 - C_8$) distributes to $\sigma^*(C_6 - C_7, C_7 - C_{12}$ and $C_8 - C_9$ of the ring. On the other hand, side the $\pi(C_7 - C_8)$ in the ring conjugate to the anti-bonding orbital of $\pi^*(N_2 - C_6)$, $\pi^*(C_9 - C_{10})$ and $\pi^*(C_{11} - C_{12})$ which leads to strong delocalization of 27.97, 24.32 and 20.70 kJ/mol respectively. The $\sigma$ system shows some contribution to the delocalization corresponds to the donor - acceptor interactions are $(N_1 - N_2) \rightarrow (C_3 - O_4)$, $(C_6 - C_7)$, $(N_1 - C_3) \rightarrow (N_2 - C_6)$, $(N_1 - H_{14}) \rightarrow (C_3 - N_5)$, $(N_2 - C_6) \rightarrow (N_1 - C_3)$, $(C_6 - C_7)$ $(C_7 - C_8)$ bondings are shown in the Table 3.7. LP (1) $N_5$ antibonding acceptor $\pi^*(C_3 - O_4)$ of the 4BSC energy of 54.81 kJ/mol. The most important interaction energy, related to the resonance in the molecule is electrons donating from antibonding donor $\pi^*(C_9 - C_{10})$ to the antibonding acceptor $\pi^*(C_7 - C_8)$,

$\pi^*(C_{11} - C_{12})$ with large stabilization energy of 250.04, 204.06 kJ/mol as shown in Table 3.7.

### 3.10. Other molecular properties

#### 3.10.1. Molecular electrostatic potentials (MEP)

The molecular electrostatic potential (MEP) is related to the electronic density and is a very useful descriptor for determining sites for electrophilic and nucleophilic reactions as well as hydrogen bonding interactions [52-54]. Molecular electrostatic potential (MEP) simultaneously displays molecular shape, size, and electrostatic potential in terms of colour grading. MEPs map has been found to be a very helpful tool in the analysis of the correlation amid molecular structures with its physiochemical property relationship, including biomolecules and drugs [55]. MEPs map of the (E)-1-(4-bromobenzylidene)semicarbazide (4BSC) generated at the optimized geometry of the title molecule using GaussView 5.0 program is shown in Fig 3.11.



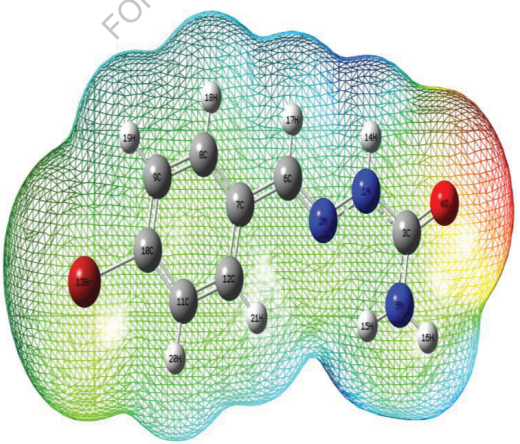

**Fig. 3.11**. Total electron density mapped with molecular electrostatic potential surface of 4BSC

The various values of the electrostatic potential at the surface are represented by various colours. The colour scheme for the MEP surface is red-electron rich, partially negative charge (electrophilic reactive center); blue-electron deficient, partially positive charge; light blue-slightly electron deficient region (nucleophilic reactive center); yellow-slightly electron rich region; green- neutral, respectively. The potential increases in the order red < orange < yellow < green < cyan < blue. It can be seen that the negative regions are mainly over the $O_4$ atoms. Negative (red colour) and positive (blue) regions of electrostatic potential are associated with electrophilic and nucleophilic reactivity. The majority of light green region MEP surface resemble a potential halfway between two extremes red and dark blue colour. The negative molecular electrostatic potential resembles an attraction of the proton by the evaluate electron density in the molecule (shades of red), the positive electrostatic potential corresponds to the repulsion of the protons by the atomic nuclei (shades of blue). According to these calculated results, the MEP map illustrates that the negative potential sites are on oxygen and nitrogen atoms and the positive potential sites as well are around the hydrogen atoms. These active sites found to be clear evidence of biological activity in the title compound.



**3.10.2. Antimicrobial activity**

Synthesized compound was screened for its in-vitro antimicrobial activity against bacterial and fungal strains by agar well diffusion method. The activity was determined by measuring the inhibition zone diameter values (mm/ml) of the investigated compound and antimicrobial activity of 4BSC against bacterial and fungal pathogens are shown in Fig. 3.12 and 3.13. The antimicrobial and solvent sensitivity test for both bacterial and fungal strains were measured and mentioned in the Tables 3.8(a) and

3.8(b). It is noted that the solvent itself has no activity on the microbes. 4BSC dissolved at two concentrations (100 µl and 200 µl ) were screened for their antibacterial activity against four bacterial strains such as, *Enterobacter*, *Bacillus subtillis*, *Escherichia coli* and *K. pneumoniae* and three fungal strains such as, *Candida albicans*, *A.niger* and *A.fumicatus* which were selected for the present investigation by the agar well diffusion method. From Tables 3.8(a) and 3.8(b) shows a good activity of 4BSC against the three fungal strains *Candida albicans*, *A.niger* and *A.fumicatus*. Moreover, it is found that synthesized compound exhibits higher antifungal activity than antibacterial activity and the highest activity is against *A.niger*.

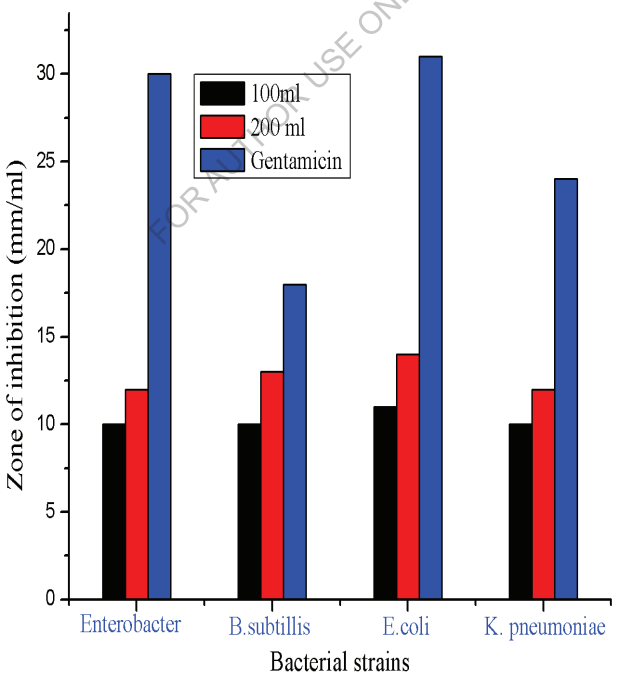



**Fig. 3.12.** A bar diagram for the antibacterial activity of 4BSC.

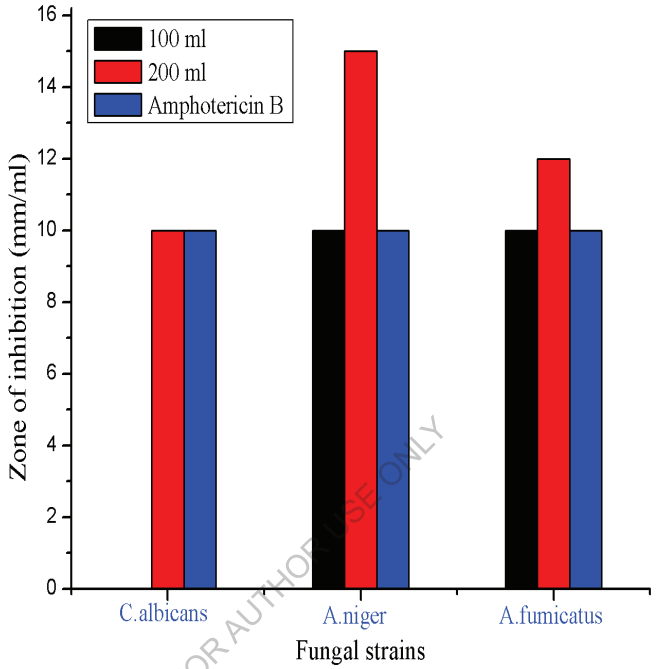



**Fig. 3.13.** A bar diagram for the antifungal activity of 4BSC.

**Table 3.8(a)** Antibacterial activity of DMSO extracts

| **Bacterial pathogen** | **DMSO Extract added and Zone of inhibition (mm/ml)** | | | |
|---|---|---|---|---|
| | **100 µl** | **200 µl** | **DMSO** | **Gentamicin** |
| *Enterobacter* | 10 | 12 | - | 30 |
| *Bacillus subtillis* | 10 | 13 | - | 28 |
| *E.coli* | 11 | 14 | - | 31 |
| *K. pneumoniae* | 10 | 12 | - | 24 |

**Table 3.8(b)** Antifungal activity of DMSO extracts

| Fungal pathogen | DMSO Extract added and Zone of inhibition (mm/ml) | | | |
|---|---|---|---|---|
| | **100 µl** | **200 µl** | **DMSO** | **Amphotericin B** |
| *Candida albicans* | - | 10 | - | 10 |
| *A.niger* | 10 | 15 | - | 10 |
| *A.fumicatus* | 10 | 12 | - | 10 |

### 3.10.3. Molecular docking study

AutoDock suite 4.2.6 is a recently been used as an expedient to ol to get insights into the molecular mechanism of protein-ligand interactions, bind to a receptor of known three-dimensional structure. With the aim to investigate the binding mode, a molecular modeling study was performed using AutoDock Tools 1.5.6 for docking. The synthesis molecule was selected to be docked into the active site of three receptors 3GFX [56], 4HOE [57] and 3EQA [58] of antimicrobial proteins which were downloaded from RCSB protein data bank. The ligand was docked into the functional sites of the respective proteins individually and the docking energy was examined to achieve a minimum value. AutoDock results indicate the binding position and bound conformation of the peptide, together with a rough estimate of its interaction. Docked conformation which had the lowest binding energy was chosen to investigate the mode of binding. The molecular docking binding energies (kcal/mol) and inhibition constants (µm) were also obtained and listed in Table 3.9.

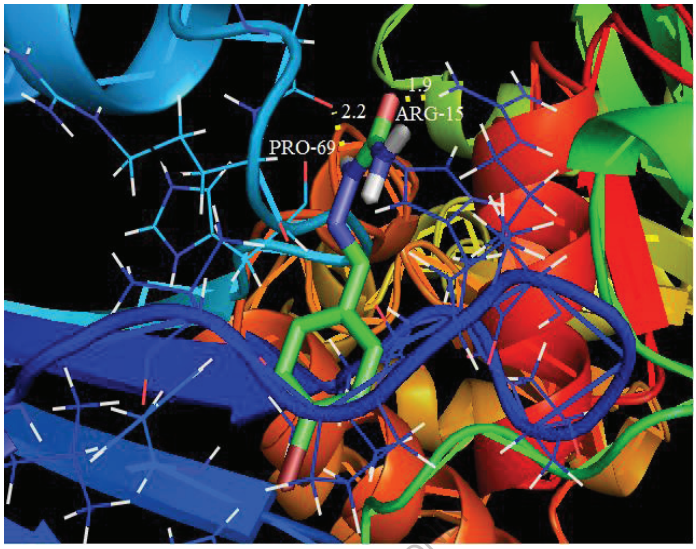


**Fig. 3.14.** Docking and Hydrogen bond interactions of 4BSC with chain A of 3GFX protein structure

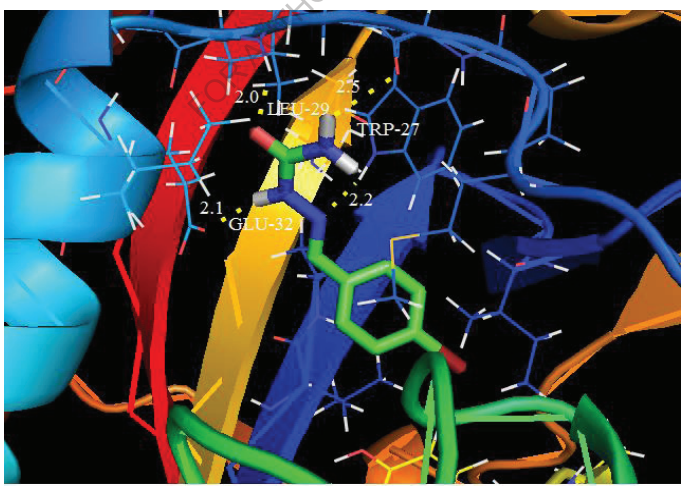


**Fig. 3.15.** Docking and Hydrogen bond interactions 4BSC with chain A of 4HOE protein structure

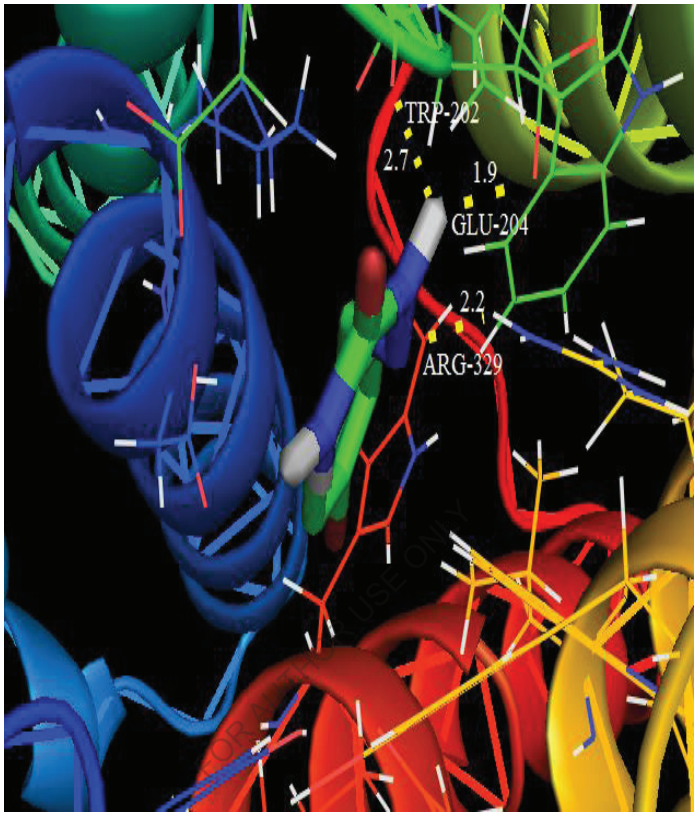


**Fig. 3.16.** Docking and Hydrogen bond interactions 4BSC with chain A of 3EQA protein structure

Among them, 4HOE exhibited the lowest free energy at −6.98 kcal/mol and most docked inhibitors interacted with the ligand within the 4HOE binding site. They exhibited up to four N H· · ·O hydrogen bonds involving LEU 29, GLU 32, TRP 27and TRP 27 with RMSD being 7.65˚A. The docking simulation shows the binding mode of the 4BSC into 34HOE. The 4BSC ligand interacts with different receptors are shown in Figs. 3.14-3.16.

**Table 3.9**

Hydrogen bonding and molecular docking with antimicrobial protein targets

| Protein (PDB ID) | Bonded residues | No. of hydrogen bond | Bond distance (Å) | Estimated Inhibition Constant (μm) | Binding energy (kcal/mol) | Reference RMSD (Å) |
|---|---|---|---|---|---|---|
| 3GFX | PRO 69 | 2 | 2.2 | 20.12 | -6.41 | 53.18 |
| | ARG 15 | | 1.9 | | | |
| 4HOE | LEU 29 | 4 | 2.0 | 7.65 | -6.98 | 28.56 |
| | GLU 32 | | 2.1 | | | |
| | TRP 27 | | 2.2 | | | |
| | TRP 27 | | 2.5 | | | |
| 3EQA | GLU 204 | 3 | 1.9 | 73.94 | -5.64 | 24.44 |
| | ARG 329 | | 2.2 | | | |
| | TRP 202 | | 2.7 | | | |



### 3.10.4. Thermodynamical properties

On the basis of vibrational investigations at B3LYP/6-311++G(d,p) basis set, the standard statistical thermodynamic properties such as heat capacity $\left(C^{0}_{p,m}\right)$, entropy $\left(S^{0}_{m}\right)$ and enthalpy changes $\left(H^{0}_{m}\right)$ for the (E)-1-(4-bromobenzylidene) semicarbazide (4BSC) were calculated using perl script THERMO.PL [59] and are shown in Table 3.10. From Table 3.10 shows, the thermodynamic functions are all values increasing with the temperature ranging from 100 to 1000K due to the fact that the molecular vibrations intensities increase with temperature. The correlation equation among heat capacity, entropy, enthalpy changes with temperatures were fitted by quadratic formulas and the corresponding fitting factors ($R^2$) these

thermodynamic properties are 0.99956, 0.99984 and 0.99938 respectively. The correlations plot is shown in Fig. 3.17. The corresponding fitting equations are follows:

$$\left(C\,^{0}_{p,m}\right) = 25.9038 + 0.6436T - 2.8331 \times 10^{-4}T^{2} \quad (R^{2} = 0.99956) \quad (3.10)$$

$$\left(S\,^{0}_{m}\right) = 258.885 + 0.7796T - 2.1163 \times 10^{-4}T^{2} \quad (R^{2} = 0.99984) \quad (3.11)$$

$$\left(H\,^{0}_{m}\right) = -8.2479 + 0.09863T - 1.6577 \times 10^{-4}T^{2} \quad (R^{2} = 0.99938) \quad (3.12)$$

The thermodynamic functions grant very useful information for the further study on the 4BSC. They can be used to calculate the other thermodynamic energy according to the relationship of thermodynamic functions and evaluate directions of chemical behavior according to the second law of thermodynamics in the thermochemical field [60]. Notice: All thermodynamic computation were done in the gas phase and without be used in the solution.



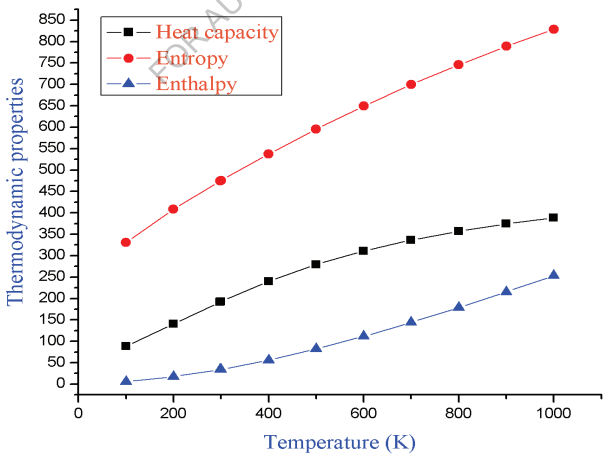


**Fig . 3.17.** Correlation plot of thermodynamic properties at different temperature of the 4BSC compound.

**Table 3.10**

Temperature dependence of thermodynamic properties of 4BSC at B3LYP /6-311++G(d,p)

| T(K) | $C^{0}_{p,m}$ (J/ mol K) | $S^{0}_{m}$ (J/ mol K) | $H^{0}_{m}$ (kJ/ mol) |
|---|---|---|---|
| 100 | 88.56 | 331.14 | 6.210 |
| 200 | 140.79 | 408.43 | 17.66 |
| 298 | 191.97 | 474.26 | 34.00 |
| 300 | 192.9 | 475.45 | 34.36 |
| 400 | 240.11 | 537.58 | 56.07 |
| 500 | 279.44 | 595.54 | 82.12 |
| 600 | 311.04 | 649.39 | 111.7 |
| 700 | 336.41 | 699.31 | 144.12 |
| 800 | 357.08 | 745.63 | 178.83 |
| 900 | 374.21 | 788.7 | 215.42 |
| 1000 | 388.6 | 828.9 | 253.58 |

## Reference


[1] J.D. Warren, D.L. Woodward, R.T. Hargreaves, 4-Substituted semicarbazones of mono- and dichlorobenzaldehydes as antihypertensive agents, J. Med. Chem. 20(11) (1977) 1520-1521.

[2] S. Chandra , L.K. Gupta, Spectroscopic and biological studies on newly synthesized nickel(II) complexes of semicarbazones and thiosemicarbazones, Spectrochim. Acta A 62 (2005) 1089-1094.

[3] V.K. Jain, A. Handa, R. Pandya, P. Shrivastav, Y.K. Agrawal, Polymer supported calix[4]arene-semicarbazone derivative for separation and preconcentration of La(III), Ce(III), Th(IV) and U(VI). React. Funct. Polym. 51 (2012) 101–110.

[4] N. Fahmi, R.V. Singh, Spectroscopic, antifungal and antibacterial studies of some manganese heterochelates, J. Indian Chem. Soc. 73 (1996) 257–259.

[5] A. Dhandapani , S. Manivarman, S. Subashchandrabose, H. Saleem, Molecular structure and vibrational analysis on (E)-1-(3-methyl-2,6-diphenyl piperidin-4-ylidene) semicarbazide, J. Mol. Struct. 1058 (2014) 41-50.

[6] R. Sharma, S. Mudgal, B. Shrivastava, P. Sharma, Synthesis, characterization & biological evaluation of newer 4-(4-substituted aryl) semicarbazones as anticonvulsant and anti-microbial agents, Indo American. J. Pharm Rech. 3 (2013) 5522-5540.

[7] G. Saravanan, V. Alagarsamy, C. Rajaram Prakash, Synthesis, characterization and in vitro antimicrobial activity of some 1-(substitutedbenzylidene)-4-(4-(2-(methyl/phenyl)-4-oxoquinazolin-3(4H) yl)phenyl)semicarbazide derivatives, J. Saudi Chem. Soc. 19 (2015) 3-11.

[8] Abelardo P. Martinez, William W. Lee, Some Semicarbazones and Thiosemicarbazones, J. Med. Chem. 10 (6) (1967) 1192-1192.

[9] M. Ibrahim, Molecular spectroscopic study of acid treated fenugreek seeds, Spectrochim. Acta A 77 (2010) 1034-1038.

[10] M. Ibrahim, A. Aziz Muhmouda, O. Osmana, A. Refaata, M. El-Sayed, Molecular spectroscopic analysis of nano-chitosan blend as biosensor, Spectrochim. Acta A 77 (2010) 802-806.

[11] S. S. Gupta, A. Marchno, R. D. Pradhan, C. F. Desai, J. Melikechi, Pump-probe thermal lens near-infrared spectroscopy and Z-scan study of zinc (tris) thiourea sulfate, J. Appl. Phys. 89 (2001) 4939-4943.

[12] S. P. Karna, Electronic and nonlinear optical materials: The role of theory and modeling, J. Phys. Chem. A104 (2000) 4671-4673.

[13] D. R. Kanis, M. A. Ratner, T. J. Marks, Design and construction of molecular assemblies with large second-order optical nonlinearities. Quantum chemical aspects, Chem. Rev. 94 (1994), 195-242.

[14] H. S. Nalwa, S. Miyata, Nonlinear optical properties of organic molecules and polymers, CRC Press, Boca Raton, FL, 1996.

[15] D.C. Young, Computational Chemistry A Practical Guide for Applying Techniques to Real-World Problems (Electronics), John Wiley and Sons, New York, 2001.

[16] N. Sundaraganesan, S. Illakiamani, H. Saleem, P.M. Wojciechowski, D. Michaliska, FT-Raman and FT-IR spectra, vibrational assignments and density functional studies of 5-bromo-2-nitropyridine, Spectrochim. Acta 61A (2005) 2995-3001.

[17] B. Sylaja, S. Srinivasan, Ab Initio and Density Functional Theory (DFT) Study on Clonazepam, Open Journal of Biophysics, 2, (2012) 80-87.

[18] GaussView, Version 5, Roy Dennington, Todd Keith, and John Millam, Semichem Inc., Shawnee Mission, KS, 2009.

[19] M. J. Frisch, G. W. Trucks, H. B. Schlegel, G. E. Scuseria, M. A. Robb, Gaussian 09, Revision **E.01,** Gaussian, Inc., Wallingford CT, 2009.

[20] M.H. Jamroz, Vibrational Energy Distribution Analysis VEDA 4, Warsaw, 2004.

[21] M.H. Jamroz, J.C. Dobrowolski, R. Brzozowski, Vibrational modes of 2,6-, 2,7- and 2,3-diisopropylnaphthalene. A DFT study, J. Mol. Struct. 787 (2006) 172-183.

[22] C. Cırak, S. Demir, F. Ucun, O. Cubuk, Experimental and theoretical study on the structure and vibrational spectra of β-2-aminopyridinium dihydrogenphosphate, Spectrochim. Acta Part A 79 (2011) 529-532.

[23] H. Arslan, O. Algul, Vibrational spectrum and assignments of 2-(4-methoxyphenyl)-1*H*-benzo[*d*]imidazole by ab initio Hartree-Fock and density functional methods, Spectrochim. Acta Part A 70 (2008) 109-116.

[24] Y. Kia, H. Osman, Vikneswaran a/l Murugaiyah, M. Hemamalinic, Hoong-KunFun, (E)-2-(4-Methyl benzy lidene) hydrazine carboxamide, Acta Cryst. E67 (2011) o242.

[25] N. Swarnalatha, S.Gunasekaran, S. Muthu, M. Nagarajan, Molecular structure analysis and spectroscopic characterization of 9-methoxy-2H-furo[3,2-g]chromen-2-one with experimental (FT-IR and FT-Raman) techniques and quantum chemical calculations, spectrochim. Acta part A 137 (2015) 721-729.

[26] L.G. Wade (Ed), Advanced Organic Chemistry, 4th ed., Wiley, New York,1992. p.723.

[27] D. Lin-Vien, N.B. Colthup, W.G. Fately, J.G. Grasselli, The Handbook of Infrared and Raman Characteristic Frequencies of Organic Molecules, Academic Press Boston, MA, 1991.

[28] M. Silverstein, G.C. Basseler, C. Morill, Spectrometric Identification of Organic Compounds, Wiley, New York, 1981.

[29] V. Krishnakumar, R. Ramasamy, Scaled quantum chemical studies of the structure and vibrational spectra of 2-(methylthio) benzimidazole, Spectrochim. Acta Part A 62 (2005) 570-577.

[30] L.J. Bellamy, The Infrared Spectra of Complex Molecules, vol. 2, Chapman and Hall, London, 1980.

[31] N. Sundaraganesan, S.Illakiamani, C. Meganathan, B.D. Joshua, Vibrational spectroscopy investigation using ab initio and density functional theory analysis on the structure of 3-aminobenzotrifluoride, Spectrochim. Acta A 67 (2007) 214-224.

[32] G. Varsanyi, Aassignments for vibrational Spectra of Seven Hundred Benzene Derivatives, vol. 1, Adam Hilger, London, 1974.

[33] V. Udayakumar, S. Periandy, S. Ramalingam, Experimental (FT-IR and FT-Raman) and theoretical (HF and DFT) investigation, IR intensity, Raman activity and frequency estimation analyses on 1-bromo-4-chlorobenzene, Spectrochim. Acta A 79 (2011) 920-927.

[34] N. Subramanian, N. Sundaraganesan, J.Jayabharathi, Molecular structure, spectroscopic (FT-IR, FT-Raman, NMR, UV) studies and first-order molecular hyperpolarizabilities of 1,2-bis(3-methoxy-4-hydroxybenzylidene)hydrazine by density functional method, Spectrochim. Acta A 76 (2010) 259-269.

[35] D.F.V. Lewis, C. Ioannides, D.V. Parke, Interaction of a series of nitriles with the alcohol-inducible isoform of P450: computer analysis of structure-activity relationships, Xenobiotica 24 (1994) 401-408.

[36] R. G. Pearson, Absolute electronegativity and hardness correlated with molecular orbital theory, Proc. Natl. Acad. Sci. 83 (1986) 8440-8441.

[37] V.K. Rastogi, M.A. Palafox, L. Mittal, N. Peica, W. Kiefer, K. Lang, S.P. Ojha, FTIR and FT-Raman spectra and density functional computations of the vibrational spectra, molecular geometry and

atomic charges of the biomolecule: 5-bromouracil, J. Raman Spectroscopy. 38 (2007) 1227-1241.

[38] S.Gunasekaran, R.A. Balaji, S. Kumaresan, G. Anand, S. Srinivasan, Experimental and theoretical investigations of spectroscopic properties of N-acetyl-5-methoxytryptamine, Canadian J Anal. Sci, Spectrosc. 53 (2008) 149-160.

[39] H.O. Kalinowski, S. Berger, S. Brawn, Carbon-$^{13}$NMR Spectroscopy, John Wiley and Sons, Chichester, 1988.

[40] K. Pihlajer, E. Kleinprter (Eds.), Carbon-$^{13}$Chemical Shifts in Structure and Spectrochemical Analysis, VCH publishers, Deerfield Beach, 1994.

[41] G. Varsanyi, Vibrational spectra of Benzene Derivatives, Academic press, New York, 1969.

[42] Y.X. Sun, Q.L. Hao, W. X. Wei, Z. X. YU, D.D. LU. X. Wang, Y. S. Wang, Experimental and density functional studies on 4-(3,4-dihydroxybenzylideneamino)antipyrine, and 4-(2,3,4-trihydroxybenzylideneamino) antipyrine, J. Mol. Struct. Theochem. 904 (2009) 74-82.

[43] M. Nakano, H. Fujita, M. Takcathata, K. Yamaguchi, Theoretical Study on Second Hyperpolarizabilities of Phenylacetylene Dendrimer: Toward an Understanding of Structure-Property Relation in NLO Responses of Fractal Antenna Dendrimers, J. Am. Chem. Soc. 124 (2002) 9648-9655.

[44] D. Sajan, H. Joe, V. S. Jajakumar, J. Zaleski, Structural and electronic contributions to hyperpolarizability in methyl p-hydroxy benzoate, J. Mol. Struct. 785 (2006) 43-53.

[45] K. S. Thanthiri Watte, K. M. Nalin de silva, Non-linear optical properties of novel fluorenyl derivatives-ab initio quantum chemical calculations, J. Mol. Struct. Theochem. 617 (2002) 169-175.

[46] S. G. Sagdinc, A. Esme, Theoretical and vibrational studies of 4,5-diphenyl-2-2 oxazole propionic acid (oxaprozin), Spectrochim. Acta Part A 75 (2010) 1370-1376.

[47] S. Muthu, G. Ramachandran, Spectroscopic studies (FTIR, FT-Raman and UV–Visible), normal coordinate analysis, NBO analysis, first order hyper polarizability, HOMO and LUMO analysis of (1R)-N-(Prop-2-yn-1-yl)-2,3-dihydro-1H-inden-1-amine molecule by ab initio HF and density functional methods, Spectrochim. Acta part A 121 (2014) 394-403.

[48] R. Srinivasaraghavan, S. Thamaraikannan, S. Seshadri, T. gnanasambandan, Molecular conformational stability and Spectroscopic analysis of Parared with experimental techniques and quantum chemical calculations, Spectrochim. Acta A 137 (2015) 1194-1205.

[49] C. James, A. Amal Raj, R. Reghunathan, V.S. Jayakumar, I.Hubert Joe, Structural conformation and vibrational spectroscopic studies of 2,6-bis(*p*-*N*,*N*-dimethyl benzylidene) cyclohexanone using density functional theory, J. Raman Spectrosc. 37 (2006) 1381-1392.

[50] J. Liu, Z. Chen, S. Yuan, Study on the prediction of visible absorption maxima of azobenzene compounds, J. Zhejing Univ. Sci B. 6 (2005) 584-589.

[51] M. Szafran, A. komasa, E.B. Adamska, Crystal and molecular structure of 4-carboxypiperidinium chloride (4-piperidinecarboxylic acid hydrochloride), J Mol. Struct. THEOCHEM 827 (2007) 101-107.

[52] E. Scrocco, J. Tomasi, Topics in Current Chemistry, vol. 7, Springer, Berlin, 1973.

[53] F.J. Luque, J.M. Lopez, M. Orozco, Perspective on "Electrostatic interactions of a solute with a continuum. A direct utilization of ab initio molecular potentials for the prevision of solvent effects", Theor. Chem. Acc. 103 (2000) 343–345.

[54] N. Okulik, A.H. Jubert, Theoretical Analysis of the Reactive Sites of Non-steroidal Anti-inflammatory Drugs, Internet Electronic. J. Mol. Des. 4 (2005) 17-30.

[55] S.K. Pathak, R. Srivastava, A.K. sachan, O. Prasad, L. Sinha, A.M. Asiri, M. Karabacak, Experimental (FT-IR, FT-Raman, UV and NMR) and quantum chemical studies on molecular structure, spectroscopic analysis, NLO, NBO and reactivity descriptors of 3,5-Difluoroaniline , Spectrochim. Acta A 135 (2015) 283-295.

[56] A. Ravi Kumar, G Sathaiah, A. Chandra Shekhar, K. Raju, P. Shanthan Rao, B. Narsaiah, Y. Kanaka Raju, U. S. N. Murthy, V. Srimai, M. Ramesh, and T. Parthasarathy, Synthesis of 6-Fluoro-7-cyclic Amino-substituted Dicarboxylic Acid Quinolones and their Antibacterial Activity, J. Hetercycl Chem. 51 (2014) 114-122.

[57] N. G. Dayanandan, L. Paulsen, K.Viswanathan, S. Keshipeddy, N. Lombardo, W. Zhou, M. Lamb, E. Sochia, J B. Alverson, D. Priestley, L. Wright and C. Anderson, Propargyl-Linked Antifolates are Dual Inhibitors of Candida albicans andCandida glabrata, J. Med. Chem, 57 (2014) 2643- 2656.

[58] Jaeyong Lee and Mark Paetzel, Structure of the catalytic domain of glucoamylase from Aspergillus niger, Acta Cryst. F67 (2011)

[59] K.K. Irikura, THERMO.PL, National Institute of Standards and Technology, Gaithersburg, MD, 2002.

[60] S. Muthu, E. Isac Palulraj, Spectroscopic and molecular structure (monomeric and dimeric structure) investigation of 2-[(2-hydroxyphenyl) carbonyloxy] benzoic acid by DFT method: A combined experimental and theoretical study, J. Mol. Struct 1038 (2013) 145-162.

# CHAPTER – IV

## Synthesis, Spectroscopic (FT-IR, FT-Raman, NMR, UV-Visible), NLO, NBO, HOMO-LUMO, Fukui Function and Molecular Docking Study of (E)-1-(5-Bromo-2-Hydroxy Benzylidene) Semicarbazide

### 4.1. Introduction

Semicarbazide derivatives have received wide attention in the current years because of their diverse biological activities and form an important part of the molecular structures of significant drugs. This class are important tridentate O, N, O-donor ligand. As biologically active compounds, semicarbazides and its derivatives of (E)-1-(5-bromo-2-hydroxybenzylidene) semicarbazide (15BHS) have exhibit interesting biological activities, such as anticonvulsant, tuberculosis, antinociceptive [1-3], anticancer, antifungal and antibacterial activity [4, 5]. Its chemical formula is $C_8H_8BrN_3O_2$. Therefore it is important to analyze the characterization of the title compound for future studies. Furthermore, researchers are also very helpful for the theoretical calculation of the experimental evidences since computational methods are reliable to characterize the molecule because of their efficiency and exactness with regard to the estimation of molecular properties. Vibrational spectroscopy is a precious tool for the clarification of molecular structure and gives a dynamical picture of the molecule.



V.L. Siji et al. [6] reported FT-IR and FT-Raman spectral studies and DFT calculations of tautomeric forms of benzaldehyde-N(4)-phenylsemicarbazone. A. Dhandapani et al. [7] reported synthesis, structural, spectroscopic studies, NLO, NBO and HOMO-LUMO of (E)-1-(3-methyl-2,6-diphenyl piperidin-4-ylidene) semicarbazide with

experimental and theoretical approaches. S. Subashchandrabose et al. [8] reported Vibrational studies on (E)-1-((pyridine-2-yl)methylene) semicarbazide using experimental and theoretical method.

Literature survey reveals that to the best of our knowledge, there is no DFT studies, vibrational assignments, NLO activity and molecular docking studies for title compound 15BHS. Considering these biological importance of (E)-1-(5-bromo-2-hydroxybenzylidene) semicarbazide, this work is mainly focused to the detailed structural behavior of the molecule. FT-IR and FT-Raman spectra of 15BHS have been reported together with the assignments of the vibrational modes supported by PED. The linear polarizability ($\alpha$) and the first order hyperpolarizability ($\beta$) values investigated molecule have been computed using DFT calculations. HOMO-LUMO a study has been performed which aid to explain charge transfer occurring in the molecule. Global reactivity descriptors such as chemical hardness, softness potential, electrophilicity index and electronegativity have been computed. Docking investigation has been performed to find out the hydrogen bond lengths and binding energy and drug activity of the molecule.



## 4.2. Materials and Methods

### 4.2.1. Synthesis

For the synthesis of (E)-1-(5-bromo-2-hydroxybenzylidene) semicarbazide (15BHS) compound, solution of 2-hydroxy-5-bromobenzaldehyde (1.56 g, 10 mmol) in ethanol (5 mL) was added with aqueous solution of semicarbazide hydrochloride (1.11 g, 10 mmol) and followed by 0.5 mL of con. HCl was added and the reaction mixture stirred at room temperature for one hour. After completion of the reaction, the solid product was filtered and washed with cold water and air dried.

Finally the crude sample was recrystallised from ethanol. The scheme of the synthesis is shown in Fig. 4.1.

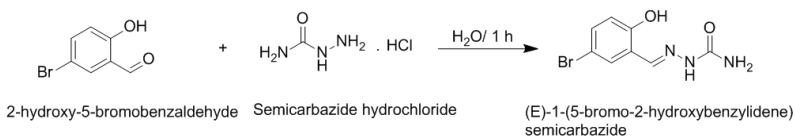


**Fig. 4.1.** The scheme of the synthesis of 15BHS

### 4.2.2. Experimental

The FT-IR spectrum of the synthesis compound (E)-1-(5-bromo-2-hydroxybenzylidene)semicarbazide (15BHS) was recorded in the region 4000-450 $cm^{-1}$ in evacuation mode using a KBr pellet technique with 1.0 $cm^{-1}$ resolution on a PERKIN ELMER FT-IR spectrophotometer. The FT-Raman spectrum of the (15BHS) compound was recorded in the region 4000-100 $cm^{-1}$ in a pure mode using Nd: YAG Laser of 100 mW with 2 $cm^{-1}$ resolution on a BRUCKER RFS 27 at SAIF, IIT, Chennai, India. Carbon($^{13}C$) NMR and Proton ($^{1}H$) NMR spectra were recorded in DMSO-$d_6$ using TMS as an internal standard on a Bruker high-resolution NMR spectrometer at 400 MHz at CAS in Crystallography & Biophysics, University of Madras, Chennai, India. The ultraviolet absorption spectrum of the sample is examined in the range 250-600 nm using UV-1700 series recording spectrometer.



### 4.2.3. Computational details

Gaussian ’09 program package [9] has been used to calculate optimized molecular geometry, vibrational wavenumbers and NLO activity using DFT/B3LYP method with the 6-311++G(d,p) basis set. To avoid the systematic errors caused by basis set incompleteness, negligence of

electron correlation and vibrational anharmonicity a general scaling factor of 0.961was used to scale the computed wavenumbers. Additionally, the compute vibrational frequencies were revealed by means of the potential energy distribution (PED) investigation of all the fundamental vibration modes by using VEDA 4 program [10] used in previous studies by many researchers [11-13]. NBO 3.1 program was implemented for natural bonding orbital calculation [14]. In order to understand the electronic properties, the theoretical UV-Vis spectra have been investigated by TD-DFT method with 6-311++G(d,p) basis set for the DMSO and gas phase. The proton and carbon NMR chemical shift were calculated with the gauge-including atomic orbital (GIAO) approach by applying B3LYP/6-311++G(d,p) method of the title molecule and compared with the experimental NMR spectra. Molecular docking (ligand-protein) simulations have been performed by using autoDock 4.2.6 software package.



## 4.3. Results and discussion

### 4.3.1. Molecular geometry

The numbering system adopted in the molecular structure of 15BHS is obtained from Gaussian 09W and GaussView 5.0 programs are shown in Fig. 4.2. The bond parameters (bond length and bond angles) of the 15BHS molecules are listed in Table 4.1 using DFT/B3LYP method with 6-311++G(d,p) basis set.

**Table 4.1**

Geometrical parameters optimized in (E)-1-(5-bromo-2-hydroxybenzylidene)semicarbazide bond length (Å) and bond angle (°).

| **Bond length(Å)** | **Experimental[a]** | **B3LYP/6-311++G(d,p)** | **Bond angle(°)** | **Experimental[a]** | **B3LYP/6-311++G(d,p)** |
|---|---|---|---|---|---|
| N1-N2 | 1.378 | 1.35 | N1-C3-N5 | 117.4 | 114.8 |
| N1-C3 | 1.376 | 1.396 | N2-C6-C7 | 120.6 | 121.7 |
| N1-H15 | 0.944 | 1.016 | N2-C6-H18 | 118.9 | 121.3 |
| N2-C6 | 1.287 | 1.284 | O4-C3-N5 | - | 125.2 |
| C3-O4 | - | 1.219 | C3-N5-H16 | 124.0 | 121 |
| C3-N5 | 1.350 | 1.359 | C3-N5-H17 | 117.2 | 117.7 |
| N5-H16 | 0.944 | 1.006 | H16-N5-H17 | 120.5 | 121.2 |
| N5-H17 | 0.944 | 1.005 | C7-C6-H18 | 118.9 | 117 |
| C6-C7 | 1.446 | 1.463 | C6-C7-C8 | 120.8 | 119.7 |
| C6-H18 | 0.960 | 1.091 | C6-C7-C12 | 121.4 | 122 |
| C7-C8 | 1.406 | 1.408 | C8-C7-C12 | 117.3 | 118.3 |
| C7-C12 | 1.406 | 1.404 | C7-C8-C9 | 120.8 | 120.5 |
| C8-C9 | 1.385 | 1.395 | C7-C8-O13 | 117.6 | 117.5 |
| C8-O13 | 1.360 | 1.369 | C7-C12-C11 | 120.8 | 120.6 |
| C9-C10 | 1.387 | 1.39 | C7-C12-H21 | 118.3 | 118.7 |
| C9-H19 | 0.960 | 1.086 | C9-C8-O13 | 120.6 | 121.9 |
| C10-C11 | 1.387 | 1.393 | C8-C9-C10 | 120.8 | 120.6 |
| C10-H20 | 0.960 | 1.082 | C8-C9-H19 | 119.6 | 119.8 |
| C11-C12 | 1.387 | 1.384 | C8-O13-H22 | - | 110 |
| C11-Br14 | - | 1.918 | C10-C9-H19 | 119.6 | 119.6 |
| C12-H21 | 0.960 | 1.081 | C9-C10-C11 | 120.6 | 118.9 |
| O13-H22 | 0.874 | 0.963 | C9-C10-H20 | 119.7 | 120.3 |
| **Bond angle(°)** | **Experimental[a]** | **B3LYP/6-311++G(d,p)** | C11-C10-H20 | 119.7 | 120.7 |
| N2-N1-C3 | 120.3 | 122.7 | C10-C11-C12 | 20.8 | 121.1 |
| N2-N1-H15 | 121.8 | 121.8 | C10-C11-Br14 | - | 119.4 |
| N1-N2-C6 | 120.3 | 118.2 | C12-C11-Br14 | - | 119.6 |
| C3-N1-H15 | 117.2 | 115.5 | C11-C12-H21 | 119.6 | 120.7 |
| N1-C3-O4 | - | 120 | | | |

[a] Taken from Ref [17]

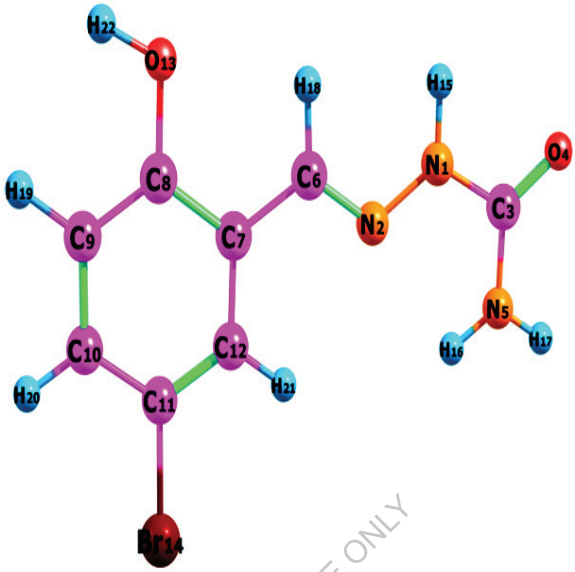


**Fig. 4.2.** Optimized geometric structure with atoms numbering of 15BHS



To the best of our knowledge, exact experimental data on the geometrical parameters of 15BHS are not available in the literature. Therefore, the crystal data of a closely related molecule such as 2-[(E)-4-Diethylamino-2-hydroxybenzylidene] hydrazinecarboxamide [15] is compared with that of the title compound. From the calculated values, it is found that most of the optimized molecular bond lengths are slightly higher than the experimental values due to the fact that the experimental XRD results were carried out in the solid state and theoretical calculations were carried out in the gas phase.

This title molecule has seven C - C bond lengths, four C - H bond lengths, three (C - N, N - H) bond lengths, two C – O bond lengths and one (N - N, C - Br, O - H) bond lengths respectively. The highest bond length was calculated for $C_6 – C_7$ found to be 1.466 Å (experimental) and 1.463 Å

(theoretical) respectively. The calculated bond length values for C-C and C-H in the benzene ring vary from 1.385-1.446 Å and 0.960-1.091 Å by B3LYP/6-311++G(d,p) basis set and well agreed with experimental values [15]. They found to be slightly difference at all levels of calculations. The homonuclear bond lengths (C-C and N-N) are higher than the heteronuclear bond lengths (C-H and N-H). The important reasons for the same charges are repulsive and opposite charges are attractive.

### 4.3.2. Vibrational analysis

Vibrational spectroscopy is used extensively in organic chemistry for the identification of functional groups of organic compounds, the study of molecular confirmations, kinetics, reaction etc. The complete vibrational assignments of fundamental modes of 15BHS along with the PED are given in Table 4.2. The title molecule consists of 22 atoms, which has 60 normal modes of vibration. Potential energy distribution (PED) was computed for each normal mode among the symmetry coordinates of the molecule. Based on the computed PED values and FT-IR intensities and FT-Raman band activities a detailed assignment of the fundamentals was proposed. The calculated wavenumbers are scaled using the scaling factor 0.961 [16]. The comparative observed and simulated FT-IR and FT-Raman spectra are shown in Fig. 4.3 and 4.4. The calculated vibrational frequencies (Unscaled and Scaled), IR intensity, Raman activity are tabulated in Table 4.2.



#### *4.3.2.1. $NH_2$ vibrations*

The $NH_2$ group has two (N-H) stretching vibrations, first one asymmetric and another one symmetric. The asymmetric stretching for the $NH_2$, $CH_2$ and $CH_3$ has a magnitude higher than the symmetric stretching [17].The aromatic structure shows the presence of C-H and N-H stretching

vibrations above 3000 $cm^{-1}$ which is the characteristic region for ready identification of this structure [18, 19]. The title compound has only one $NH_2$ group and hence one symmetric and one asymmetric N-H stretching vibrations in $NH_2$ group are expected. The symmetric $NH_2$ stretching vibrations appear from 3420 to 3500 $cm^{-1}$ [20]. The theoretical wavenumbers computed using the B3LYP/6-311++G(d,p) method identified at 3603 and 3470 $cm^{-1}$ [mode no 59, 58] are assigned to $NH_2$ asymmetric and symmetric stretching vibrations contributing 60 and 99% to the PED. In this work, the FT-Raman band at 3617(vw) $cm^{-1}$ has been assigned to $NH_2$ asymmetric stretching vibrations. The $NH_2$ symmetric stretching vibrations observed in the FT-IR and FT-Raman have strong and very weak intensity bands. The experimental FT-IR and FT-Raman symmetric stretching bands found at 3469(s) $cm^{-1}$ and 3470(vw) $cm^{-1}$.



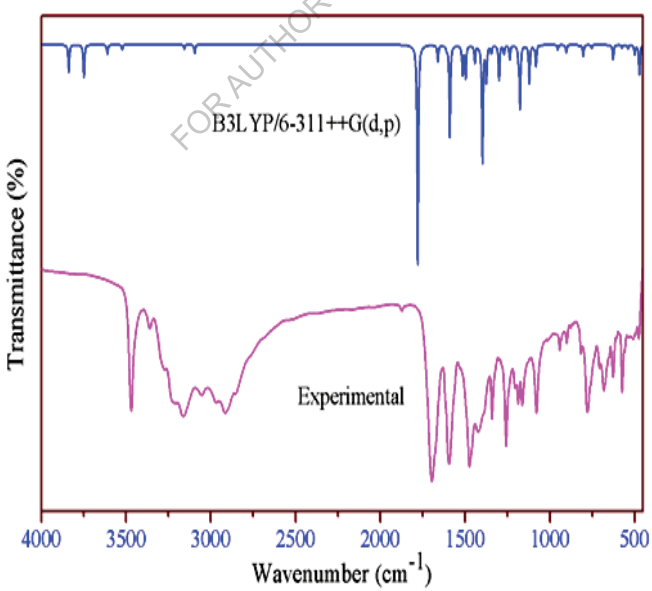


**Fig. 4.3.** FT- IR spectra of 15BHS

**Table 4.2**

Observed and calculated vibrational frequency of 15BHS at B3LYP method with 6-311++G(d,P) basis set.

| Experimental wave number ($cm^{-1}$) | | Theoretical wave number($cm^{-1}$) | | Assignments (PED)[a] |
|---|---|---|---|---|
| **FTIR** | **FT-Raman** | **Unscaled** | **Scaled[b]** | |
| - | - | 3838 | 3689 | γ OH(100) |
| - | 3617(vw) | 3749 | 3603 | $\gamma_{as}$ $NH_2$(60) |
| 3469(s) | 3470(vw) | 3611 | 3470 | $\gamma_s$ $NH_2$(99) |
| 3360(w) | 3385(vw) | 3523 | 3386 | γ NH(100) |
| - | - | 3216 | 3091 | γ CH(100) |
| - | 3077(m) | 3206 | 3081 | γ CH(97) |
| 3051(m) | 3059(m) | 3157 | 3034 | γ CH(97) |
| 2968(m) | 2970(w) | 3095 | 2974 | γ CH(100) |
| 1696(vs) | 1711(w) | 1780 | 1710 | γ OC(69) |
| 1594(vs) | 1602(vs) | 1661 | 1596 | γ NC(64) |
| - | 1568(vs) | 1633 | 1569 | γ CC(44)+β CCC(10) |
| - | - | 1609 | 1547 | γ CC(44)+β CCC(12) |
| - | 1517(w) | 1591 | 1529 | β HNH(75) |
| 1475(vs) | 1476(s) | 1516 | 1457 | β HNN(13)+β HCC(28) |
| 1424(s) | 1432(w) | 1497 | 1439 | β HCN(12)+β HNN(35) |
| | 1386(w) | 1443 | 1386 | γ CC(48)+β HCC(15) |
| 1341(s) | 1345(w) | 1398 | 1343 | γ NC(38)+β OCN(14)+β HNH(13)+β HNN(16) |
| - | - | 1375 | 1322 | γ NC(10)+β HCN(52)+β HNN(12) |
| 1300(w) | 1301(s) | 1346 | 1293 | β HOC(21)+γ CC(48)+β HCC(11) |
| 1258(s) | 1242(m) | 1300 | 1249 | γ OC(13)+β HCC(42) |

| | | | | |
|---|---|---|---|---|
| 1204(m) | 1208(w) | 1271 | 1221 | γ CC(24)+β HCC(21) |
| 1186(s) | 1161(s) | 1236 | 1188 | γ CC(18)+β HOC(16)+β CCC(11)+β HCN(11) |
| 1163(s) | | 1186 | 1140 | β HOC(21)+β HCC(18)+γ CC(14) |
| | 1128(w) | 1176 | 1130 | γ NN(49)+β HOC(10) |
| 1079(s) | 1081(m) | 1122 | 1078 | γ CC(20)+β HCC(14)+β HOC(13) |
| | | 1095 | 1052 | γ CC(35)+β HCC(16) |
| | 1019(m) | 1082 | 1040 | β HNC(51) |
| 942(w) | 937(m) | 998 | 960 | β NNC(12)+γ NC(58) |
| | - | 953 | 916 | τ HCNN(80) |
| 900(w) | 902(m) | 936 | 900 | τ HCCC(62) |
| 875(w) | - | 903 | 868 | γ BrC(25)+β CCC(17)+γ CC(17)+γ NC(15) |
| | - | 900 | 865 | τ CCCC(10)+τ HCCC(64) |
| 817(w) | 784(m) | 827 | 794 | β CCC(29)+γ OC(17) |
| 778(s) | - | 803 | 772 | OUT OCCC(15)+τ HCCC(79) |
| 707(m) | - | 753 | 724 | OUT ONNC(87) |
| 681(m) | - | 708 | 681 | τ CCCC(33)+OUT CCCC(40) |
| 627(m) | 631(m) | 663 | 637 | β NCC(11)+β NCN(11)+β CCC(30) |
| - | 613(w) | 627 | 602 | γ OC(10)+γ BrC(15)+β OCN(11)+β NNC(14)+β CCC(15) |
| | | 627 | 603 | β CCC(26)+β NCN(12)+β CNN(11) |
| 558(w) | | 574 | 552 | τ HNCN(80)+τ HNNC(13) |

| | | | | |
|---|---|---|---|---|
| | | 562 | 540 | OUT BrCC(12)+τ CCCC(64)+OUT CCCC(14) |
| 509(w) | | 539 | 518 | β OCN(54) |
| 475(w) | 470(w) | 500 | 480 | β CCC(14)+β OCC(32)+β NCN(14) |
| - | - | 479 | 460 | τ HNNC(16)+τ CCCC(13)+OUT OCCC(25)+OUT CCCC(13) |
| - | 430(m) | 472 | 454 | τ HNNC(64) |
| - | 358(m) | 397 | 382 | β CCC(10)+β OCC(17)+β NNC(13)+β NCN(23)+β CCC(11) |
| - | - | 351 | 337 | τ NNCC(12)+OUT BrCC(18)+τ CCCC(35)+OUT OCCC(18) |
| - | 279(m) | 292 | 280 | β NCC(10)+β CCC(10)+τ NNCC(32)+γ BrC(25)+OUT BrCC(15) |
| - | - | 292 | 281 | β BrCC(12)+γ BrC(33) |
| - | - | 283 | 272 | τ HOCC(59) |
| - | - | 256 | 246 | τ CNNC(16)+τ HOCC(38) |
| - | - | 226 | 217 | β CNN(10)+β CCC(11)+β OCC(17)+β BrCC(18) |
| - | - | 224 | 216 | β CNN(25)+β NNC(13)+β CCC(13)+β BrCC(29) |
| - | 156(m) | 161 | 155 | γ OC(32) |

| | | | | |
|---|---|---|---|---|
| - | - | 118 | 113 | τ NCCC(12)+τ CNNC(23)+τ CCCC(12)+OUT BrCC (19)+OUT CCCC(21) |
| - | 106(s) | 105 | 101 | τ CCCC(46)+OUT BrCC(13) |
| - | - | 57 | 55 | τ NCNN(33)+τ CNNC(17)+τ NNCC(20)+OUT CCCC(14) |
| - | - | 51 | 49 | β NCC(32)+β NNC(19)+β CCC(26) |
| - | - | 30 | 29 | τ NCCC(67)+τ CNNC(24) |
| - | - | 18 | 17 | τ HNCN(43)+τ HNCN(32)+τ NCNN(14) |



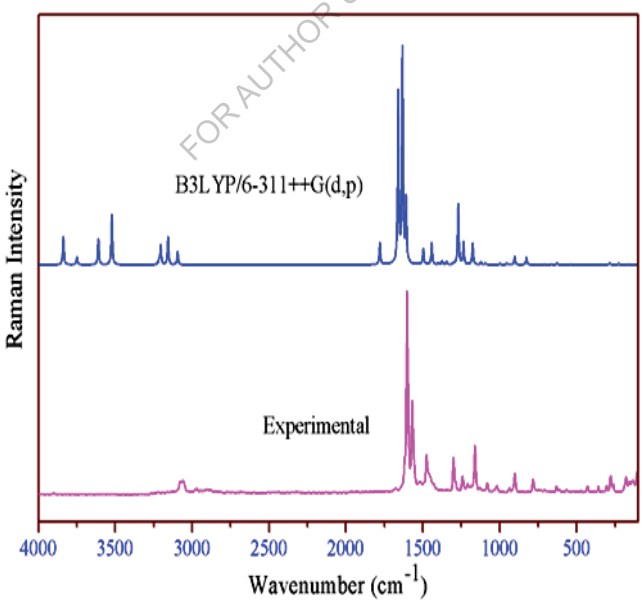


**Fig. 4.4.** FT-Raman spectra of 15BHS

#### *4.3.2.2. C-H vibrations*

In the aromatic compounds, the C-H stretching wavenumbers appear in the range 3000-3100 $cm^{-1}$ which are the characteristic region for the ready identification of C-H stretching vibrations [21]. The C-H stretching and bending regions are of the most difficult regions to interpret in infrared spectra. The nature and position of the substituent cannot affect these vibrations. Most of the aromatic compounds have almost four infrared peaks in the region 3080-3010 $cm^{-1}$ due to ring C-H stretching bands [22]. In this present study, the C-H stretching vibrations are observed at 3091, 3081, 3034 and 2974 $cm^{-1}$[mode nos 56-53] by B3LYP/6-311++G(d,P) method show good agreements with experimental vibrations. The bands observed in the recorded FT-IR spectrum 3051(m), 2968(m) $cm^{-1}$ and with the FT-Raman spectrum bands at 3077(m), 3059(m), 2970(w) $cm^{-1}$. The PED corresponding to this pure mode of title molecule contributed 100, 97, 97 and 100% is shown in Table 5.2.



#### *4.3.2.3. C-Br Vibrations*

The most aromatic bromo compounds C-Br stretching vibrations occur in the region 650-395 $cm^{-1}$ [23]. The vibration belonging to the bond between the ring and the Bromine atom is salient as a combination of vibrations is possible owing to the presence of heavy atom [24]. The C-Br stretching vibrations for title molecule is assigned at 868, 602, 280 $cm^{-1}$ (mode no 30, 23, 13) in B3LYP/6-311++G(d,p) and 875(w) $cm^{-1}$ in FT-IR and 613(w), 279(m) $cm^{-1}$ in FT-Raman with a PED of 25, 15 and 25%.

#### *4.3.2.4. C-C ring vibrations*

The C-C stretching vibrations are expected in the range from 1650 to 1100 $cm^{-1}$ which are not significantly influenced by the nature of the

substituents [25]. The C-C stretching vibrations of the 15BHS compound were observed from1570 to 865 $cm^{-1}$. In this present study, the C-C stretching vibrations are found at 1300(w), 1204(m), 1186(s), 1163(s), 1079(s), 875(w) $cm^{-1}$ in FT-IR and 1568(vs), 1386(w), 1301(s), 1208(w), 1161(s), 1081(m) $cm^{-1}$ in FT-Raman respectively. The theoretical wavenumbers at 1569, 1386, 1293, 1221, 1188, 1140, 1078 and 868 $cm^{-1}$ (mode no 50, 45, 42, 40, 39, 38, 36, 30) are assigned as C-C stretching vibrations with PED contribution of 44, 48, 48, 18, 24, 18, 40 and 17% respectively.

#### *4.3.2.5. C-N vibrations*

The C-N stretching frequency is a very tough task since it falls in a composite region of the vibrational spectrum, i.e., mixing of several bands are possible in this region [18] assigned C-N stretching absorption in the region 1386-1266 $cm^{-1}$ for the aromatic compound. The bands observed at 1594(vs), 1341(s), 942(w), 875(w) $cm^{-1}$ in FT-IR and 1602(vs), 1345(w), 937(m) $cm^{-1}$ in FT-Raman are assigned as N-C stretching vibrations. The theoretically scaled wavenumbers calculated at 1596, 1343, 960 and 868 $cm^{-1}$ (mode no 57, 38, 33, 30) are assigned as C-N stretching vibrations with PED contribution of 64, 38, 58 and 15% respectively.



### 4.4. NMR spectral analysis

The NMR spectroscopy is one of the most important techniques for the structural conformational analysis for the organic compounds. We used this technique ($^{1}H$ and $^{13}C$ NMR) due to the useful, common to have more information about the studied molecule. The experimental and theoretical values for carbon ($^{13}C$) and proton ($^{1}H$) NMR of the title compound are given in Table 4.3. The experimental $^{13}C$ and $^{1}H$ NMR spectra were recorded in a DMSO-$d_6$ solvent are shown in Figs. 4.5 and 4.6. The

theoretical $^{13}C$ and $^{1}H$ chemical shifts are calculated for the optimized geometry to obtain from B3LYP/6-311++G(d,p) using GIAO method [26].

There are eight carbon atoms (in the ring) in the 15BHS molecule. The result in Table 5.3 shows that the range carbon ($^{13}C$) NMR chemical shifts of the typical organic molecule usually > 100 ppm [27-29]. In this work, aromatic carbons are observed from 123 to 157 ppm in carbon (13C) NMR spectrum for the 15BHS molecule. The oxygen (O) and nitrogen (N) atom's high electronegative property polarizes the electron distribution in its bond to the adjacent carbon atom and decreases the electron density at the bridge for the title molecule. Therefore, the chemical shift value seems to be moderately high for the title molecule DMSO-d6 solvent under study at 156.78 and 154.93 ppm (C3, C8). The calculated $^{13}C$ NMR chemical shift values well coincides with the experimental values.



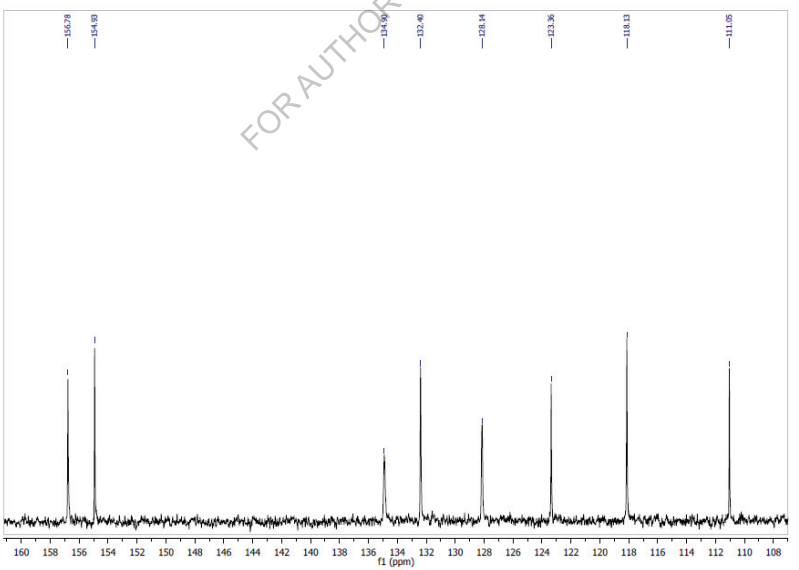


**Fig. 4.5.** $^{13}C$ NMR spectrum of 15BHS (Experimental)

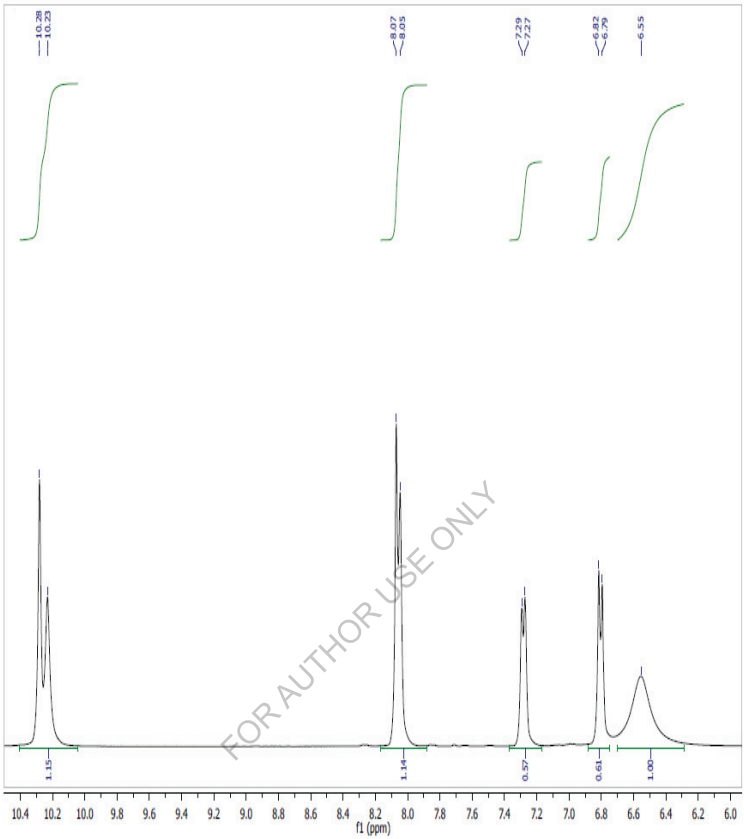



**Fig. 4.6**. $^{1}$H NMR spectrum of 15BHS (Experimental)

There are also eight hydrogen atoms (ring, NH and $NH_2$ group) in the title molecule. The $^{1}$H NMR observed chemical shift values at 8.07, 6.82, 6.55, 10.23, 7.29, 8.05, 10.28, 6.79 ppm with the theoretical chemical shift values at 8.71, 6.54, 5.57, 9.39, 7.89, 8.41, 10.54, 6.03 ppm for $H_{15}$, $H_{16}$, $H_{17}$, $H_{18}$, $H_{19}$, $H_{20}$, $H_{21}$ and $H_{22}$. The predicted all chemical shift values are in good agreement with the experimental values.

**Table 4.3**

Theoretical and experimental $^{13}C$ and $^{1}H$ isotropic chemical shifts [with respect to TMS, all values in ppm] for 15BHS molecule

| Atom | Chemical shifts (ppm) | |
|---|---|---|
| | Experimental | B3LYP/6-311++G(d,p) |
| C3 | 156.78 | 156.81 |
| C6 | 132.40 | 133.17 |
| C7 | 111.05 | 111.95 |
| C8 | 154.93 | 153.50 |
| C9 | 118.13 | 120.02 |
| C10 | 134.90 | 135.60 |
| C11 | 128.14 | 128.83 |
| C12 | 123.36 | 123.94 |
| H15 | 8.07 | 8.71 |
| H16 | 6.82 | 6.54 |
| H17 | 6.55 | 5.57 |
| H18 | 10.23 | 9.39 |
| H19 | 7.29 | 7.89 |
| H20 | 8.05 | 8.41 |
| H21 | 10.28 | 10.54 |
| H22 | 6.79 | 6.03 |

## 4.5. Electronic properties

UV-Visible spectra analyses of 15BHS have been investigated by experimental and theoretical calculation. Time-dependent density functional theory (TD-DFT) has recently emerged as a great tool for examining the static and dynamic properties of the molecules in their excited states, allowing for the best compromise between accuracy. The experimental and theoretical UV-Visible comparison spectrum of title molecule is shown in Fig. 4.7. Absorption maximum ($\lambda_{max}$) of our title molecule is calculated by TD-DFT/B3LYP method with 6-311++G(d,p) basis set. The calculation of molecular orbital geometry shows that the visible absorption maxima of the 15BHS resemble the electronic transition from HOMO to LUMO. The experimental UV-Vis spectra of 15BHS molecule were used to DMSO solvent and theoretical calculations were carried out in the DMSO and gas phase. The UV-Vis spectra absorption maximum ($\lambda_{max}$) values 286 (Experimental), 290 and 288 nm (Theoretical) are listed in Table 4.4. The $\lambda_{max}$ is a function of substitution, the more electrons pushed into the ring, the larger $\lambda_{max}$ [30]. The band gap energy was calculated by the formula, $E = hc/\lambda$. Here h and c are constant; $\lambda$ is the cut off wavelength. The calculated results involving the absorption wavelength, band gap energy, excitation energies and oscillating strength are carried out compared with experimental data. The energy difference between HOMO and LUMO orbits is called as band gap that is important stability for structure [31]. HOMO and LUMO is related to the ionization potential and electron affinity. The HOMO and LUMO energies, the energy gap ($\Delta E$), the ionization potential (I), the electron affinity (A), the absolute electronegativity ($\chi$), and softness (S) and the absolute hardness ($\eta$) for the 15BHS molecule have been calculated at B3LYP/6-311++G(d,P) basis set (Fig 4.8) and the result are given in the Table 4.5.

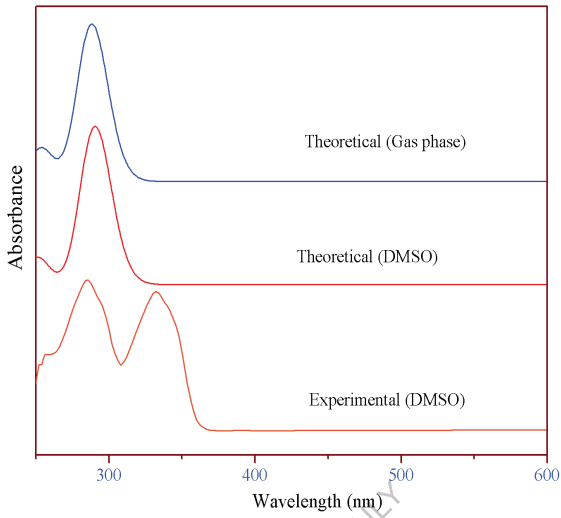


**Fig. 4.7.** UV–Vis spectra of 15BHS (Experimental, Theoretical (DMSO, GAS phase))



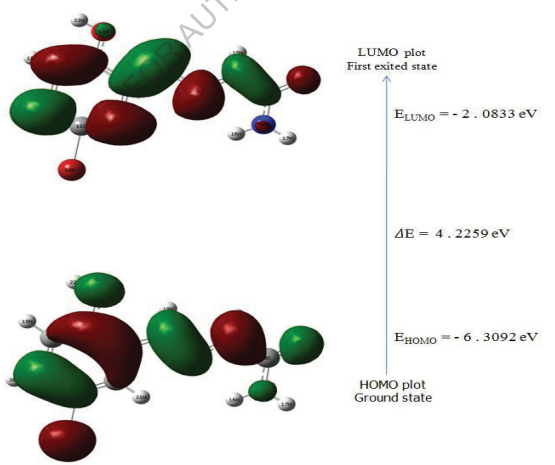


**Fig. 4.8.** Atomic orbital HOMO – LUMO composition of the frontier molecular orbital for 15BHS

**Table 4.4** The UV–vis wavelength (λ), band gap energy (ΔE), and oscillator strength (f) for 15BHS calculated by TD-DFT/B3LYP method

| **Experimental** | | **TD-DFT/B3LYP-311++G(d,p)** | | | | | |
|---|---|---|---|---|---|---|---|
| | | **DMSO** | | | **Gas phase** | | |
| **$\lambda_{max}$ (nm)** | **Band gap (ev)** | **$\lambda_{cal}$ (nm)** | **Band gap (eV)** | **Energy ($cm^{-1}$)** | **$\lambda_{cal}$ (nm)** | **Band gap (eV)** | **Energy ($cm^{-1}$)** |
| **286** | 4.3465 | 290 | 4.2866 | 34457 | 288 | 4.3164 | 34721 |
| | | 250 | 4.9725 | 39850 | 253 | 4.9135 | 39456 |
| | | 232 | 5.3582 | 42992 | 228 | 5.4523 | 43768 |

**Table 4.5**

Calculated energy values of title compound by B3LYP/6-311++G(d,p) method.



| **Basis set** | **B3LYP/6-311++G(d,p)** |
|---|---|
| $E_{HOMO}$ (eV) | -6.3092 |
| $E_{LUMO}$ (eV) | -2.0833 |
| Ionization potential | 6.3092 |
| Electron affinity | 2.0833 |
| Energy gap (eV) | 4.2259 |
| Electronegativity | 4.1962 |
| Chemical potential | -4.1962 |
| Chemical hardness | 2.1129 |
| Chemical softness | 0.2366 |
| Electrophilicity index | 4.1668 |

By using HOMO and LUMO energy values for a molecule, electronegativity and chemical hardness can be calculated as follow:

$$\chi = \frac{I+A}{2} \text{ (Electronegativity)} \qquad (5.1)$$

$$\mu = -\frac{(I+A)}{2} \text{ (Chemical potential)} \quad (5.2)$$

$$\eta = \frac{I-A}{2} \text{ (Chemical hardness)} \quad (5.3)$$

$s=1/2\eta$ (chemical softness), $\omega=\mu^2/2\eta$ (Electrophilicity index)

Where I and A are ionization potential and electron affinity; $I = -E_{HOMO}$ and $A = -E_{LUMO}$ respectively [32]. The energy gap of title molecule is calculated experimentally by UV-Visible spectrum is 4.3465 eV, the Energy gap is calculated theoretically by TD-DFT (DMSO and gas phase) method is 4.2866 and 4.3164 eV and from HOMO-LUMO diagram is 4.2259 eV. All energy gap values are very good agreements which are listed in Table 4.4 and 5.5.



## 4.6. Hyperpolarizability calculations

The first order hyperpolarizability ($\beta_{total}$) of this novel molecular system the related properties ($\mu$, $\alpha$ and $\Delta\alpha$) of 15BHS were investigated by DFT/ Becke-3-Lee-Yang-Parr method with 6-311++G(d,P) basis set, is based on the finite-field approach. Non-linear optical (NLO) is the forefront of present research because of its significance in grants the key functions of frequency shifting, optical modulation, optical switching, optical logic, and optical memory for the emerging technologies in areas such as telecommunications, signal processing, and optical interconnections [33]. Hyperpolarizability are very sensitive to the basis sets and level of theoretical approach employed [34-36], that the electron correlation can change the value of hyperpolarizability.

The non-linear optical response of an isolated molecule in an electric field $E_i$ (ω) can be represented as a Taylor series enlargement of the total dipole moment, $\mu_{tot}$, induced by the field:

$$\mu_{tot} = \mu_0 + \alpha_{ij}E_j + \beta_{ijk}E_jE_k + \ldots, \quad (5.4)$$

Where α is the linear polarizability, $\mu_0$ is the permanent dipole moment and $\beta_{ijk}$ are the first hyperpolarizability tensor components. The isotropic (or average) linear polarizability is defined as:

$$\alpha = \frac{\alpha_{xx} + \alpha_{yy} + \alpha_{zz}}{3} \quad (5.5)$$

The first order hyperpolarizability is a third rank tensor that can be described by 3×3×3 matrix. The 27 components of 3D matrix can be abridged to 10 components owing to the Kleinman symmetry [37]

.Components of the first hyperpolarizability can be reckoned using the following equation:

$$\beta_i = \beta_{iii} + \sum_{i \neq j}(\beta_{ijj} + \beta_{jij} + \beta_{jji}) \quad (5.6)$$

Using the x, y and z components of β, the magnitude of the first hyperpolarizability tensor can be calculated by:

$$\beta_{tot} = \sqrt{(\beta_x^2 + \beta_y^2 + \beta_z^2)} \quad (5.7)$$

The entire equation for reckoning the magnitude of β from Gaussian 09W program output is given a follows:

$$\beta_{tot} = \sqrt{(\beta_{xxx} + \beta_{xyy} + \beta_{xzz})^2 + (\beta_{yyy} + \beta_{yzz} + \beta_{xxy})^2 + (\beta_{zzz} + \beta_{xxz} + \beta_{yyz})^2} \quad (5.8)$$

The calculations of the total molecular dipole moment (μ), linear polarizability (α) and first-order hyperpolarizability (β) from the Gaussian output have been explained in detail previously [38], and DFT

has been widely used as an efficient method to investigate the organic NLO materials [39,40]. In addition, the polar properties of the 15BHS and urea were computed at the DFT (B3LYP)/6-311++G(d,p) level using Gaussian 09W program package.

**Table 4.6**

The values of calculated dipole moment μ(D), polarizability ($\alpha_0$), first order hyperpolarizability (βtot) components of 15BHS and Urea

| Parameters | B3LYP/6-311++G(d,p) | | Parameters | B3LYP/6-311++G(d,p) | |
|---|---|---|---|---|---|
| | 15BHS | Urea | | 15BHS | Urea |
| $\mu_x$ | -0.6634 | 1.0100 | $\beta_{xxx}$ | 491.0058 | 24.2998 |
| $\mu_y$ | 2.0401 | -1.4506 | $\beta_{xxy}$ | 463.5538 | -31.4542 |
| μz | 0 | 0 | $\beta_{xyy}$ | 397.2556 | 5.9597 |
| μ(D) | 2.1452 | 1.7676 | $\beta_{yyy}$ | 223.9906 | -72.1057 |
| $\alpha_{xx}$ | 198.2782 | 25.3561 | $\beta_{zxx}$ | -0.1970 | -0.01325 |
| $\alpha_{xy}$ | 31.9154 | 0.5087 | $\beta_{xyz}$ | 0.0292 | 0.0078 |
| $\alpha_{yy}$ | 199.3002 | 40.6306 | $\beta_{zyy}$ | 0.4411 | 0.0187 |
| $\alpha_{xz}$ | 0 | 0 | $\beta_{xzz}$ | -15.2079 | -0.9717 |
| $\alpha_{yz}$ | 0 | 0 | $\beta_{yzz}$ | 0 | 37.6625 |
| $\alpha_{zz}$ | 76.5808 | 40.1710 | $\beta_{zzz}$ | 0 | 0 |
| $\alpha_0$ (e.s.u) | $2.3423X10^{-23}$ | $0.5244X10^{-23}$ | βtot (e.s.u) | $9.6007X10^{-30}$ | $0.6230X10^{-30}$ |
| α (e.s.u) | $5.4023X10^{-23}$ | $0.6880X10^{-23}$ | | | |



Urea is the prototypical molecule utilized in investigating of the NLO properties of the compound. For this reason, urea was used often as a threshold value for comparative purpose. The calculated dipole moment and hyperpolarizability values obtained from B3LYP/6-311++G(d,p) methods are collected in Table 4.6. The first order hyperpolarizability of 15BHS with B3LYP/6-311++G(d,p) basis set is 9.6007 x $10^{-30}$ fifteen

times greater than the value of urea ($\beta_o$ = 0.6230 x $10^{-30}$ esu). From the computation, the high values of the hyperpolarizabilities of 15BHS are probably attributed to the charge transfer existing amid the benzene rings within the molecular skeleton. This is evidence for the nonlinear optical (NLO) property of the molecule.

### 4.7. Donor- acceptor interactions

The second order fock matrix was carried out to investigate the donor-acceptor interactions in the NBO analysis [41]. NBO analysis has been carried out on the (E)-1-(5-bromo-2-hydroxybenzylidene) semicarbazide at the B3LYP/6-311++G(d,p) level in order to elucidate the intra molecular, rehybridization and delocalization of electron density within the molecule. The higher the E(2) value, the molecular interaction between electron donors and electron acceptors is more intensive and the greater the extent of conjugation of the entire system. Delocalization of electron density amid occupied Lewis-type (bond or lone pair) NBO orbitals and properly unoccupied (antibond or Rydgberg) non-Lewis NBO orbitals resemble to a stabilizing donor-acceptor interaction.



The strong intramolecular hyper conjugative interaction of the $\sigma$ and $\pi$ electrons of C-C to the anti C - C bond of the ring leads to stabilization and evidence of some part of ring values are listed in Table 5.7. The strong intramolecular hyperconjugative interaction of σ ($C_7$-$C_8$) distributes to σ $^*$ ($C_6 - C_7$, $C_7 - C_{12}$ and $C_8 - C_9$ of the ring. On the other hand, side the π $C_7$- $C_8$ in the ring conjugate to the anti-bonding orbital of π*($N_2 - C_6$), π*($C_9 - C_{10}$) and π*($C_{11}$ - $C_{12}$) which leads to strong delocalization of

**Table 4.7** Second order perturbation theory analysis of Fock matrix in NBO basis for 15BHS

| Donor(i) | Type | Acceptor(i) | Type | [a]E(2) (KJ mol$^{-1}$) | [b]E(J)-E(i) (a.u.) | [c]F(I,j) (a.u.) |
|---|---|---|---|---|---|---|
| $N_1$-$C_3$ | σ | $N_2$-$C_6$ | σ* | 2.27 | 1.49 | 0.052 |
| $N_1$-$H_{15}$ | σ | $C_3$-$N_5$ | σ* | 3.79 | 1.14 | 0.06 |
| $N_2$-$C_6$ | σ | $C_6$-$C_7$ | σ* | 4.38 | 1.56 | 0.074 |
| $N_2$-$C_6$ | π | $C_7$-$C_8$ | π* | 12.89 | 0.38 | 0.069 |
| $C_3$-$O_4$ | π | $C_3$-$O_4$ | π* | 2.56 | 0.38 | 0.031 |
| $N_5$-$H_{16}$ | σ | $C_3$-$O_4$ | σ* | 4.12 | 1.31 | 0.066 |
| $N_5$-$H_{17}$ | σ | $N_1$-$C_3$ | σ* | 4.33 | 1.11 | 0.063 |
| $C_6$-$C_7$ | σ | $N_1$-$N_2$ | σ* | 4.54 | 1.13 | 0.064 |
| | | $N_2$-$C_6$ | σ* | 4.44 | 1.39 | 0.071 |
| | | $C_7$-$C_8$ | σ* | 5.67 | 1.38 | 0.079 |
| | | $C_7$-$C_{12}$ | σ* | 6.84 | 1.40 | 0.087 |
| $C_6$-$H_{18}$ | σ | $C_7$-$C_{12}$ | σ* | 4.72 | 1.19 | 0.067 |
| $C_7$-$C_8$ | σ | $C_6$-$C_7$ | σ* | 6.20 | 1.38 | 0.083 |
| | | $C_7$-$C_{12}$ | σ* | 7.10 | 1.40 | 0.089 |
| | | $C_8$-$C_9$ | σ* | 5.98 | 1.38 | 0.081 |
| $C_7$-$C_8$ | π | $N_2$-$C_6$ | π* | 26.58 | 0.29 | 0.082 |
| | | $C_9$-$C_{10}$ | π* | 19.57 | 0.31 | 0.071 |
| | | $C_{11}$-$C_{12}$ | π* | 25.11 | 0.31 | 0.08 |
| $C_7$-$C_{12}$ | σ | $C_6$-$C_7$ | σ* | 7.25 | 1.36 | 0.089 |
| | | $C_6$-$H_{18}$ | σ* | 3.05 | 1.11 | 0.052 |
| | | $C_7$-$C_8$ | σ* | 7.06 | 1.37 | 0.088 |
| | | $C_8$- $O_{13}$ | σ* | 4.53 | 1.08 | 0.063 |
| | | $C_{11}$-$C_{12}$ | σ* | 5.76 | 1.39 | 0.08 |
| | | $C_{11}$-$Br_{14}$ | σ* | 6.27 | 0.84 | 0.065 |
| $C_8$-$C_9$ | σ | $C_6$-$C_7$ | σ* | 3.51 | 1.39 | 0.062 |

| | | | | | | |
|---|---|---|---|---|---|---|
| | | $C_7$-$C_8$ | σ* | 6.89 | 1.39 | 0.088 |
| | | $C_9$-$C_{10}$ | σ* | 4.81 | 1.40 | 0.073 |
| $C_9$-$C_{10}$ | σ | $C_8$-$C_9$ | σ* | 4.38 | 1.38 | 0.07 |
| | | $C_8$-$O_{13}$ | σ* | 4.46 | 1.10 | 0.063 |
| | | $C_{11}$-$Br_{14}$ | σ* | 6.14 | 0.86 | 0.065 |
| $C_9$-$C_{10}$ | π | $C_7$-$C_8$ | π* | 23.26 | 0.32 | 0.079 |
| | | $C_{11}$-$C_{12}$ | π* | 18.65 | 0.31 | 0.069 |
| $C_{10}$-$C_{11}$ | σ | $C_{11}$-$C_{12}$ | σ* | 5.40 | 1.42 | 0.078 |
| $C_{10}$-$H_{20}$ | σ | $C_{11}$-$C_{12}$ | σ* | 4.69 | 1.17 | 0.066 |
| $C_{11}$-$C_{12}$ | σ | $C_7$-$C_{12}$ | σ* | 5.30 | 1.41 | 0.077 |
| | | $C_{10}$-$C_{11}$ | σ* | 5.34 | 1.41 | 0.077 |
| $C_{11}$-$C_{12}$ | π | $C_7$-$C_8$ | π* | 17.93 | 0.32 | 0.07 |
| | | $C_9$-$C_{10}$ | π* | 24.07 | 0.32 | 0.079 |
| $C_{11}$-$Br_{14}$ | σ | $C_7$-$C_{12}$ | σ* | 2.99 | 1.32 | 0.056 |
| | | $C_9$-$C_{10}$ | σ* | 3.24 | 1.31 | 0.058 |
| $C_{12}$-$H_{21}$ | σ | $C_7$-$C_8$ | σ* | 4.48 | 1.15 | 0.064 |
| | | $C_{10}$-$C_{11}$ | σ* | 4.74 | 1.16 | 0.066 |
| $N_1$ | LP(1) | $N_2$-$C_6$ | π* | 30.76 | 0.29 | 0.086 |
| | | $C_3$-$O_4$ | π* | 52.73 | 0.30 | 0.114 |
| $N_2$ | LP(1) | $N_1$-$H_{15}$ | σ* | 8.69 | 0.76 | 0.074 |
| | | $C_6$-$H_{18}$ | σ* | 9.61 | 0.77 | 0.078 |
| $O_4$ | LP(2) | $N_1$-$C_3$ | σ* | 24.29 | 0.68 | 0.117 |
| | | $C_3$-$N_5$ | σ* | 23.55 | 0.69 | 0.116 |
| $N_5$ | LP(1) | $C_3$-$O_4$ | π* | 54.89 | 0.28 | 0.116 |
| $O_{13}$ | LP(1) | $C_8$-$C_9$ | σ* | 5.90 | 1.21 | 0.076 |
| $O_{13}$ | LP(2) | $C_7$-$C_8$ | π* | 26.09 | 0.38 | 0.097 |
| $Br_{14}$ | LP(3) | $C_{11}$-$C_{12}$ | π* | 10.02 | 0.33 | 0.055 |

[a]$E^{(2)}$ means energy of hyper conjugative interaction (stabilization energy)

26.58, 19.57 and 25.11 kJ/mol respectively. Some important second order perturbation energies and molecular orbital interactions investigated from the NBO calculation are listed in Table 4.7, which shows the very important interactions between Lewis and non-Lewis orbital with Oxygen and nitrogen lone pairs. The very significant interaction between them was the electron donation of LP(1) $N_1$, LP(1) $N_5$, LP(2) $O_{13}$ and LP (2) $O_4$ to the neighbouring antibonding acceptor $\sigma^*(N_2\text{-}C_6)$, $\sigma^*(C_3\text{-}O_4)$, $\pi^*(C_3\text{-}O_4)$, $\pi^*(C_7\text{-}C_8)$, $\sigma^*(N_1\text{-}C_3)$ and $\sigma^*(C_3\text{-}N_5)$ of the 15BHS energy by 30.76, 52.73, 54.89, 26.09, 24.29 and 23.55 kJ/mol.

## 4.8. Molecular electrostatic potentials (MEP)

Molecular electrostatic potential (MEP) simultaneously displays molecular shape, size, and electrostatic potential in terms of colour grading. MEPs map has been found to be a very helpful tool in the analysis of the correlation amid molecular structures with its physiochemical property relationship, including biomolecules and drugs [42]. MEPs map and contour plot of the (E)-1-(5-bromo-2-hydroxybenzylidene) semicarbazide (15BHS) generated at the optimized geometry of the title molecule using GaussView 5.0 program is shown in Fig 4.9 and 4.10. The various values of the electrostatic potential are represented by various colours; red represented the regions of the most negative electrostatic potential, blue represents the regions of the most positive electrostatic potential and green presents the region of zero potential. The potential increases in the order red < orange < yellow < green < cyan < blue. It can be seen that the negative regions are mainly over the $O_4$ atoms. Negative (red colour) and positive (blue) regions of electrostatic potential are associated with electrophilic and nucleophilic reactivity. The majority of light green region MEP surface resemble a potential halfway between two

extremes red and dark blue colour. The negative molecular electrostatic potential resembles to an attraction of the proton by the evaluate electron density in the molecule (shades of red), the positive electrostatic potential corresponds to the repulsion of the protons by the atomic nuclei (shades of blue). According to these calculated results, the MEP map illustrates that the negative potential sites are on oxygen and nitrogen atoms and the positive potential sites as well are around the hydrogen atoms. These active sites found to be clear evidence of biological activity in the title compound.

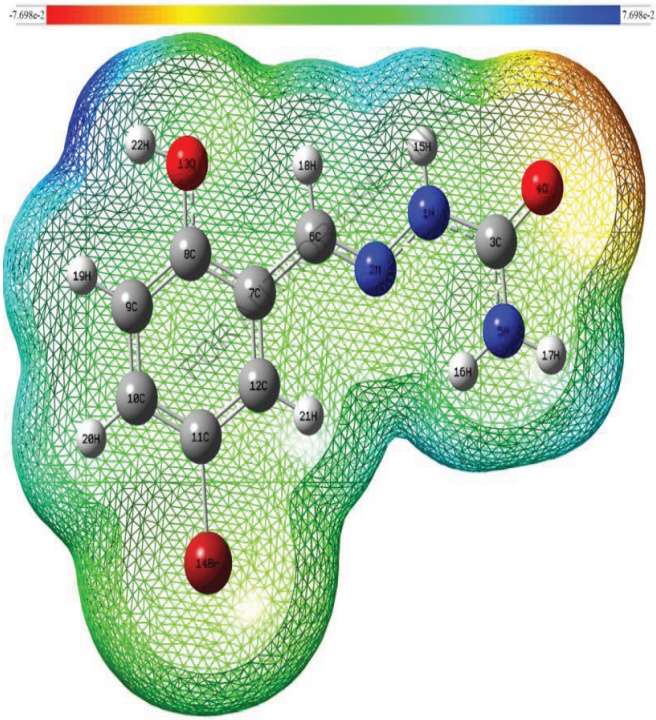


**Fig. 4.9**. Total electron density mapped with molecular electrostatic potential surface of 15BHS.

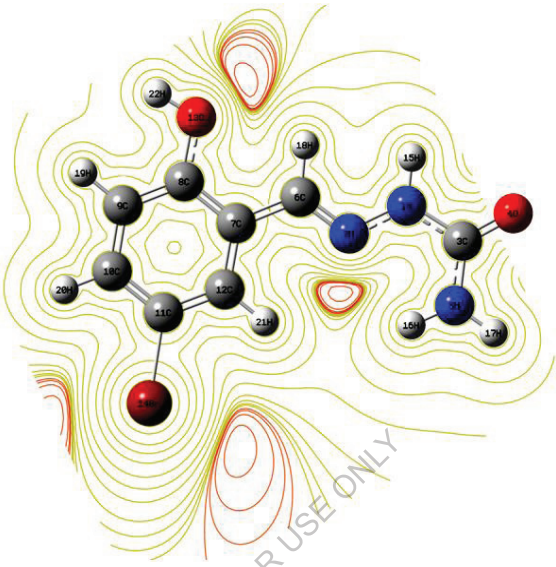

**Fig. 4.10**. The contour map of electrostatic potential of 15BHS.



## 4.9. Fukui function

Fukui function plays a central role in study of chemical reactivity and selectivity. It indicates the propensity of density to deform at a given position in order to accept or donate electrons which are more prone to undergo a nucleophilic or an electrophilic attack respectively. Fukui functions such as nucleophilic attack, electrophilic attack and radical attack have been calculated [43,44]. Fukui functions and local softness for selected atomic sites in 15BHS have been listed in Table 4.8. It has been found that MPA schemes predict $Br_{14}$ has lower $f_r^-$ value indicates the possible site for electrophilic attack. From Table 5.8 shows, MPA schemes predict the reactivity order for the electrophilic case as $Br_{14} > C_{11}$

> $O_4$ > $N_1$ > $O_{13}$ > $C_{10}$ > $C_{12}$ > $C_8$ > $N_5$. The calculated $f_r^+$ values predicts that the possible sites for nucleophilic attack is $C_7$ and $N_1$ site and the radical attack was predicted at $C_7$ and $C_3$ site. The title compound more electrophilic attack than nucleophilic attack and radical attack. These results show 15BHS compound act as more biological activity.

**Table 4.8**

Condensed fukui function $f_r$ and new descriptor $(sf)_r$ for 15BHS.

| Atoms | $f_r^+$ | $f_r^-$ | $f_r^0$ | $s_r^+ f_r^+$ | $s_r^- f_r^-$ | $s_r^0 f_r^0$ |
|---|---|---|---|---|---|---|
| $N_1$ | 0.0203 | -0.0930 | -0.0363 | 0.0048 | -0.0220 | -0.0086 |
| $N_2$ | -0.1205 | -0.0484 | -0.0845 | -0.0285 | -0.0115 | -0.0200 |
| $C_3$ | -0.0010 | 0.0145 | 0.0068 | -0.0002 | 0.0034 | 0.0016 |
| $O_4$ | -0.0830 | -0.1209 | -0.1020 | -0.0196 | -0.0286 | -0.0241 |
| $N_5$ | -0.0188 | -0.0248 | -0.0218 | -0.0044 | -0.0059 | -0.0052 |
| $C_6$ | -0.0584 | -0.0121 | -0.0353 | -0.0138 | -0.0029 | -0.0083 |
| $C_7$ | 0.1045 | -0.0105 | 0.0470 | 0.0247 | -0.0025 | 0.0111 |
| $C_8$ | -0.0349 | -0.0379 | -0.0364 | -0.0083 | -0.0090 | -0.0086 |
| $C_9$ | -0.0238 | -0.0042 | -0.0140 | -0.0056 | -0.0010 | -0.0033 |
| $C_{10}$ | -0.0595 | -0.0191 | -0.0393 | -0.0141 | -0.0045 | -0.0093 |
| $C_{11}$ | -0.1917 | -0.1116 | -0.1717 | -0.0454 | -0.0359 | -0.0406 |
| $C_{12}$ | -0.0523 | 0.0514 | -0.0005 | -0.0124 | 0.0122 | -0.0001 |
| $O_{13}$ | -0.0166 | -0.0653 | -0.0409 | -0.0039 | -0.0154 | -0.0097 |
| $Br_{14}$ | -0.1209 | -0.1166 | -0.1387 | -0.0286 | -0.0371 | -0.0328 |



## 4.10. Thermodynamic properties

Standard statistical thermodynamics function, heat capacity$\left(C_{p,m}^{0}\right)$, entropy $\left(S_{m}^{0}\right)$ and enthalpy changes $\left(H_{m}^{0}\right)$ were computed at B3LYP/6-311++G(d,p) basis set by using perl script THERMO.PL [45] and are listed in Table 4.9. Thermodynamic functions are all values increasing

with temperature ranging from 100 to 1000K due to the fact that the molecular vibrations intensities increase with temperature.

The correlation equation among heat capacities, entropies, enthalpy changes with temperatures were fitted by quadratic formulas and the corresponding fitting factors ($R^2$) these thermodynamic properties are 0.9993, 0.9997 and 0.9993 respectively. The correlations plot of those shown in Fig 4.11.

The thermodynamic correlation fitting equation is follows:

$$\left(C_{p,m}^{0}\right) = 33.8900 + 0.6906T - 3.1650 \times 10^{-4}T^2 \ (R^2 = 0.9993) \qquad (5.9)$$

$$\left(S_{m}^{0}\right) = 262.2796 + 0.8729T - 2.5363 \times 10^{-4}T^2 \ (R^2 = 0.9997) \qquad (5.10)$$

$$\left(H_{m}^{0}\right) = -10.0536 + 0.1164T - 1.6958 \times 10^{-4}T^2 \ (R^2 = 0.9993) \qquad (5.11)$$



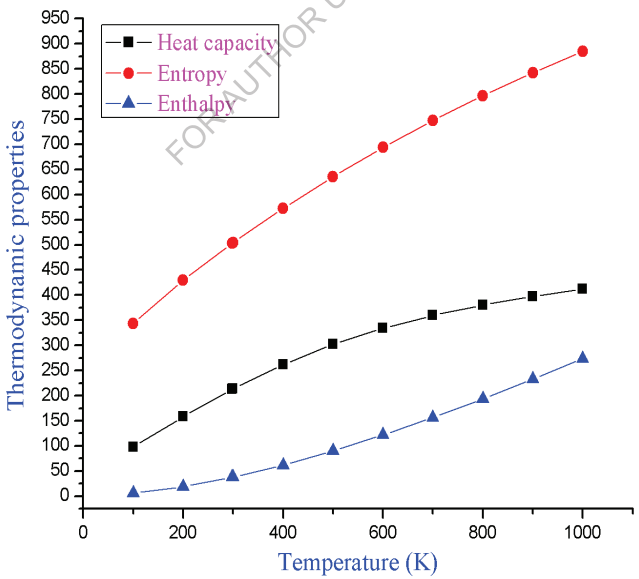


**Fig . 4.11.** Correlation plot of thermodynamic properties at different temperature of the 15BHS compound.

**Table 4.9**

Temperature dependence of thermodynamic properties of 15BHS at B3LYP /6-311++G(d,p)

| T(K) | $C^{0}_{p,m}$ (J/ mol K) | $S^{0}_{m}$ (J/ mol K) | $H^{0}_{m}$ (kJ/ mol) |
|---|---|---|---|
| 100 | 97.84 | 342.9 | 6.56 |
| 200 | 158.42 | 429.6 | 19.41 |
| 298.15 | 212.78 | 503.16 | 37.68 |
| 300 | 213.75 | 504.48 | 38.07 |
| 400 | 262.21 | 572.81 | 61.94 |
| 500 | 302.16 | 635.77 | 90.23 |
| 600 | 334.08 | 693.79 | 122.1 |
| 700 | 359.6 | 747.28 | 156.83 |
| 800 | 380.33 | 796.69 | 193.86 |
| 900 | 397.46 | 842.51 | 232.77 |
| 1000 | 411.86 | 885.15 | 273.26 |



All thermodynamic data provide useful information for further studies. They can be used to compute other thermodynamic energies according to relationships of thermodynamic functions and estimate directions of chemical reactions according to the second law of thermodynamics in thermo chemical field [46].

### 4.11. Antibacterial activity

Biological evaluations have been checked in term of antimicrobial activities of target compounds against gram-positive (Enterobacter and Bacillus subtilis), gram-negative (Escherichia coli and Klebsiella pneumoniae) and three strains of fungus (Candida albicans, A.niger and A.fumicatus). Result for antimicrobial activities of target compounds are presented in Table 4.10(a) and 4.10(b) and illustrated in Figs. 4.12 and

4.13. Activity has been determined by measuring inhibition zone diameter values (mm) of investigated compound. It is noted that the solvent itself has no activity on the microbes. 15BHS dissolved at different concentrations has been screened for their activity against bacterial strains. The nutrient agar medium was prepared and sterilized by autoclaving at 121˚C 15 lbs pressure for 15 minutes then aseptically poured the medium into the sterile petriplates and allowed to solidify the Bacterial broth culture was swabbed on each petriplates using a sterile buds. Then wells were made by well cutter.

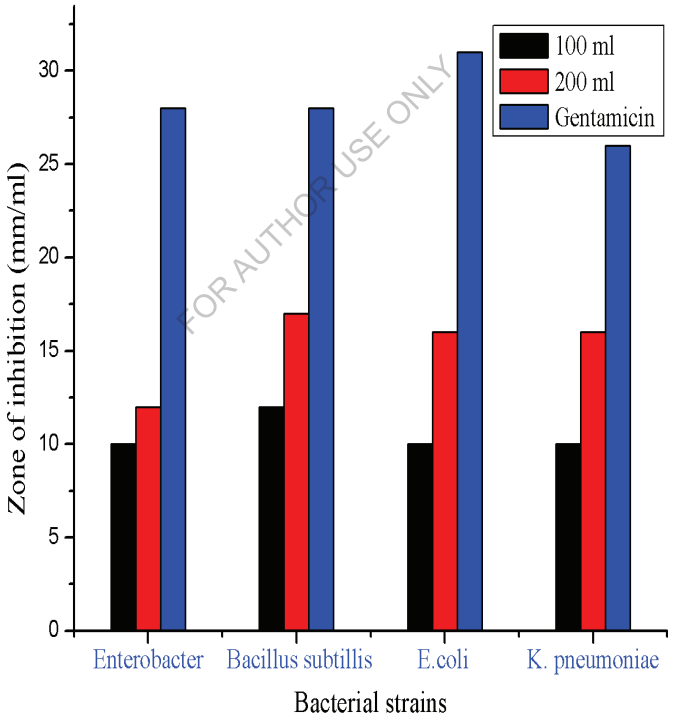



**Fig. 4.12.** A bar diagram for the antibacterial activity of 15BHS.

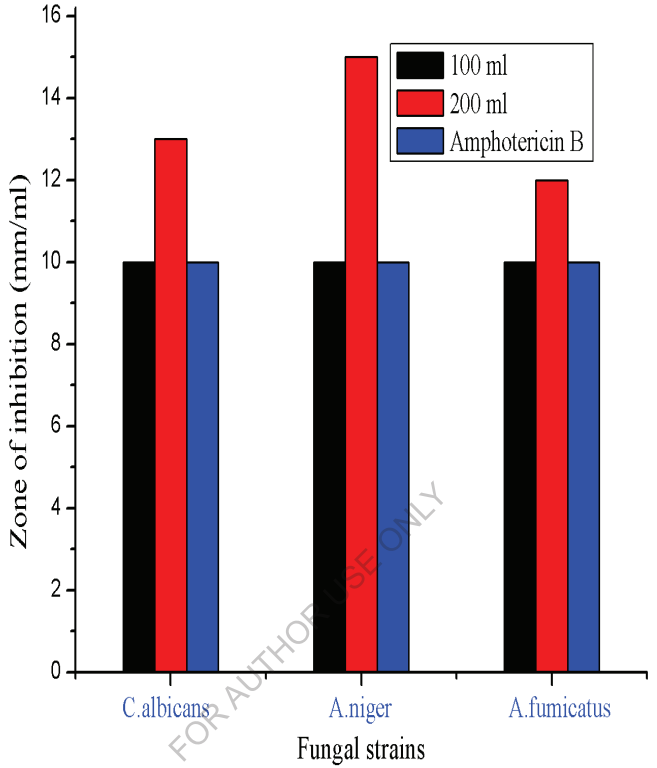



**Fig. 4.13.** A bar diagram for the antifungal activity of 15BHS.

The organic solvent extracts of leaves were added to each well aseptically. This procedure was repeated for each Petri plates then the petriplates were incubated at 37˚C for 24 hrs. After incubation the plates were observed for the zone of inhibition. 15BHS possess remarkable antifungal activity against Candida albicans but it is comparatively low when compared to the other pathogen A.niger. It is found that 15BHS has high activity on A.niger with increase in concentration. So, antifungal activity is more when compared with antibacterial activity.

**Table 4.10(a)** Antibacterial activity of DMSO extracts

| Bacterial pathogen | DMSO Extract added and Zone of inhibition (mm/ml) | | | |
|---|---|---|---|---|
| | 100 µl | 200 µl | DMSO | Gentamicin |
| *Enterobacter* | 10 | 12 | - | 28 |
| *Bacillus subtillis* | 12 | 17 | - | 28 |
| *E.coli* | 10 | 16 | - | 31 |
| *K. pneumoniae* | 10 | 16 | - | 26 |

**Table 4.10(b)** Antifungal activity of DMSO extracts

| Fungal pathogen | DMSO Extract added and Zone of inhibition (mm/ml) | | | |
|---|---|---|---|---|
| | 100 µl | 200 µl | DMSO | Amphotericin B |
| *Candida albicans* | 10 | 13 | - | 10 |
| *A.niger* | 10 | 15 | - | 10 |
| *A.fumicatus* | 10 | 12 | - | 10 |



## 4.12. Molecular docking study

Molecular docking is playing an increasingly important role in drug design for the treatment of many diseases. This technique provides insight into plausible protein-ligand interactions which can substantiate the experimental result. The title molecule was selected to be docked into the active site of three receptors Aspergillus fumigates (2X8R), Candida albicans (4HOE) and Aspergillus niger (3EQA) of three fungal proteins which was downloaded from RCSB protein data bank [47, 48]. However, people with weakened immune systems or lung diseases are at a higher risk of developing health problems due to 2X8R, 4HOE and 3EQA.

The Graphical User Interface program ‘‘Auto- Dock Tools’’ was used to prepare, run, and analyze the docking simulations. Kollman united atom charges, salvation parameters and polar hydrogen’s were added to the receptor for the preparation of protein in docking simulation.

Molecular docking software AutoDock 4.2.6 [49] Program supplied with AutoGrid 4.0 and AutoDock 4.0 was used to produce grid maps. The Lamarckian Genetic Algorithm (LGA) was chosen to investigate for the best conformers [50]. During the docking process, a maximum of 100 conformers was considered for title compound. All the AutoDock docking runs were performed in Intel(R) Pentium(R) CPU A1018 @ 2.10 GHz of Acer system origin, with 2 GB RAM. AutoDock 4.2.6 was compiled and run under Microsoft Windows7 operating system.

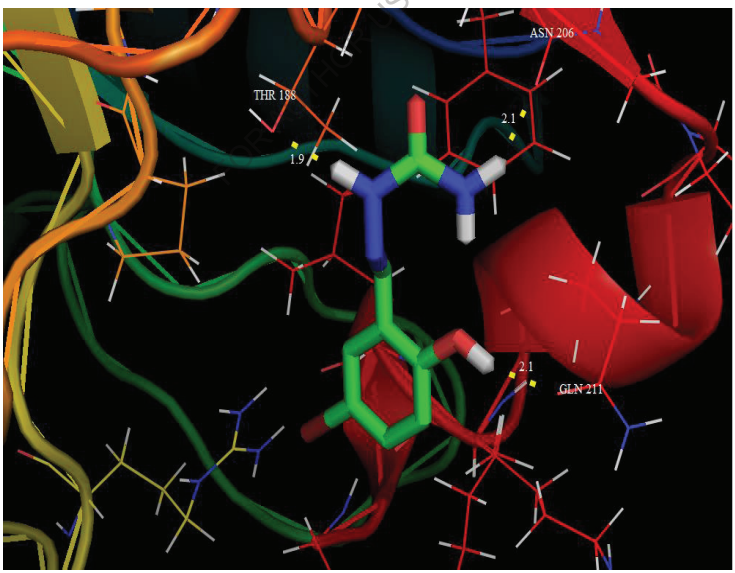


**Fig. 4.14.** Docking and Hydrogen bond interactions of 15BHS with chain A of 2X8R protein structure

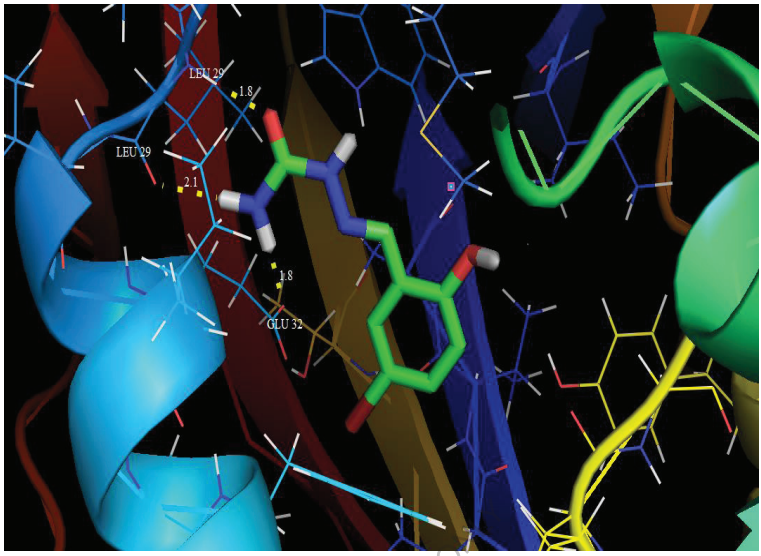


**Fig. 4.15.** Docking and Hydrogen bond interactions of 15BHS with chain A of 4HOE protein structure

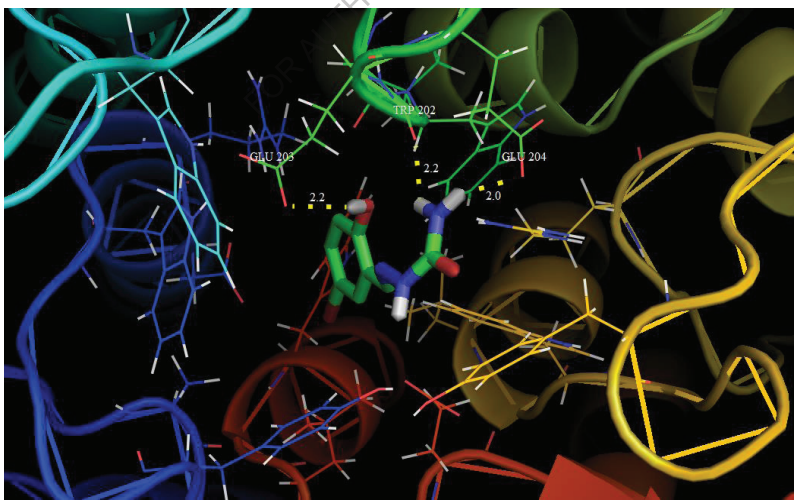


**Fig. 5.16.** Docking and Hydrogen bond interactions of 15BHS with chain A of 3EQA protein structure

**Table 4.11**

Hydrogen bonding and molecular docking with antifungal protein targets

| Protein | Bonded residues | hydrogen bond interaction | Bond distance (Å) | EIC (µm) | BE (kcal/mol) | RMSD (Å) |
|---|---|---|---|---|---|---|
| 2X8R | ASN 206 | NH…O | 2.1 | 103.5 | -5.44 | 33.94 |
| | GLN 211 | OH…O | 2.1 | | | |
| | THR 188 | NH…O | 1.9 | | | |
| 4HOE | GLU 32 | NH…O | 1.8 | 11.76 | -6.73 | 28.13 |
| | LEU 29 | NH…O | 2.1 | | | |
| | LEU 29 | O…NH | 1.8 | | | |
| 3EQA | GLU 204 | NH…O | 2.0 | 41.62 | -5.98 | 24.38 |
| | TRP 202 | NH…O | 2.2 | | | |
| | GLU 203 | OH…O | 2.2 | | | |



The ligand was docked into the functional sites of the respective proteins individually and the docking energy was examined to achieve a minimum value. AutoDock results indicate the binding position and bound conformation of the peptide, together with a rough estimate of its interaction. Docked conformation which had the lowest binding energy was chosen to investigate the mode of binding. The molecular docking binding energies (kcal/mol) and inhibition constants (µm) were also obtained and listed in Table 4.11. Among them, 4HOE exhibited the lowest binding energy at -6.73 kcal/mol and most docked inhibitors interacted with the ligand within the 4HOE binding site. They exhibited up to three hydrogen bonds involving NH…O, NH…O and O…NH with RMSD being 28.13 Å. The docking simulation shows the binding mode of the 15BHS into 4HOE. The 15BHS ligand interacts with different receptors are shown in Figs. 4.13-4.15 reapectively.

## Reference


[1] G. Saravanan, V. Alagarsamy, C. Rajaram Prakash, Synthesis, characterization and in vitro antimicrobial activity of some 1-(substitutedbenzylidene)-4-(4-(2-(methyl/phenyl)-4-oxoquinazolin-3(4H) yl)phenyl)semicarbazide derivatives, J. Saudi Chem. Soc. 19 (2015) 3-11.

[2] S. Chandra , L.K. Gupta, Spectroscopic and biological studies on newly synthesized nickel(II) complexes of semicarbazones and thiosemicarbazones, Spectrochim. Acta A 62 (2005) 1089-1094.

[3] R. Sharma, S. Mudgal, B. Shrivastava, P. Sharma, Synthesis, characterization & biological evaluation of newer 4-(4-substituted aryl) semicarbazones as anticonvulsant and anti-microbial agents, Indo American. J. Pharm Rech. 3 (2013) 5522-5540.

[4] J.R. Dimmock, K.K Sidhu, S.D. Tumber, S.K. Basranl, M. Chen, J.W. Quail, J. Yang, I. Rozas, D.F. Weaver, Some aryl semicarbazones possessing anticonvulsant activities, Eur. J. Med. Chem. 30 (1995) 287-301.

[5] A.P. Martinez, W.W. Lee, Some Semicarbazones and Thiosemicarbazones, *J. Med. Chem.* 10 (1967) 1192.

[6] V.L. Siji, M.R. Sudarsanakumar, S. Suma, A. Geogre, P.V. Thomas, FT-IR and FT-Raman spectral studies and DFT calculations of tautomeric forms of benzaldehyde-N(4)-phenylsemicarbazone, Indian journal of chemistry 50A (2011) 793-797

[7] A. Dhandapani, S. Manivarman, S. Subashchandrabose, H. Saleem, Molecular structure and vibrational analysis on (E)-1-(3-methyl-2,6-diphenyl piperidin-4-ylidene) semicarbazide, J. Mol. Struct. 1058 (2014) 41-50.

[8] S. Subashchandrabose, N. Ramesh Babu, H. Saleem, M. Syed Ali Padusha, Vibrational studies on (E)-1-((pyridine-2-yl)methylene)semicarbazide using experimental and theoretical method, J. Mol. Struct. 1094 (2015) 254–263.

[9] M.J. Frisch, G.W. Trucks, H.B. Schlegel, G.E. Scuseria, M.A. RobbGaussian 09, Revision **E.01,** Gaussian, Inc., Wallingford CT, 2009.

[10] M.H. Jamroz, Vibrational energy distribution analysis (VEDA): scopes and limitations, Spectrochim. Acta A 114 (2004) 220-230.

[11] S. Murugavel, V. Vetri velan, D. Kannan, M. Bakthadoss, Synthesis of a novel methyl(2*E*)-2-{[*N*-(2-formylphenyl)(4-methylbenzene)sulfonamido]methyl}-3-(2-methoxyphenyl)prop-2-enoate:molecular structure, spectral, antimicrobial, molecular docking and DFT computational approaches, , J. Mol. Struct. 1127 (2017) 457–475.

[12] M. Raja, R. Raj Muhamed, S. Muthu, M. Suresh, K. Muthu, Synthesis, spectroscopic (FT-IR, FT-Raman, NMR, UV-Visible), Fukui function, antimicrobial and molecular docking study of (E)-1-(3-bromobenzylidene)semicarbazide, J. Mol. Struct. 1130 (2017) 374–384.

[13] M. Cinar, M. Karabacak , A.M. Asiri, An experimental and density functional study on conformational and spectroscopic analysis of 5-methoxyindole-2-carboxylic acid, Spectrochim. Acta Part A 137 (2015) 670-676.

[14] E.D. Glendening, A.E. Reed, J.E. Carpenter, F. Weinhold, NBO Version 3.1, Theoretical Chemistry Institute and Department of Chemistry, University of Wisconsin, Madison, 1998.

[15] H.K. Fun, C.W.Ooi, S. Malladi, A.M. Isloor , K.N. Shivananda, 2-[(E)-4-Diethylamino-2-hydroxybenzylidene]hydrazinecarboxamide, Acta Cryst. E68 (2012) o380.

[16] M.T. Gulluoglu, Y.Erdogu, J. Karpagam, N. Sundaraganesan, S.Yurdakal, DFT, FT-Raman, FT-IR and FT-NMR studies of 4-phenylimidazole, J. Mol. Struct. 990 (2011) 14- 20.

[17] D. Lin-Vien, N.B. Colthup, W.G. Fately, J.G. Grasselli, The Handbook of Infrared and Raman Characteristic Frequencies of Organic Molecules, Academic Press Boston, MA, 1991.

[18] M. Silverstein, G.C. Basseler, C. Morill, Spectrometric Identification of Organic Compounds, Wiley, New York, 1981.

[19] V. Krishnakumar, R. Ramasamy, Scaled quantum chemical studies of the structure and vibrational spectra of 2-(methylthio) benzimidazole, Spectrochim. Acta Part A 62 (2005) 570-577.

[20] L.J. Bellamy, the Infrared Spectra of Complex Molecules, vol. 2, Chapman and Hall, London, 1980.

[21] N. Swarnalatha, S.Gunasekaran, S. Muthu, M. Nagarajan, Molecular structure analysis and spectroscopic characterization of 9-methoxy-2H-furo[3,2-g]chromen-2-one with experimental (FT-IR and FT-Raman) techniques and quantum chemical calculations, spectrochim. Acta part A 137 (2015) 721-729.

[22] L.G. Wade (Ed), Advanced Organic Chemistry, 4th ed., Wiley, New York,1992. p.723.

[23] G. Varsanyi, Aassignments for vibrational Spectra of Seven Hundred Benzene Derivatives, vol. 1, Adam Hilger, London, 1974.

[24] V. Udayakumar, S. Periandy, S. Ramalingam, Experimental (FT-IR and FT-Raman) and theoretical (HF and DFT) investigation, IR intensity, Raman activity and frequency estimation analyses on 1-bromo-4-chlorobenzene, Spectrochim. Acta A 79 (2011) 920-927.

[25] N. Sundaraganesan, S.Illakiamani, C. Meganathan, B.D. Joshua, Vibrational spectroscopy investigation using ab initio and density functional theory analysis on the structure of 3-aminobenzotrifluoride, Spectrochim. Acta A 67 (2007) 214-224.

[26] M.A. Quarishi, D. Jamal, Dianils: New and Effective Corrosion Inhibitors for Oil-Well Steel (N-80) and Mild Steel in Boiling Hydrochloric Acid, Corros. Sci. 56 (2000) 156-160.

[27] G. Varsanyi, Vibrational spectra of Benzene Derivatives, Academic press, New York, 1969.

[28] G. Socrates, Infrared Characteristic Group Frequencies, John Wiley Interscience, New York, 1980.

[29] B.T. Gowda, K. Jyothi, J.D. D'Souza, Infrared and NMR Spectra of Arylsulphonamides, 4-X-C6H4SO2NH2 and i-X, j-YC6H3SO2NH2 (X¼H; CH3; C2H5; F; Cl; Br; I or NO2 and i-X, j-Y¼2,3-(CH3)2; 2,4-(CH3)2; 2,5-(CH3)2; 2-CH3, 4-Cl; 2-CH3, 5-Cl; 3-CH3, 4-Cl; 2,4-Cl2 or 3,4-Cl2), Z. Natureforsch. 57a (2002) 967-973.

[30] N. Subramanian, N. Sundaraganesan, J. Jayabharathi, Molecular structure, spectroscopic (FT-IR, FT-Raman, NMR, UV) studies and first-order molecular hyperpolarizabilities of 1,2-bis(3-methoxy-4-hydroxybenzylidene)hydrazine by density functional method, Spectrochim. Acta A 76 (2010) 259-269.

[31] D.F.V. Lewis, C. Ioannides, D.V. Parke, Interaction of a series of nitriles with the alcohol-inducible isoform of P450: computer analysis of structure-activity relationships, Xenobiotica 24 (1994) 401-408.

[32] R. G. Pearson, Absolute electronegativity and hardness correlated with molecular orbital theory, Proc. Natl. Acad. Sci. 83 (1986) 8440-8441.

[33] G. Velraj, S. Soundharam, C. Sridevi, Structure, vibrational, electronic, NBO and NMR analyses of 3-methyl-2,6-diphenylpiperidin-4-one (MDPO) by experimental and theoretical approach, Journal of Molecular Structure 1060 (2014) 156-165.

[34] A.E. Reed, L.A. Curtiss, F. Weinheld, Intermolecular Interactions from a Natural Bond Orbital, Donor-Acceptor Viewpoint, Chem.Soc. 102 (1988) 899-926.

[35] J.P. Foster, F. Weinhold, Natural Hybrid Orbitals, J. AM. Chem. Soc. 102 (1980) 7211-7218.

[36] H. Sekino, R.J. Bartlett, Hyperpolarizabilities of the hydrogen fluoride molecule: A discrepancy between theory and experiment?, J. Chem. Phys. 84 (1986) 2726-2733.

[37] D. Sajan, H. Joe, V. S. Jajakumar, J. Zaleski, Structural and electronic contributions to hyperpolarizability in methyl p-hydroxy benzoate, J. Mol. Struct. 785 (2006) 43-53.

[38] K.S. Thanthiri Watte, K.M. Nalin de silva, Non-linear optical properties of novel fluorenyl derivatives-ab initio quantum chemical calculations, J. Mol. Struct. Theochem. 617 (2002) 169-175.

[39] S.G. Sagdinc, A. Esme, Theoretical and vibrational studies of 4,5-diphenyl-2-2 oxazole propionic acid (oxaprozin), Spectrochim. Acta Part A 75 (2010) 1370-1376.

[40] S. Muthu, G. Ramachandran, Spectroscopic studies (FTIR, FT-Raman and UV–Visible), normal coordinate analysis, NBO analysis, first order hyper polarizability, HOMO and LUMO analysis of (1R)-N-(Prop-2-yn-1-yl)-2,3-dihydro-1H-inden-1-amine molecule by ab initio HF and density functional methods, Spectrochim. Acta part A 121 (2014) 394-403.

[41] M. Szafran, A. komasa, E.B. Adamska, Crystal and molecular structure of 4-carboxypiperidinium chloride (4-piperidinecarboxylic acid hydrochloride), J Mol. Struct. THEOCHEM 827 (2007) 101-107.

[42] **S**.K. Pathak, R. Srivastava, A.K. sachan, O. Prasad, L. Sinha, A.M. Asiri, M. Karabacak, Experimental (FT-IR, FT-Raman, UV and NMR) and quantum chemical studies on molecular structure, spectroscopic analysis, NLO, NBO and reactivity descriptors of 3,5-Difluoroanilin, Spectrochim.Acta A 135 (2015) 283-295.

[43] R.G. Parr, W. Yang, Functional Theory of Atoms and Molecules, OxfordUniversity Press, New York, 1989.

[44] P. Politzer, P. Lane, A computational study of some nitrofluoromethanes Struct.Chem. 61 (1990) 159-164.

[45] K.K. Irikura, THERMO. PL (National Institute of Standards and Technology), Gaithersburg, MD, 2002.

[46] J.B. Ott, J.B. Goates, Chemical Thermodynamics: Principles and Applications, Academic Press, San Diego, 2000

[47] T. Joselin Beaula, I. Hubert Joe, V.K. Rastogi, V. Bena Jothy, Spectral investigations, DFT computations and molecular docking studies of the antimicrobial 5-nitroisatin dimer, Che. Phy. Letters 624 (2015) 93-101.

[48] H.M. Berman, J. Westbrook, Z. Feng, G. Gilliland, T.N. Bhat, H. Weissig, I.N. Shindyalov, P.E. Bourne, The protein data bank, Nucleic Acids Res. 28 (2000) 235-242.

[49] A.R. Katritzky, L. Mu, V.S. Lobanov, M. Karelson, Correlation of Boiling Points with Molecular Structure. 1. A Training Set of 298 Diverse Organics and a Test Set of 9 Simple Inorganics, J. Phys. Chem. 100 (1996) 10400-10407.

[50] R. Huey, G.M. Morris, A.J. Olson, D.S. Goodsell, A semiempirical free energy force field with charge-based desolvation, J. Comput. Chem. 28 (2007) 1145-1152.

# CHAPTER V

## Summary and Conclusion

As said earlier, a great deal of research is currently being directed towards the goal of accurate prediction of the vibrational spectra of the molecules. In principle, the stated goal can be reached by known theoretical methods. However in this work, rigorous theoretical analyses based on quantum mechanical calculations were done.

In line with the above statement, FT-IR and FT-Raman spectra of three semicarbazide molecules were recorded and subjected to the new trends of theoretical methods based on quantum mechanical computations by DFT/6-311++g(d,p) basis set for the spectral analyses. A detailed vibrational spectral analysis has been carried out and assignments of the observed fundamental bands have been proposed on the basis of peak positions, relative intensities, fundamentals, overtones and combination bands. The quantum mechanical computations were applied using suitable software with DFT/6-311++G(d,p) higher basis sets. The difference between the experimental and theoretical wavenumbers is very small for most of the fundamentals. Therefore, the results presented in this work indicate that this level of theory is reliable for the prediction of both infrared and Raman spectra of the compounds.



The optimized molecular geometrical parameters such as bond lengths and bond angles were calculated and compared with the related XRD data. The compound has been synthesized and characterized by UV, $^{1}$HNMR and $^{13}$CNMR spectral analysis. Moreover, Molecular electrostatic potential, Fukui functions, thermodynamical property (entropy, enthalpy and specific heat capacity), and first order hyper polarizabilites were

calculated for the molecules. HOMO-LUMO analysis, UV-Visible, Natural bond orbital analysis were carried out. In order to understand electronic transitions of the compound, TD-DFT calculations on electronic absorption spectra in gas phase and DMSO-$d_6$ solvent were performed. The biological applications of semicarbazide derivatives molecule have been screened for its antimicrobial activity and found to exhibit antifungal and antibacterial effects. In addition, the Molecular docking was also performed for the different antimicrobial receptors.

In this present study, the investigation on different structural parameters such as geometrical parameters, structure conformation, energy, NLO, NBO, MEP, Fukui function, antimicrobial and Molecular docking and other molecular properties based on the structure and substitution were elaborately discussed and reported separately. The entire results obtained by this research work on the basis of substitutions in semicarbazide derivatives, theoretical methods etc., the comparative conclusions are listed below.



- The three semicarbazide derivative compounds (3BSC, 4BSC and 15BHS) were successfully synthesized and characterized. All the molecules characterized by FT-IR, FT-Raman, UV-Vis, NMR and tools derived from the density functional theory.

- In all the molecules, the theoretically calculated optimized bond lengths are comparatively larger than the experimental values. These indicate that the theoretical calculation refer to isolated molecules in the gas phase while the experimental results belong to solid phase.

- The band gap energy was calculated. In the entire semicarbazide molecule lower band gap energy is indentified. The lower band gap

energy explains the eventual charge transfer interactions taking place within the molecule.

- The nonlinear optical (NLO) response was noticed in the 3BSC, 4BSC and 15CHS molecules. The computed first order hyperpolarizability of all the molecules were 1.0475, 7.1223 and 9.6007 X $10^{-30}$ esu respectively suggest that the investigated molecules have potential for future NLO applications.

- Reactive sites for the all semicarbazide derivative compounds were identified from MEP and Fukui function analysis. Stability of the entire molecules arising from hyperconjugative interactions and charge delocalization has been analyzed using NBO analysis.

- The antimicrobial activity of all the molecules 3BSC, 4BSC and 15BHS are found to be high. However the molecular docking results of 15BHS molecule suggests that 15BHS molecule has higher antimicrobial activity when compared to all other molecules.

- Theoretical calculations gave the thermodynamic properties (heat capacity, entropy and enthalpy) for the compounds. From these it is observed that these thermodynamic functions were found to increase with temperatures ranging from 100 to 1000 K. This can be attributed as due to the fact that the molecular vibrational intensities increase with temperature.

- By analyzing the overall results obtained in this research on different parameters, among DFT/B3LYP method, the results obtained by 6-311++G(d,p) basis set show a pleasing, accurate and precise

qualitative agreement with the experimental findings by applying suitable scaling factors.

Furthermore, we find that the results of this present work and all the calculated data and simulations provide for a newer technique for the characterization of molecule as well as provide scope for future researchers who wish to carry out further investigations on these compounds and establish their predictive activities and properties. The potency of the technique is boundless and would be of immense help as and when new frontiers are identified for its application.